

POLITECNICO DI TORINO

Corso di Laurea Magistrale in Ingegneria Aerospaziale

TESI DI LAUREA MAGISTRALE

Experimental analysis of pneumatic probes in an unsteady environment



Relator

Prof. Roberto MARSILIO

relator's signature

.....

Candidate

Gerardo Russo

candidate's signature

.....

A.A. 2018

Contents

- 1. Introduction 1**
- 2. Architecture and details of the test rig 5**
 - 2.1. Module 1 - Banc enceinte sous vide (ECL) 6
 - 2.2. Module 2 - Banc multi-physique (ECL-B3) 6
 - 2.3. Module 3 - Banc d'excitation multiaxes (INSA) 8
- 3. Parametric analysis 15**
 - 3.1. Probe geometry study 23
 - 3.1.1. Not suitable probes 24
 - 3.1.2. Kiel-head probes 28
 - 3.1.3. Multi-hole probes 32
 - 3.2. Flow characteristics study 34
 - 3.2.1. Compressibility effects 34
 - 3.2.2. Turbulence effects 37
 - 3.2.3. Approaches on the analysis of turbulent phenomena 43
- 4. Analysis of application 45**
 - 4.1. Points of strong fluctuations 50
 - 4.2. Amplitude and frequency assessment 51
- 5. Experimental study of reduced model 59**
- 6. Probes cross evaluation 67**
- 7. Conclusions 77**
- 8. Appendix 79**
 - 8.1. Kiel-head probe specifications 79
 - 8.2. MATLAB script for the probes cross evaluation 85

8.2.1. Variables definition and data loading.....	85
8.2.2. Interpolation coefficients generation.....	86
8.2.3. Critical yaw angles determination.....	87
8.2.4. Approximated curves calculation.....	87
8.2.5. Pressure coefficients calculation.....	87
8.2.6. <i>Dremel</i> off - on total pressure difference, total pressure percentage error and CP difference matrixes calculation.....	88
8.2.7. Fluctuations-related angle and corrective factors determination.....	88
9. Bibliography.....	91

Experimental analysis of pneumatic probes in an unsteady environment

Chapter 1

1. Introduction

The aim of the present dissertation deals with a comprehensive study on pneumatic probes used to measure unsteady flow conditions.

Usually, pneumatic probes are employed to measure physical amounts of a flow, such as both static and stagnation pressure and temperature. Despite, to whom that may concern aviation and turbo-machinery fields, the measurement accuracy is very important as well as the reduced size of instruments in order to not influence a lot the inter-stage environment to be analysed.

In general, these kinds of probes (there may have single or multi-hole probe, each one with its positive aspects and drawbacks to be following discussed) are calibrated in low turbulence, free-stream channels with steady conditions, despites they can be successfully used to measure highly fluctuating unsteady flow conditions.

The knowledge on the accuracy of measurements and the uncertainty induced by inappropriate measurement systems is of great importance in all fields of fluid engineering, particularly for the development of highly efficient aircraft and energy applications. To support the development of modern simulation techniques, highly accurate measurement methods are necessary to enable a substantial validation.

Within the proposed work, the author and its tutors will analyse the specific influence of periodic unsteadiness in order to investigate the validity of calibrations under steady conditions, in addition to conduce a systematic variation of flow and probe parameters so that sensitivities will be derived and measurement accuracy will be quantified.

The results will be useful to quantify systematic errors of these measurement methods.

One of the most interesting fields in turbo machinery is about the comprehension of how much the size and the geometry of pneumatic probes used in today's centrifugal compressors can affect the precision of the pressure amounts read downwards compressors' rotors, environments well known as fully unsteady.

As a matter of facts, despite these values could seem useless due to the strong importance of inter-stage pressure values, which correspond to data get downwards both rotor and stator, into performance determination, the knowledge of these values can provide very useful information about compressor stall and surge predictions, as well as they can assess and certify the good design of rotor blades.

In this way, the aim of this work happening at LMFA (*Laboratoire de Mécanique des Fluides et d'Acoustique*), sited into École Centrale de Lyon and carried out by the underwritten through the supervision of Prof. Xavier Ottavy and his assistant Christoph Brandstetter, concerns into plural tasks.

First of all it is useful to perform a parametric analysis about the study of the influence of both probe geometry (number of holes, probe's intake, length, diameter, radial position and so on) and flow characteristics (Mach number, velocity vector direction respect to the probe front axis, Reynolds number, kind of unsteadiness - if periodic or randomly fluctuating);

Then, it is important to get a prediction about the points along with the flow path where there could be strong fluctuations.

Hereafter, it is useful to quantify both amplitude and frequency in order to demonstrate that, when in service, the rotor blades won't produce deleterious oscillations that can bring to amplify unsteadiness or cause fatigue phenomena on blades' materials. As known, the frequency of fluctuations depends on the application for which a rotating machine is designed. Just to make a quick comparison, wind turbines oscillations are in the order of 1[Hz], as well as common turbojets axial compressors ones are in the range of 1[KHz] to 20 [KHz] while turbochargers fluctuations happen with a frequency of the order of 100 [KHz]. In order to provide more useful data about this concept comprehension, a table listing the most important physical characteristics for each field of application has been created and here under reported:

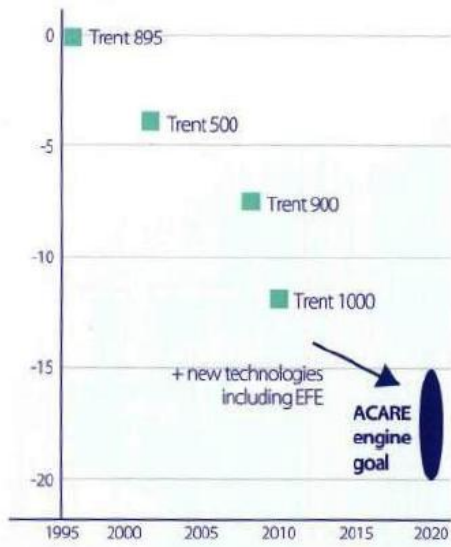
Type of rotating machine	blades number	rotational speed [rpm]	f [Hz]	Mach Number	γ	α_0 [deg]	α_1 [deg]	α [deg]	tpd [Pa]
Wind turbine	3	10	3.14	0.10	1.40	0.00	20.00	20.00	-0.02
Water turbine	22	500	1151.92	0.30	1.33	0.00	0.00	0.00	0.00
Turbojet compressor	18	15000	28274.33	0.56	1.40	40.00	7.00	47.00	-0.46
Turbocharger	13	280000	381179.91	0.70	1.40	40.00	6.00	46.00	-0.42
measured / assumed									
α_0 is the incidence angle set up into the rig									
α_1 is the additional incidence angle coming from fluctuations									
α is the overall incidence angle									

Type of rotating machine	p_s [Pa]	$p_t - p_s$ [Pa]	Δp_{tot} [Pa]	ρ [Kg/m ³]	Δv [m/s]
Wind turbine	101325.00	711.05	15.07	1.225	34.07
Water turbine	101325.00	6202.12	2.48	1000.00	3.52
Turbojet compressor	101325.00	24041.82	11021.82	1.225	198.12
Turbocharger	101325.00	39223.04	16599.58	1.225	253.06

For further details about these last tables, see chapter four, in which each value and formula will be explained.

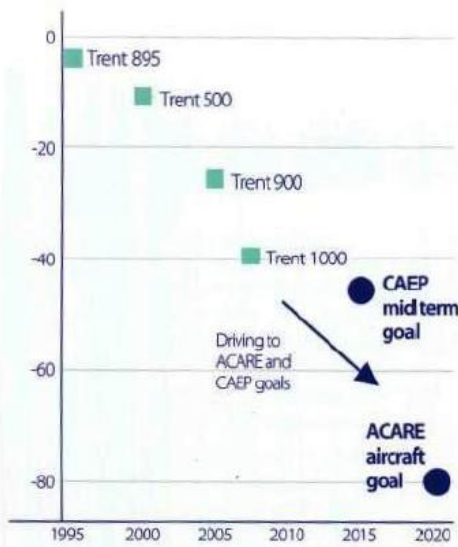
Before continuing, is important to specify that one of the most important reasons for which this project has been carried out are linked to ACARE goals (*Advisory Council for Aeronautics Research in Europe*), which aims to a reduction, until 2020, of 50% of both CO₂ and noise emissions and a decrease of 80% of both NO₂ emissions and crashes. See the under-reported picture for a best comprehension of ACARE goals and state-of-the-art aircraft power-plants.

Fuel saving¹ (%)



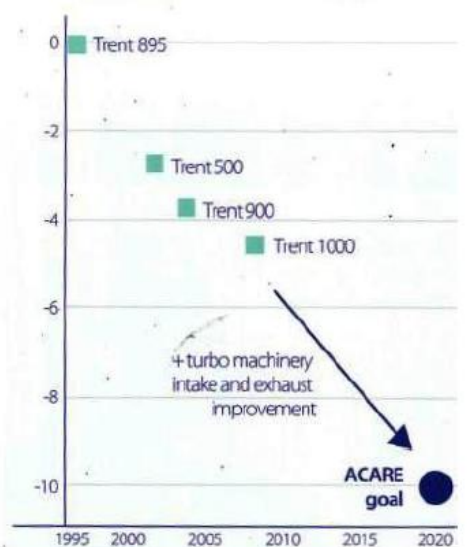
¹SFC: fuel consumption normalised for engine power

NOx reduction² (%)



²Normalised to CAEP standards for engine power

Noise reduction³ (dB)



³Corrected for aircraft weight

Figure 1.1 - ACARE goals accomplishments progresses, X.Ottavy [12]

Chapter 2

2. Architecture and details of the test rig

The work under consideration is part of a huge project called EquipEx - PHARE, word made up as acronym of the French description of the test rig: "*Plateforme macHines tournantes pour la mAîtrise des Risques Environnementaux*".

This last is a Lyon-based project, conceived in 2011, and developed in accordance with "*Ministère de l' Enseignement supérieur et de la recherche*" and the "*Commissariat Général à l'investissement*" to made up experiments with the aim to face the industrial challenges of increase the productivity of energy production and the overall efficiency of means of transportation.

This project consists of three test benches installed at École Centrale de Lyon and at INSA that process issues dealing with aerodynamic instabilities inside rotating machines, aeroacoustics and elastodynamics in order to improve:

- overall energetic efficiency;
- safety;
- environmental impact.

As a matter of facts, owing to the multidisciplinary nature of this project, there are numerous factories interested in, like Safran and EDF, and a lot of science branches are involved such as structure mechanics as well as material and fluid ones, physicians and acousticians. In addition, different limbs of knowledge may be influenced and have repercussions thanks to this research, which can space from the efficiency improvement of the present aeronautical engines up to electric power stations interests, as different physical phenomena linked to interaction of instabilities are studied, such as fluid-structure and structure-structure interaction, and so on.

In this way, three different benches have been developed:

2.1. Module 1 - Banc enceinte sous vide (ECL)

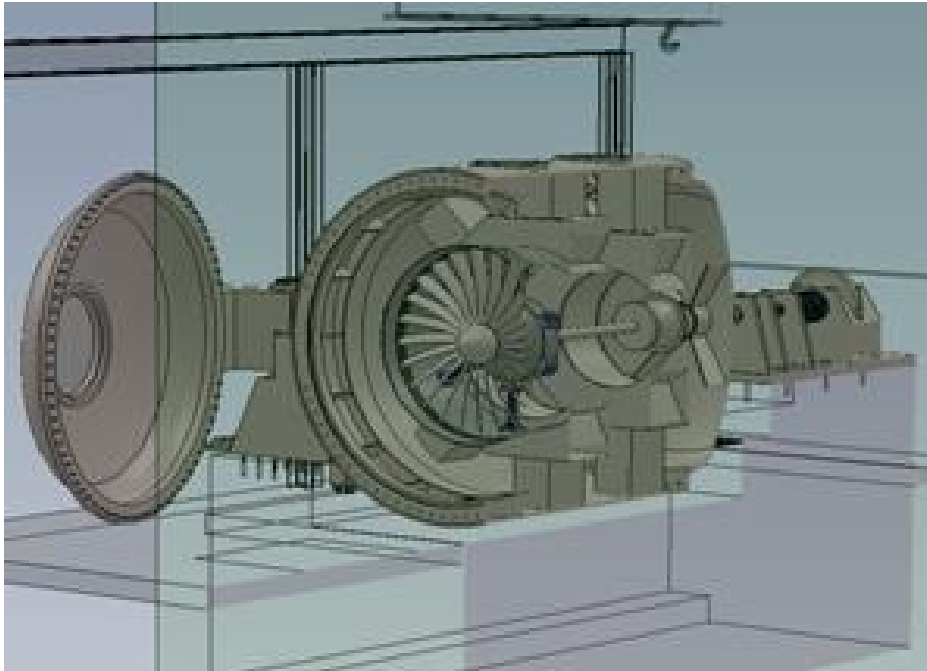


Figure 2.1 - Banc enceinte sous vide, X.Ottavy [12]

The aim of this rig is to realize vibratory experiments under vacuum, in the same scale of an aeronautical engine, so that it can concern both vibratory phenomena, such as shaft vibrations, wheels' skews and instabilities, both quick and passing dynamic aspects linked to the loss of a blade or a rotating disk burst.

(Responsible : Claude Gilbert)

2.2. Module 2 - Banc multi-physique (ECL-B3)

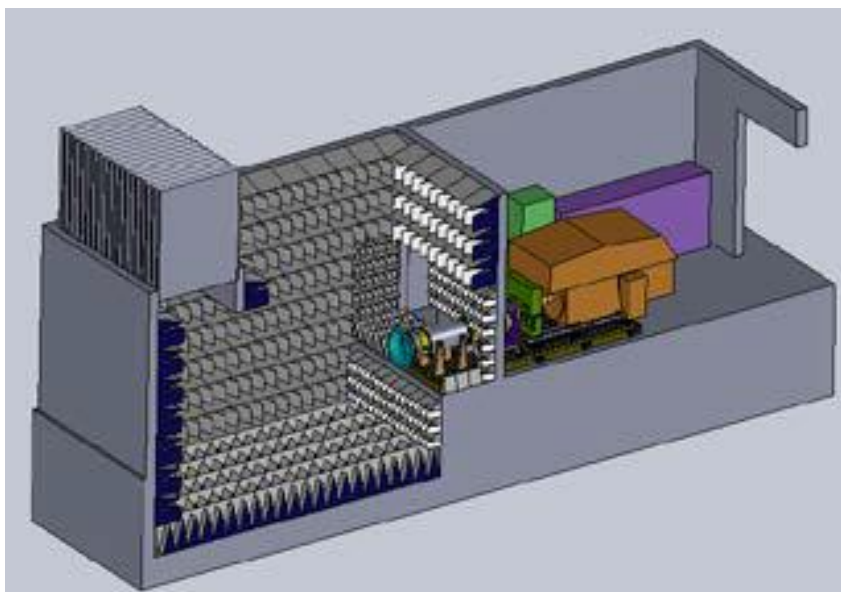


Figure 2.2 - Salle d'essais of Banc multi-physique, X.Ottavy [12]

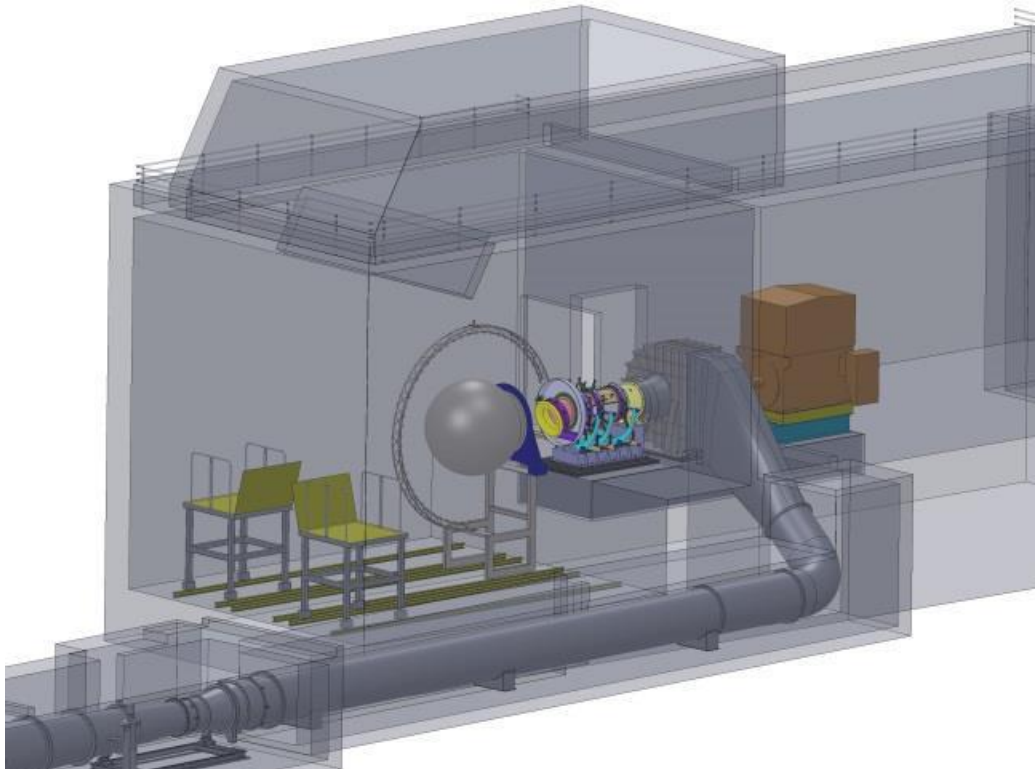


Figure 2.3 - Salle d'essais et des machines of Banc multi-physique, X.Ottavy [12]

The aim of this rig is to perform tests on instabilities owing to fluid-related interactions. Thanks to the ability to simulate a 1/3 scaled fan, this bench can allow to develop multi-physics and multi-scale approaches where a valuable role is represented by physics coupling and can analyse three scientific limbs:

- aerodynamic instabilities;
- aeroelastic instabilities;
- aeroacoustic signature.

(Responsible : Xavier Ottavy)

2.3. Module 3 - Banc d'excitation multiaxes (INSA)

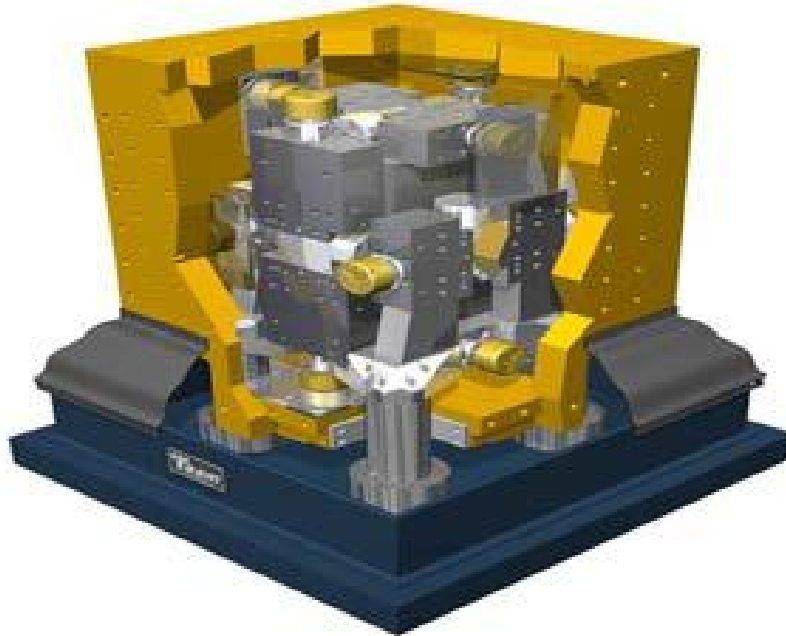


Figure 2.4 - global view of Banc d'excitation multiaxes, X.Ottavy [12]

The aim of this rig is to study the dynamics of rotating machines installed on a 6 axis excitement system in order to realize the dynamic behaviour in both passing and steady modes. In addition, there is the capability to control the stability in both active and passive ways.

(Responsible : Regis Dufour)

The last three benches are those ones employed in the project of which the current dissertation deals with. The attention, now, can be focused on the second bench, the Banc multi-physique (ECL-B3), which is currently used at LMFA for the following study.

As a matter of facts, this bench involves inner instrumentation useful to carry out the ACARE goals, that is showed in the following picture :

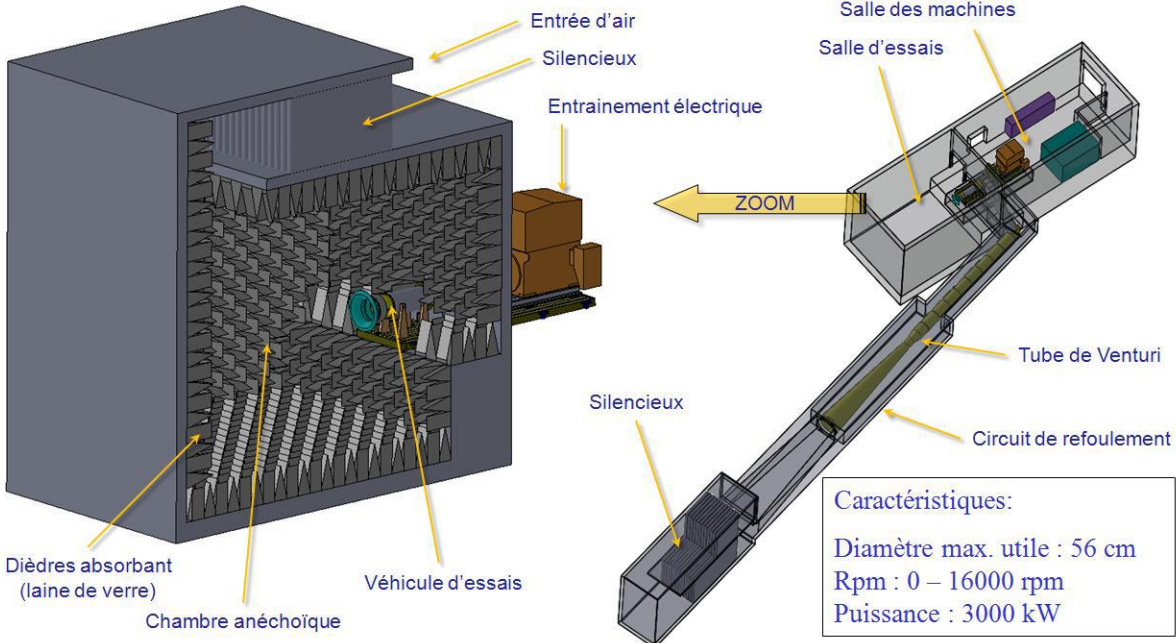


Figure 2.5 - global view of Banc multi-physique (ECL-B3), with inner and outer instrumentation, X.Ottavy [12]

As noticeable, the ECL-B3 consists of different macro-components such as :

- Air aspiration / reject : is a single component that can work both as an intake both as a nozzle and that can limit the acoustic emissions thanks to the use of sound-absorbent panels.
- test chamber : consists of a cubic-shaped anechoic chamber which fibre-glassed absorbent dihedrals and obstacles are deployed in order to provide a flow direction that directly, with no vortex or loss, goes to the bench intake.

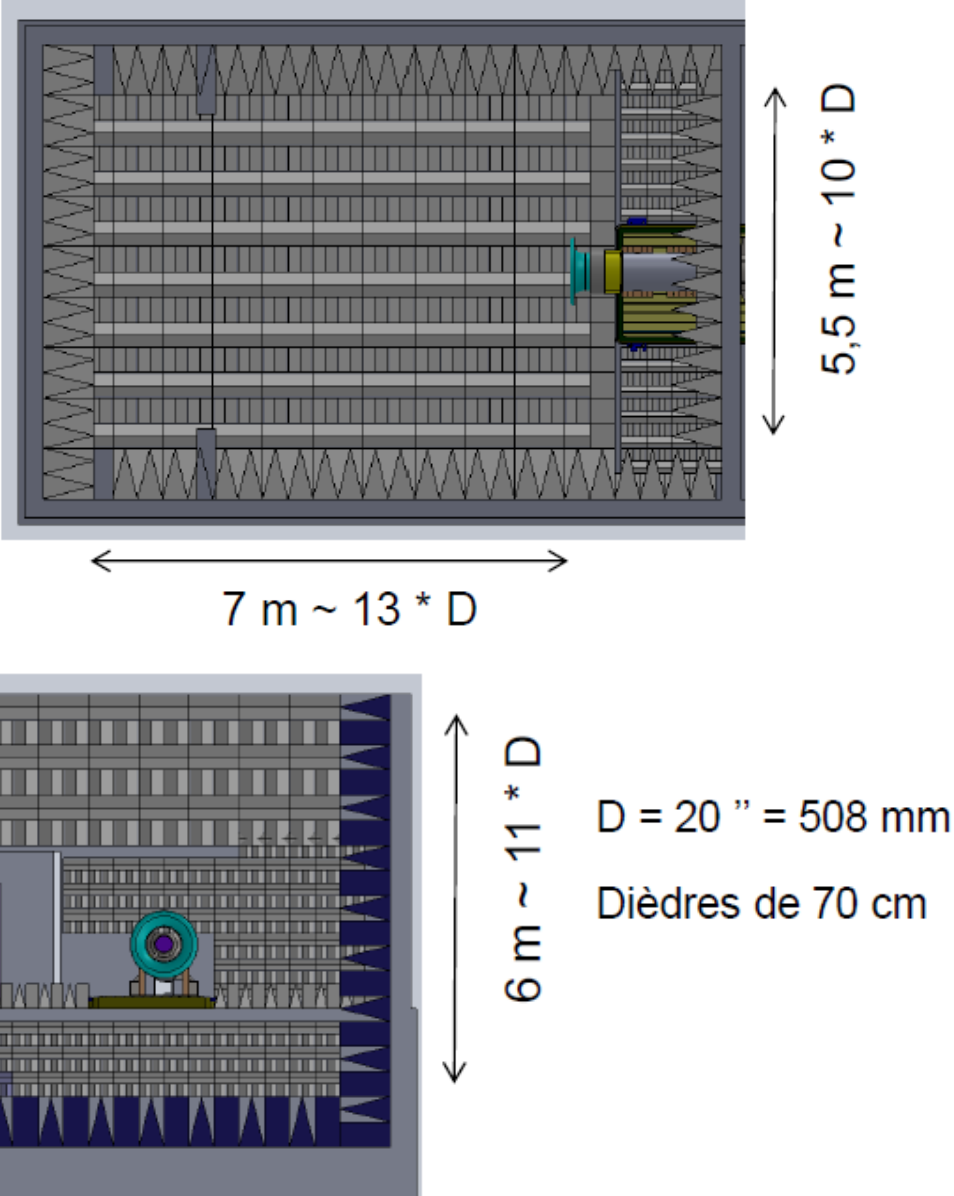


Figure 2.6 - anechoic chamber details and sizes, X.Ottavy [12]

- test rig - MARLYSA (Snecma owned) : is the focus component as it will be used to take flow field measurements about the present work. It features different 360 degrees rotating rings on which different instrumentation can be installed, such as aerodynamic related probes (static and stagnation pressure probes, both stationary and not, or total pressure probes, laser instrumentation, and so on), or other acoustic and aero-elastic related instrumentation. In addition, there are other equipments that can measure radial and angular displacement (called "*Explorateur*"), or it is possible to use telemetry to get rotating amounts measures such as the torque and axial thrust.

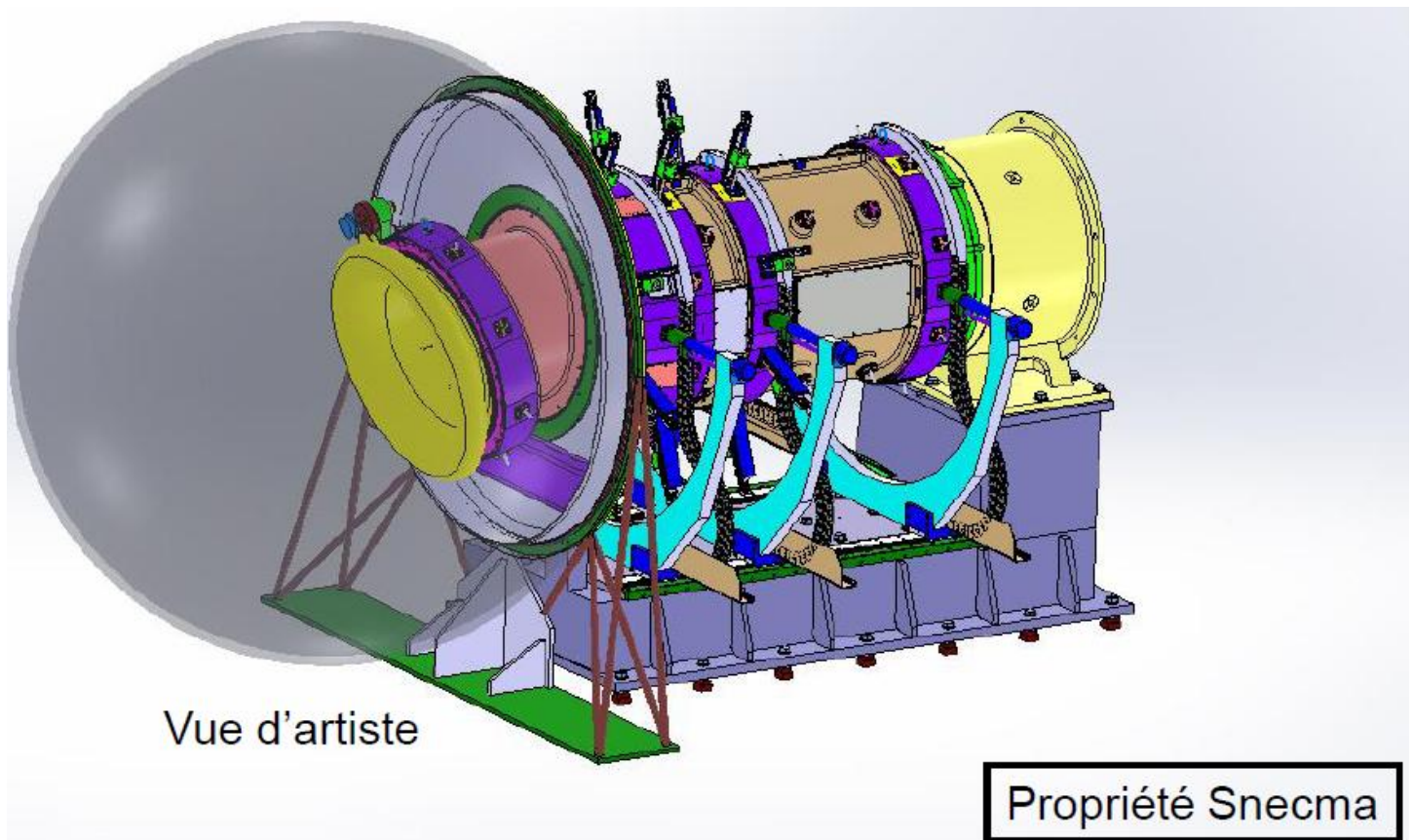


Figure 2.8 - axonometric view of the used test rig, X.Ottavy [12]

- Volute : placed downstream the test rig, it consists of a spiral coil useful to change the orientation of the environment without induce circumferential flow distortions, and so lessen the pressure load. In addition, thanks to this component, it is possible to vary the load of the test rig and so study the aerodynamic instabilities with an integrated acoustic treatment.

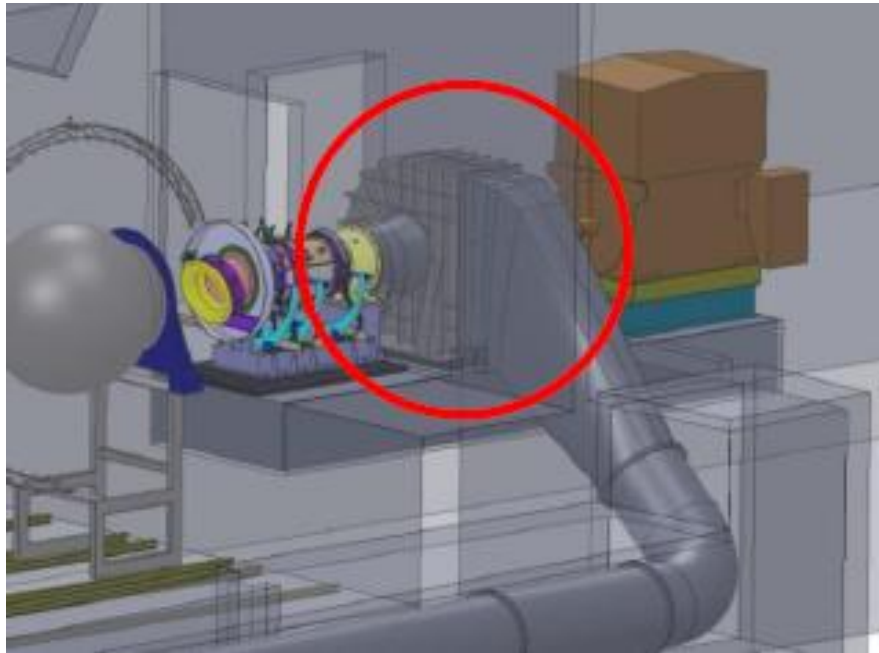


Figure 2.9 - volute, X.Ottavy [12]

- Machines chamber : consists of a set of devices useful to control a downstream-placed electric motor that provide the power to allow the work of the test rig (that simply represents a compressor). These lasts include AC to DC converter (*variateur*), multiplying gears, lubrication platform, transformer and so on. Follows a quick resume of the main test equipment features and a picture that better represent the motor:

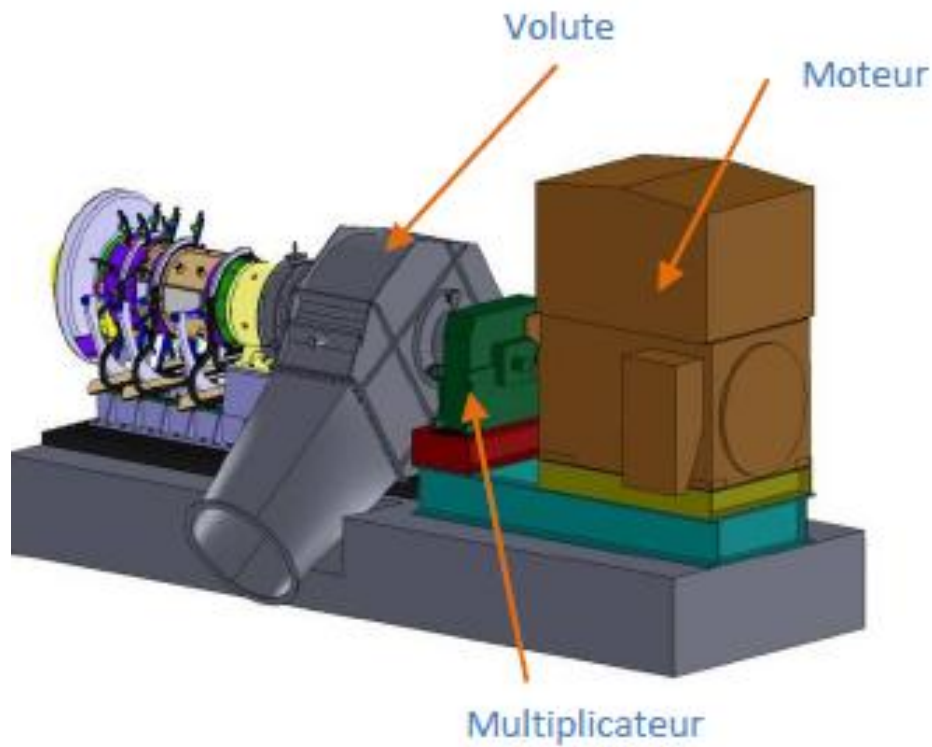


Figure 2.10 - Motor and related devices, X.Ottavy [12]

Physical amount [unit of measurement]	Value
length - L [m]	10
width - I [m]	7.3
height - H [m]	5.8
supplied power [MW]	3
maximum allowable shaft speed [rpm]	16000
maximum inter-stage pressure ratio [/]	1.8
maximum flow rate [Kg/s]	45

Table 2.1 - Sizes and power of the test rig

- Control chamber : is the last component explained and contains a control desk as well as other piloting tools.

Chapter 3

3. Parametric analysis

In this chapter, a comprehensive study about different factors that may affect the amounts read by a generic probe in an unsteady environment will be carried out.

As a matter of facts, downstream a compressor rotor and inside all other unsteady environments, thermodynamic and physical amounts are time dependent, which means that time-derived-by terms in Navier-Stokes equations must not be simplified. This feature brings intrinsically to higher solution difficulties and so there is the need to use more powerful calculus resources, such as CFD based numerical methods and solution.

Then, unsteady flow-field is highly turbulent and many fluctuation frequencies exist, which brings both to a three-dimensionality of the flow field, both to the awareness, in case of a multi-stage compressor or test rig, to take into account these fluctuating fields so that instrument-read amounts (in general static pressure, total pressure and total temperature, mass flow rate) won't be influenced;

In addition, compressor efficiency-related phenomena, such as surge and stall margin, appears when inter-stage pressure values do not respect the following compressor map:

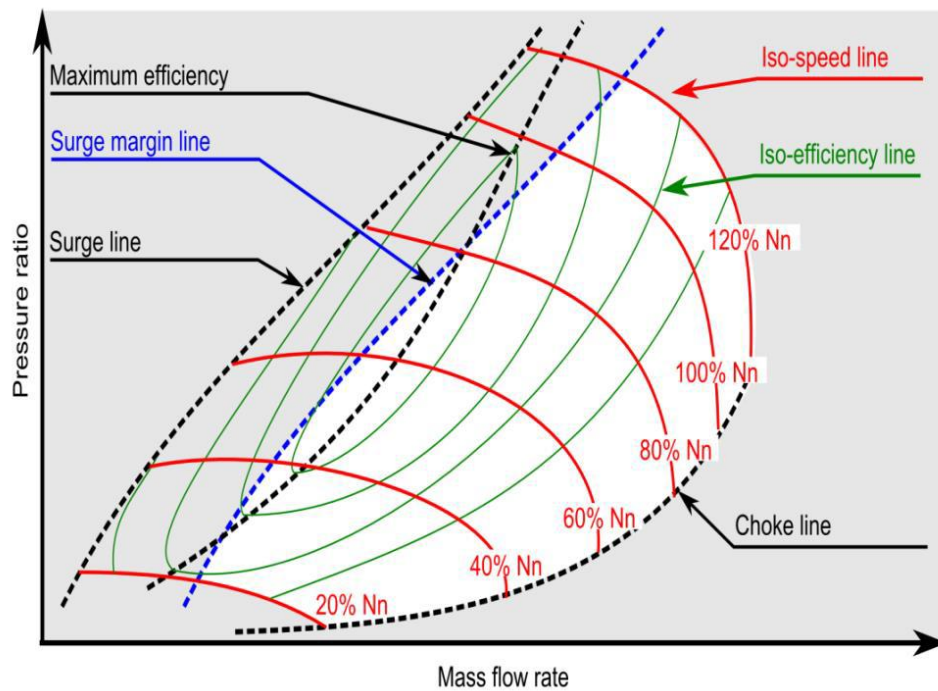


Figure 3.1 - Motor typical compressor map, valid for both axial and centrifugal geometry, X.Ottavy [12]

To avoid these deleterious phenomena, it is important not to overwhelm specific inter-stage pressure ratios as, otherwise, adverse pressure gradients may happen even if there are low flow angles and blade exit angles.

So, when a pneumatic probe is awash into an unsteady environment, there are different parameters that may have a consequence over the pressure determination which, according to S. Bauinger et al [1], could interlace:

- Mach number, so there could be effects of compressibility that have to be taken into account, that will be analysed in one of the following chapters;
- Reynolds number, which is not analysed in the present dissertation, even because the authors previously mentioned demonstrated a poor correlation between Reynolds number and unsteadiness captured by a probe steadily calibrated;
- Speed gradients & wall proximity effects, which are also not taken in consideration due to the low influence they have on the probe, as it is installed and positioned sufficiently far from ducts walls in order to minimize boundary layer induced effects and errors;
- Amplitude & frequency of time-resolved periodic pressure fluctuations. As a matter of facts, periodic fluctuations have an amplitude that does not affect the

reading as they depends on the probe-heads shape and on the hub-to-shroud position, as the following picture explains :

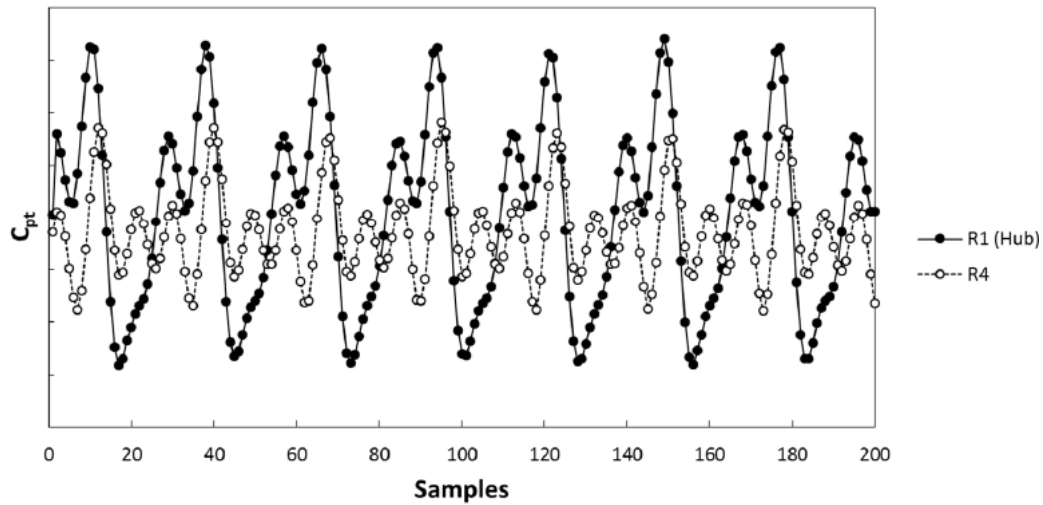


Figure 3.2 - Dependence of the total pressure coefficient in correlation with the hub-to-shroud position inside a duct containing unsteady flowfield, S. Bauinger et all [1]

- Stochastic pressure fluctuations / turbulence intensity. How it is possible to grasp, the peaks of fluctuations increase with the growth of the operating point-dependant variables, such as the mass flow rate, shaft angular speed and pressure ratio.

In addition, from the literature read, it is possible to realize that unsteady measured values can be done and reported in three different manners:

1. Time-averaged, in order to let possible a comparison of different pneumatic measurements techniques (preferred in turbo machinery). In this field can be included all the probes used in this dissertation, such as five hole probes, Kiel-head and pitot ones which, among other things, have low frequency response in comparison with the next manner reported but they are more robust to face the highly fluctuating flow fields;
2. Mass-averaged, are used to get information in the entire section of the machine duct. For this kind of measure, it is important to possess a high frequency response probe, such as FRAPP;
3. Hub-to-shroud profiles, as there is the necessity to determine the radial variation of gas properties and flow angle at each stage station, so it is important to install two probes. In this way, there will be a hub side probe

(set up at 33% of the duct thickness) and a shroud side probe (installed at 67% of the duct thickness) :

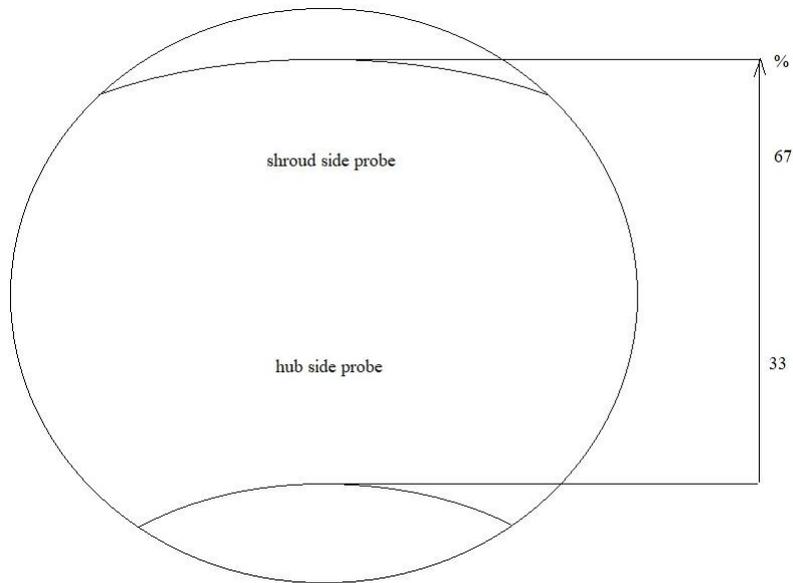


Figure 3.3 - General layout of an hub-to-shroud probes placement

Now, to better describe the compressor performances and characterize the amounts under consideration, such as blade-related angles, the following picture is provided :

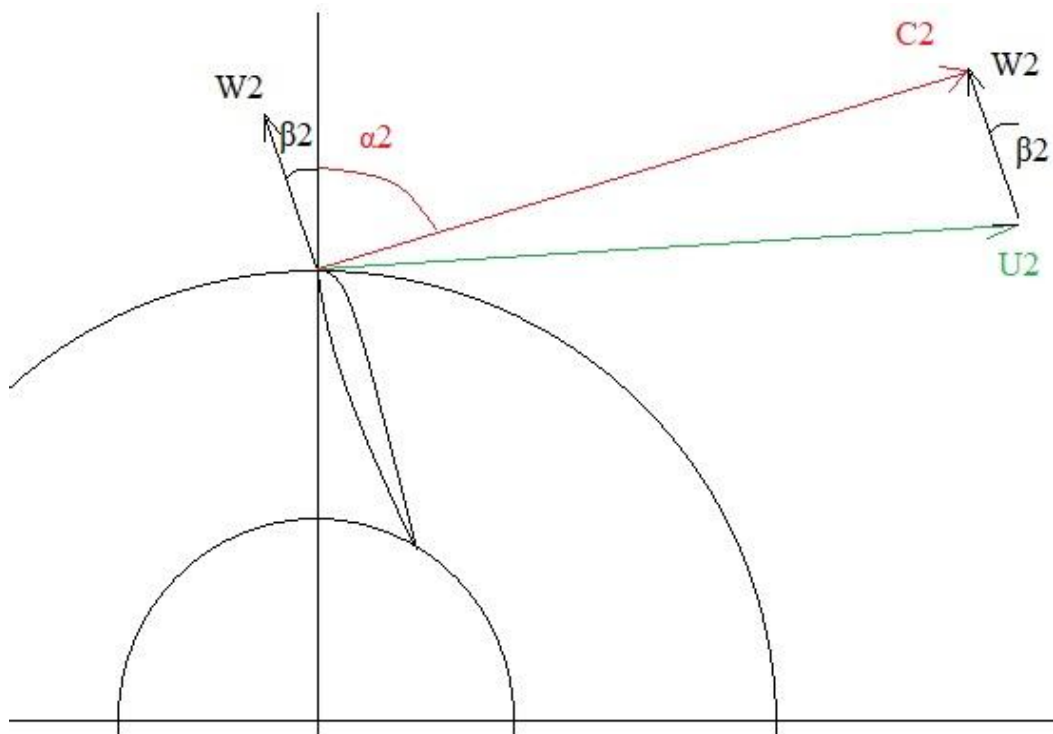


Figure 3.4 - angles and speeds that are summarily analysed

Where :

- α are absolute angles;
- β are relative angles;

As reported by different authors, such as Gilarranz et al [2], centrifugal compressors performances can be described, in addition by their working maps, by the graphs under reported, which explain the relationship among flow angle deviation (between rotor exit and stator intake) and operating conditions as well as machine mach number and radial position (in facts, hub-to-shroud measurements have been performed as explained in picture 3.3) :

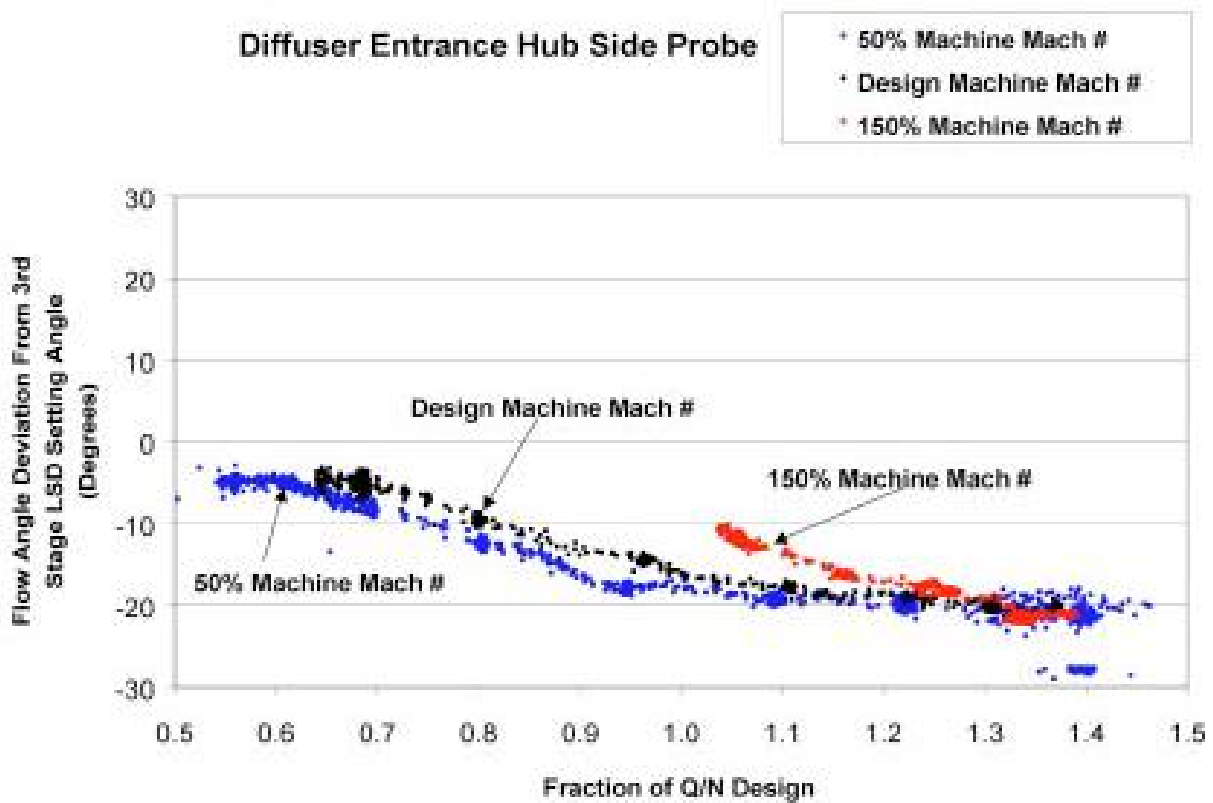


Figure 3.5 - Hub-side flow angle deviation at diffuser entrance with varying the machine flow coefficient, J. L. Gilarranz et al [2]

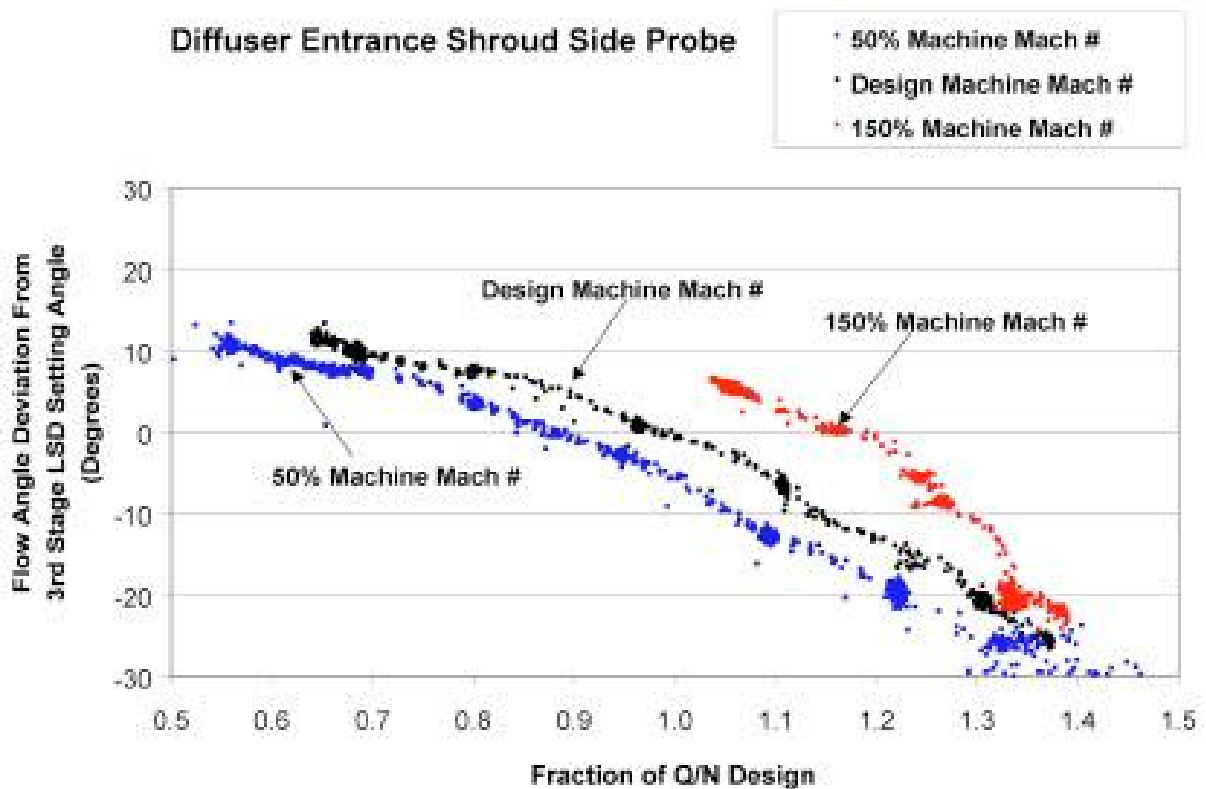


Figure 3.6 - Shroud-side flow angle deviation at diffuser entrance with varying the machine flow coefficient, J. L. Gilarranz et al [2]

where :

- flow angle deviation is $i = \alpha_2 - \beta_3$;
- α_2 is the absolute angle of the flow exiting the impeller blades;
- β_3 is the next stage's blades setting angle;
- Q/N is called "*Machine Flow coefficient*" and is a parameter that gives indications about the machine operating point respect to design condition. Notice that Q is the mass flow rate and N is the shaft's angular speed. So, in function of the amount of this coefficient, can be noticed that :
 1. if $Q/N = 1$, then the machine is operating at on design condition;
 2. if $Q/N < 1$, then the machine is operating at an off design condition close to surge;
 3. if $Q/N > 1$, then the machine is operating at an off design condition close to choke.

Other graphs follow:

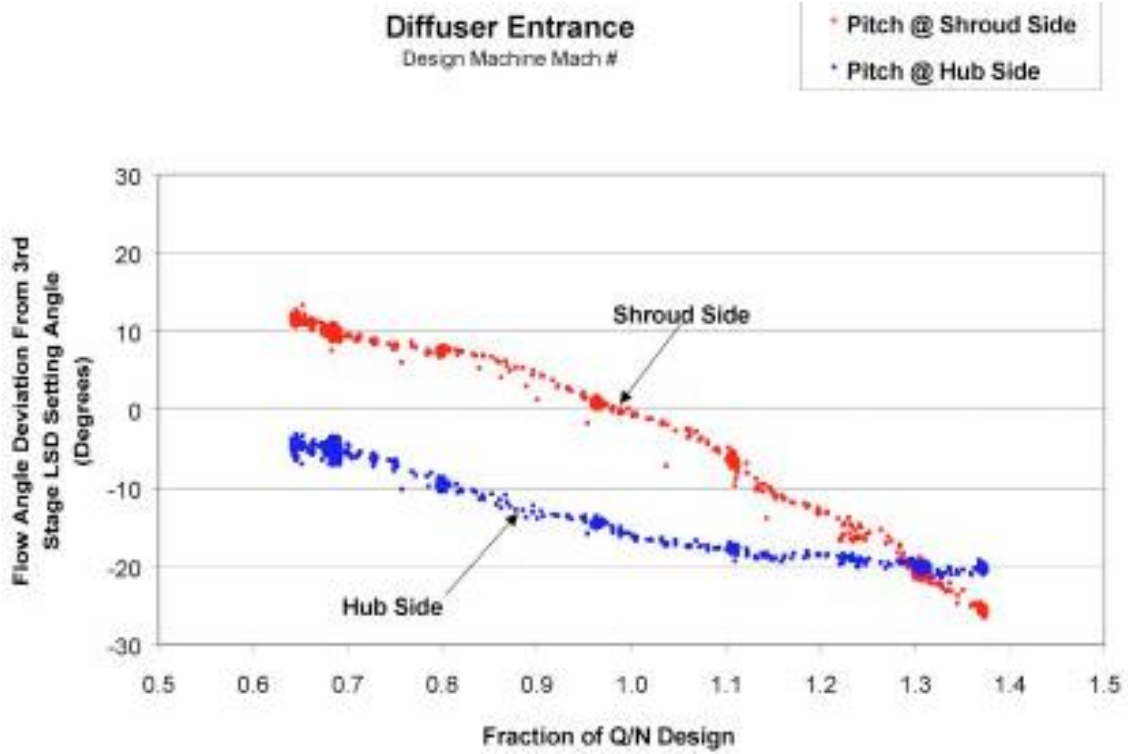


Figure 3.7 - Flow angle deviation at diffuser entrance with varying the machine flow coefficient, J. L. Gilarranz et al [2]

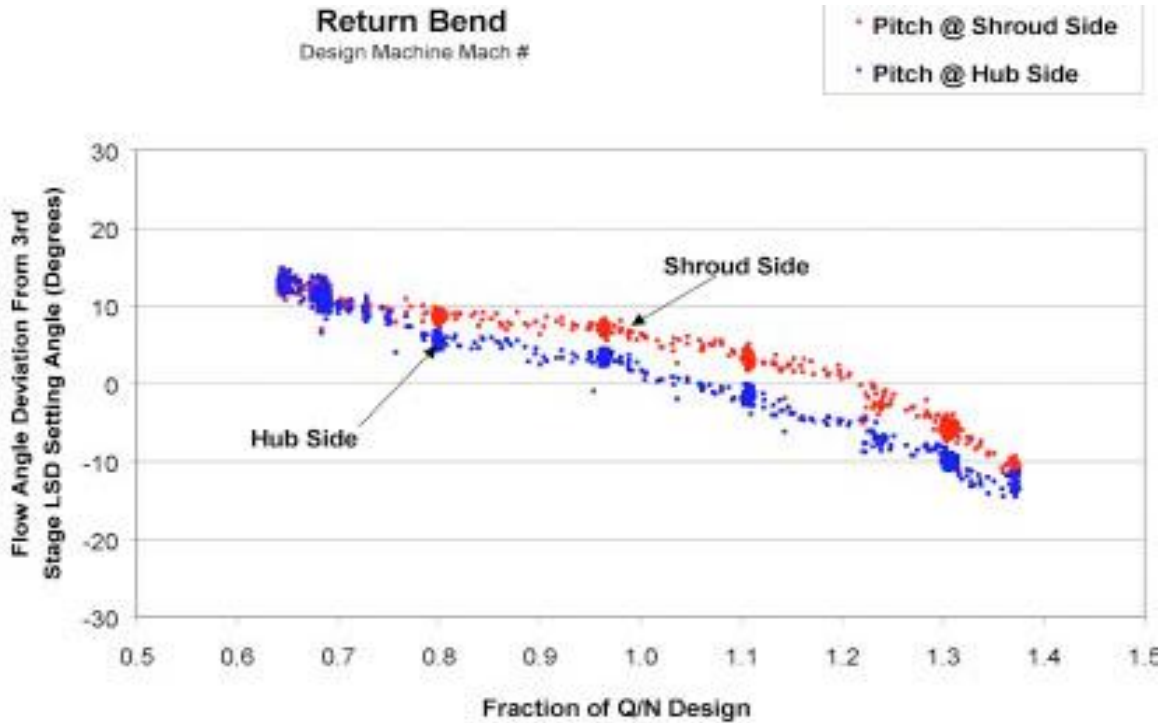


Figure 3.8 - Flow angle deviation at return bend with varying the machine flow coefficient, J. L. Gilarranz et al [2]

All these operating point-related graphs can be summarized as reported in the picture below:

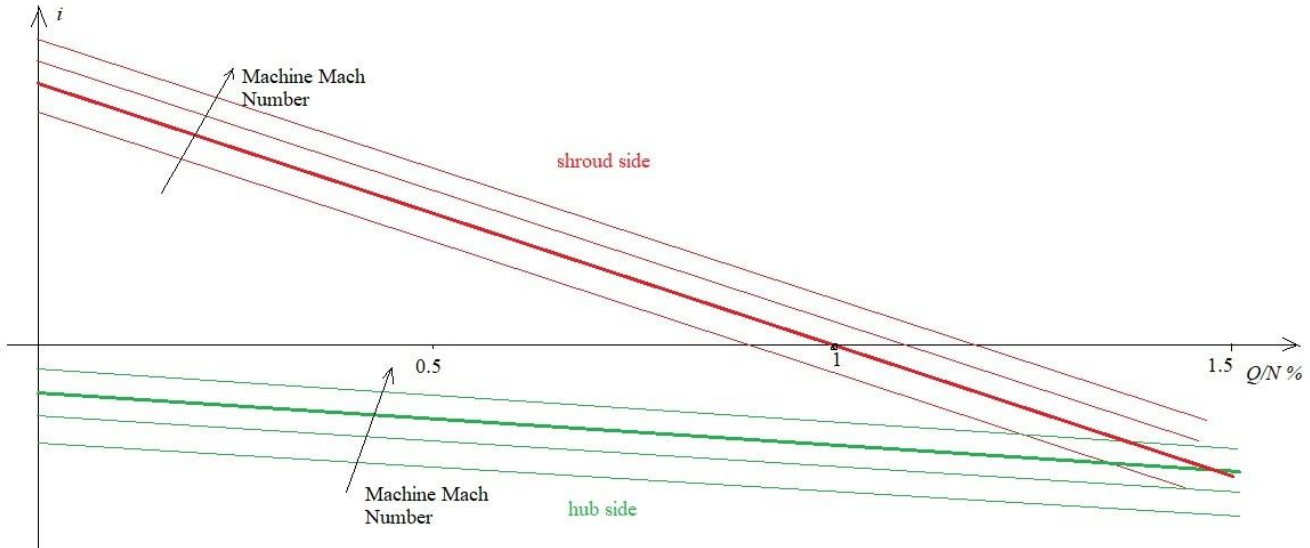


Figure 3.9 - diffuser incidence relative to the impeller exit angle with varying the machine flow coefficient. The highlighted curves are related to the machine On-Design Mach Number

Is important to specify that the authors of the previous figures (Gilarranz et al [2]) obtained these results analyzing data gathered at intermediate stages so that compressor's inlet effects would have been minimized. In addition, they used a low solidity diffuser (stage number three) which blades are optimized only for on design condition and, when the machine works off design, the polytropic efficiency would have a shortfall.

As concerns *Figures 3.7* and *3.8*, can be seen that close to the surge condition, there is a huge flow angularity difference between impeller and return bend positions because at the impeller exit, the flow is features a higher hub-to-shroud deviation.

Then, looking at *Figure 3.7* can be noticed that the flow is more radial next to the hub due to shear forces in the flow-field, which bring viscous dissipation and mixing effects. Instead, the flow-field tends to be more tangential next to the shroud.

In addition, as the authors specify, the use of ribs may reduce flow deviation, especially in the shroud-side position, due to the “routing effect”, which can provide the possibility to have a higher surge margin and overload capacity.

Anyway, in general can be affirmed that, when moving from choke ($Q/N = 1.4$) to surge ($Q/N = 0.65$), the flow angularity tends to increase.

In addition, from *Figure 3.9* can be noticed that, as expected, at design condition (bold curves) the flow angularity is null, i.e. the flow exiting the impeller is aligned with the next stage's blades setting angle.

Instead, when close to stall condition, two observations can be done:

- flow angular deviation tends to increase with approaching stall, condition at which it may amount a dozen degrees approximately;
- close-to-hub flows never reach β_3 , i.e. flow angularity is every time negative.

So, known that all kinds of probes have their own pitch and yaw ranges, all these features previously described can lead to the very important observation to check the probe axis alignment along with the machine working condition.

Now, once introduced in broad terms the parametric analysis of a general centrifugal machine and which parameters may affect its performance, the attention may be focused on the influence of flow characteristics and the different probe geometries on the value read in a test rig environment.

3.1. Probe geometry study

As written in the previous pages, there is the need to harness instrumentation useful to assess the inter-stage working condition of a compressor. In general, these sensors may be:

- total pressure probes;
- static pressure taps;
- J-type thermocouples (both shielded or unshielded).

In most cases, those ones may be integrated into a single probe, and, in general, there are a lot of probe types existing in commerce but only a narrow set of those can be employed in turbo-machinery due to the existence of different constraints that make this field very demanding in terms of robustness and frequency response.

As a matter of facts, especially for unsteady environments, fluctuations and turbulences amplitude, frequency and vortexes scale are the most important variables to take into account in order to avoid that a steady-calibrated probe submerged in a fully unsteady environment will read a wrong pressure, being it either static or stagnation one. Anyway, in the next chapter this aspect will be analysed in detail but, as concerns the aim of this subchapter, it is important to recognize which kind of probe

is suitable for highly unsteady environments such as those ones encountered in the currently used test rig.

In addition, before to undertake the different probe geometry analysis, it is important to define the *critical angle*, which is the incidence, referred to either yaw or pitch, at which the stagnation pressure error overtakes the amount of 1% of the pressure measured at a null angle of attack.

3.1.1. Not suitable probes

The most common probe is Pitot one, which features a duct linked to a differential manometer (see picture below) so that it is possible to measure dynamic pressure, consisting of the difference between stagnation pressure (captured through the probe intake) and the static pressure (captured by lateral holes, not exposed to the main flow stream).



Figure 3.10 - A classical Pitot probe, source : <http://www.unitedsensorcorp.com/pitot.html>

In this way, the flow velocity can be derived using Bernoulli's theorem:

$$p + \frac{\rho u^2}{2} = \text{const} \quad (3.1)$$

where p is static pressure, ρ is the flow density and u is the local flow speed.

The reading speed is a function of:

- the length and diameter of the flow ducts;
- the size of the pressure ducts to the manometer;
- the displacement volume of the manometer.

Whether there is the need to miniaturize the probe due to the limited ducts' section in which they have to be installed, then separate total and static tubes have to be harnessed rather than combined total-static one as the time constant (i.e. the time taken by the manometer to reach the equilibrium in terms of pressure) increases rapidly.

As noticeable in the figure below, this kind of probe is employed to get a flow field measurement in parallel to flow direction (direction along which the probe error is null, corresponding at the top of the curve) because flow misalignment, even if relatively small, can result in a huge error in total pressure reading.

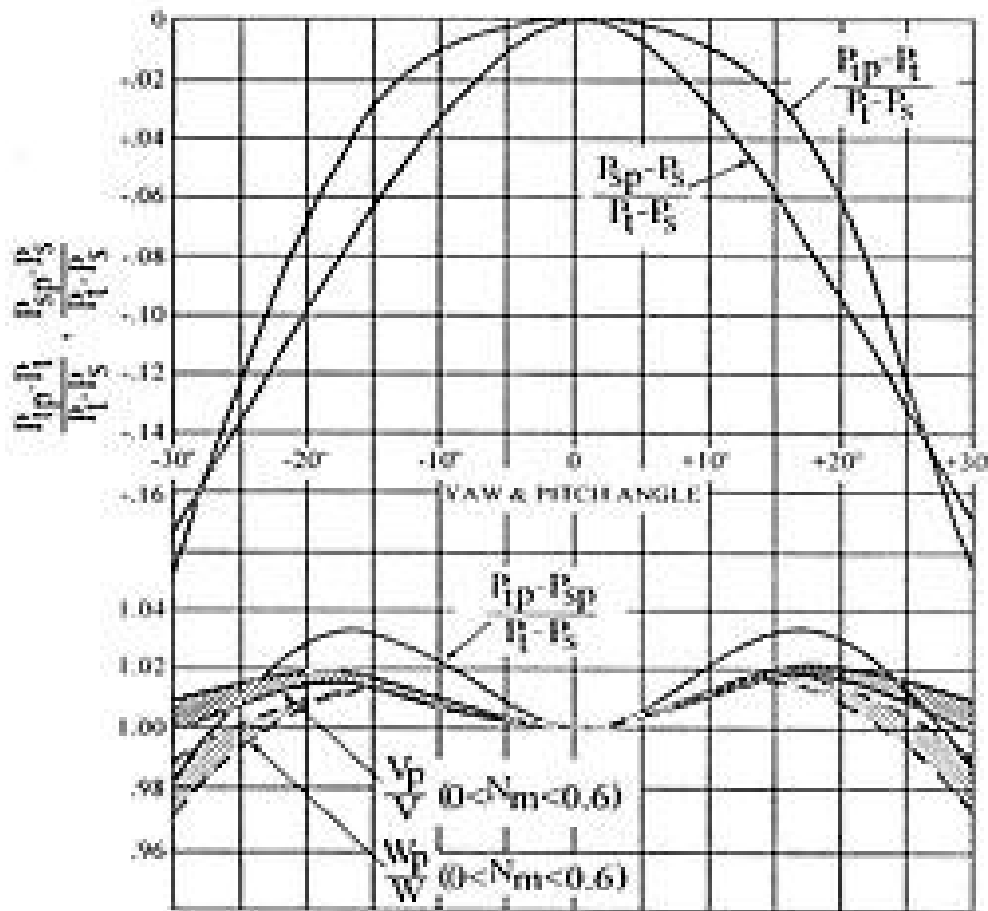


Figure 3.11 - Pitot probe pressure error with varying yaw / pitch angles, Chue [3]

Notice that misalignment can happen both having a flow field with a speed vector not aligned with the probe axis (i.e. yaw or pitch angle exist and are not null) both if the probe is immersed in highly turbulent flows so that the fluctuating components are high enough to let the probe perceive a different flow direction.

Of course, exactly for this reason, Pitot probes are not suitable for unsteady environments even if they can be harnessed over a broad set of flow regimes such as incompressible, subsonic, transonic and supersonic flow-fields.

As concerns the incompressible regime, the study carried out by Chue [3] shows an interesting result reported in *Figure 3.12* which leads to the statement that there are different Pitot probes geometries, each with a different yaw angles insensitivity range but, if compared with other kind of probes such as Kiel-head ones, they all have a critical insensitive angle much more smaller, that's why Pitot probes are not suitable for highly unsteady environments, so they won't be used in the present study.

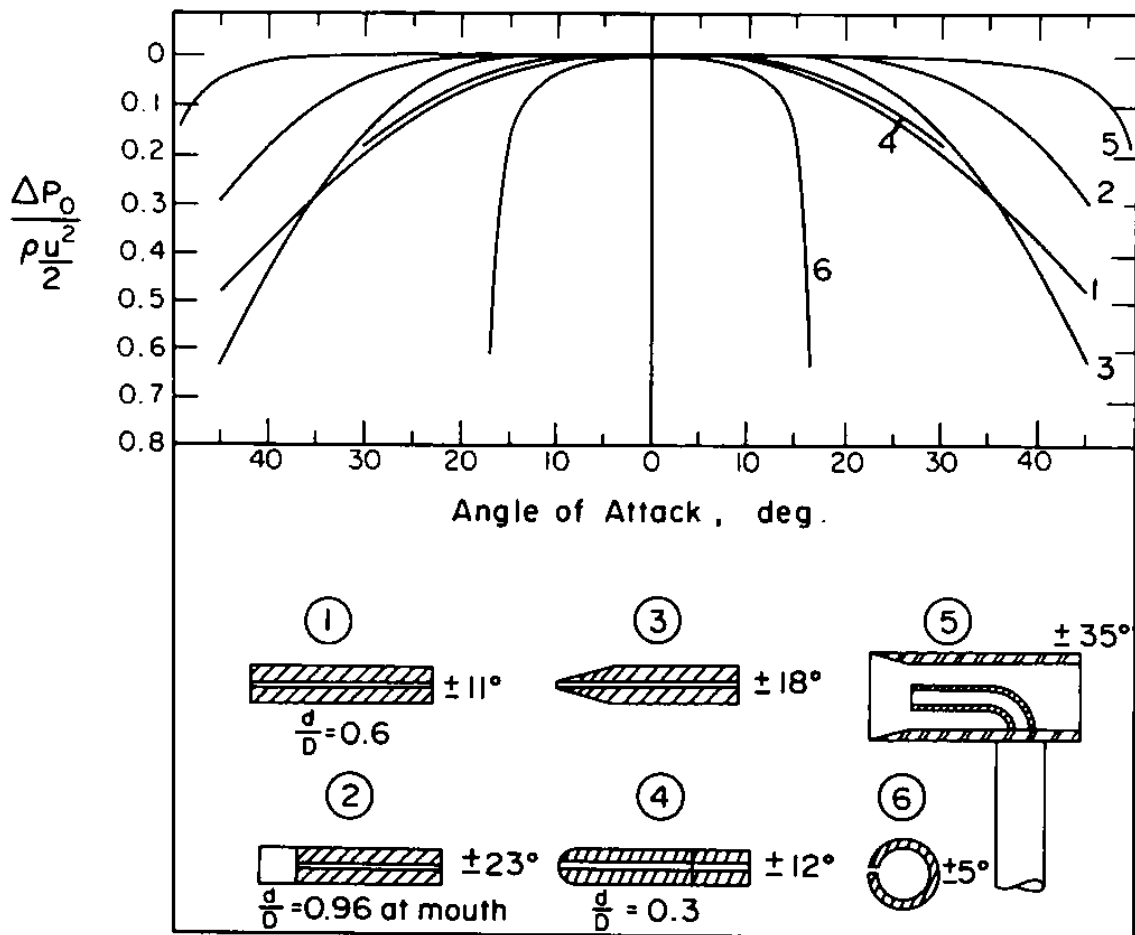


Figure 3.12 - A comparison among different Pitot probes' insensitivity ranges, Chue [3]

Anyway, it is possible to define a correlation between probe geometry (in this case the d/D ratio) and the probe errors related to flow misalignment respect to the probe axis. In facts, greater will be the Pitot intake, smaller will result the yaw-induced intake area-averaged distortion in pressure distribution. According to Chue [3], then, this

correlation may be observed in conical-shaped Pitot probes, even if there is no experimental study that may lead to this result in an unmistakable manner.

In addition, even according to Chue [3], decreasing the external probe diameter higher will be the error probe pressure reading (these two amounts are linked by a nearly proportional relationship) and a possible physical explanation deals with the additional shear stresses induced by a yawed or pitched flow direction that leads to a flow stabilization and this stabilization cannot happen if the size of the probe is excessively small.

In this way, for Pitot probes, yaw and/or pitch correction has to be performed not only taking into account geometrically-similar probes but there is the need to consider the actual diameter too.

As regards, instead, the pitch sensitivity of flattened Pitots, it is very high but it can be reduced simply producing an orthogonal flow-facing surface.

Another kind of probe studied and analysed consists of Fast Response Aerodynamic Pressure Probe (FRAPP), which is showed in *Figure 3.13* and, according to Toni et all [4], is suitable for narrow channels as their higher degree of miniaturization tends to lessen blockage effects, so their sizes do not influence a lot the stage performances.



Figure 3.13 - FRAPP probe, L. Toni et all [4]

Then, they provide a very high frequency response (100 [KHz]) about pressure, speed and, if coupled with other FRAPPs, it is possible even to accurately evaluate the turbulence level of the flow field (3D information), even if the advantage of having low encumber respect to other probes would have been reduced.

In spite of this, the high frequency response, whether useful for accurate three-dimensional turbulence determination, in the present study they have the flaw to possess a sampling frequency much higher than the one produced by turbulent phenomena (about 50 [KHz]), so their high accuracy won't be fully exploited.

Finally, just like other probes, there is the possibility to align its centerline with the incoming flow through an automatic / manual rotation but, in industrial test rigs, they

don't have practicality as they are not so robust into highly unsteady flow fields. This last flaw is just the one who did not make possible its suitability in the present study.

Hereafter, a quick description of the most commonly used probes in turbo machinery measurements will follow.

3.1.2. Kiel-head probes

As *Figure 3.14* shows, Kiel-head probe is nothing more a pitot probe which intake is shielded by a shroud and it is useful to get stagnation pressure (thanks to the pitot-derived extremity probe) and temperature (due to the presence of a J-type thermocouple with perforated half shield).

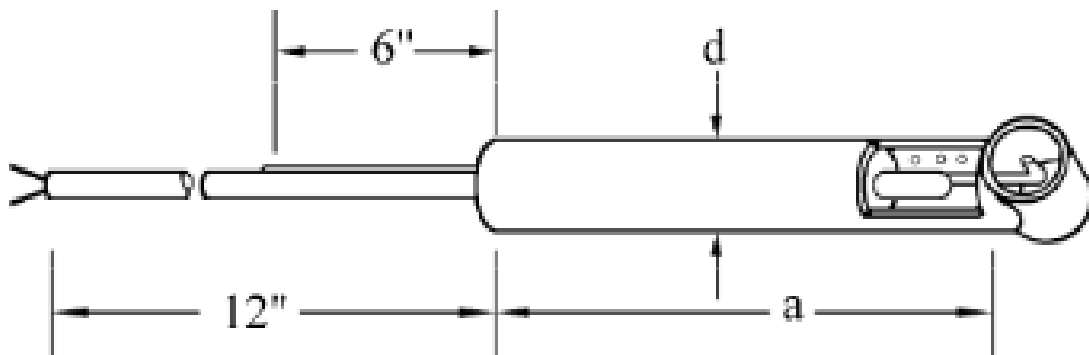
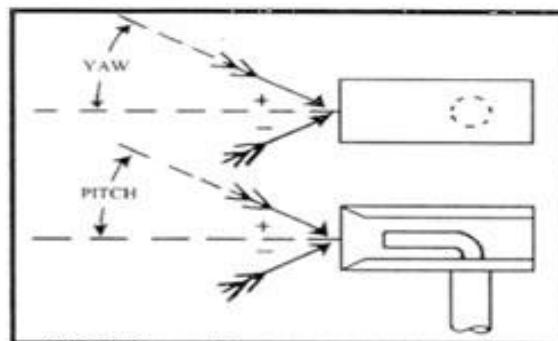


Figure 3.14 - Layout of a Kiel-head probe, source : <http://www.techmark.de>

Despite it has poor sensitivity with regards to yaw angle changes, it can be utilized if the probe axis alignment and the flow direction have a relative imprecision or incidence of almost ± 35 degrees (see *Figure 3.15*), resulting in a higher pitch/yaw applicable ranges in comparison with Pitot probes.



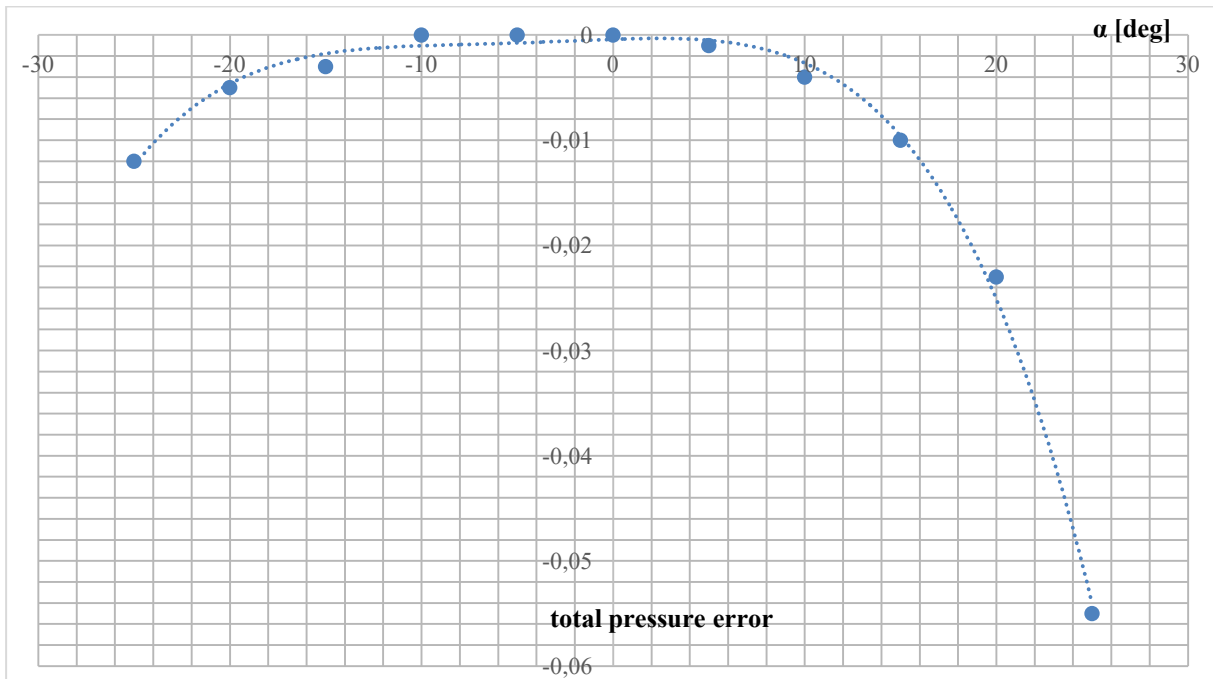


Figure 3.15 – an example of a Kiel-head probe yaw and pitch sensitivity

Being cylindrically-headed, it may be influenced by dynamic phenomena depending on the head geometry, such as inertial effects, so it must be accurately calibrated when used in highly unsteady flow fields.

Instead, as concerns the influence of this kind of probes' geometry on the reading accuracy, especially for insensitivity ranges, different producers have been consulted but, in order to have a wider vision on Kiel-heads, only the producer with the more numerous types and subtypes has been reported in *Appendix 8.1* in which, among other things, even detailed inner geometries and layouts are showed.

According to data gathered in the above-mentioned appendix, it is possible to summarize all Kiel-head geometries through the following table:

Kiel-Head probe type	sub-type	probe intake diameter [inches]	probe intake diameter [mm]	negative Yaw range [°]	positive Yaw range [°]	negative Pitch range [°]	positive Pitch range [°]	time constant [sec]
A	A	0.0625	1.59	-52	52	-40	47	36
	C	0.1250	3.18	-52	52	-40	47	36
B	A	0.0625	1.59	-48	48	-45	45	15
	C	0.1250	3.18	-48	48	-45	45	15
C	C	0.1250	3.18	-54	54	-49	49	0.6
	E	0.1875	4.76	-54	54	-49	49	0.6
	F	0.2500	6.35	-54	54	-49	49	0.6
D	C	0.1250	3.18	-54	54	-49	49	0.6
	E	0.1875	4.76	-54	54	-49	49	0.6
E	F	0.2500	6.35	-54	54	-49	49	0.6
	C	0.1250	3.18	-63	63	-58	58	0.3
	E	0.1875	4.76	-63	63	-58	58	0.3
F	F	0.2500	6.35	-63	63	-58	58	0.3
		0.2500	6.35	-67	67	-61	61	0.3
R	C	0.1250	3.18	-54	54	-49	49	0.6
	F	0.2500	6.35	-54	54	-49	49	0.6

Table 3.1 - different Kiel-head probe parameters

Here, in fact, are showed:

- type, indexed by a letter that refers to a specific inner geometry, such as the size of the clearance hole respect to the external diameter, of the inner duct geometry (if straight or converging-diverging, for example);
- sub-type, which is a letter that refers to the different diameter that two Kiel-head probes belonging to the same type may have;
- external diameter, both expressed in inches and millimeters, can be listed as a reference size of probes (not only Kiel-head ones);
- yaw and pitch insensitivity ranges, in which the amount reported refers to the critical angle (below which the read pressure is erratic less than 1% of the actual free-stream value);
- time constant, defined as the time taken by the probe to reach the inner pressure equilibrium, and so the time over which the reading can be assumed accurate. In other words, being this value related to transient phenomena (e.g. inertia of the liquid inside the attached manometer), it won't be considered as this study deals with pressure reading taken with pressure transducers at full regime.

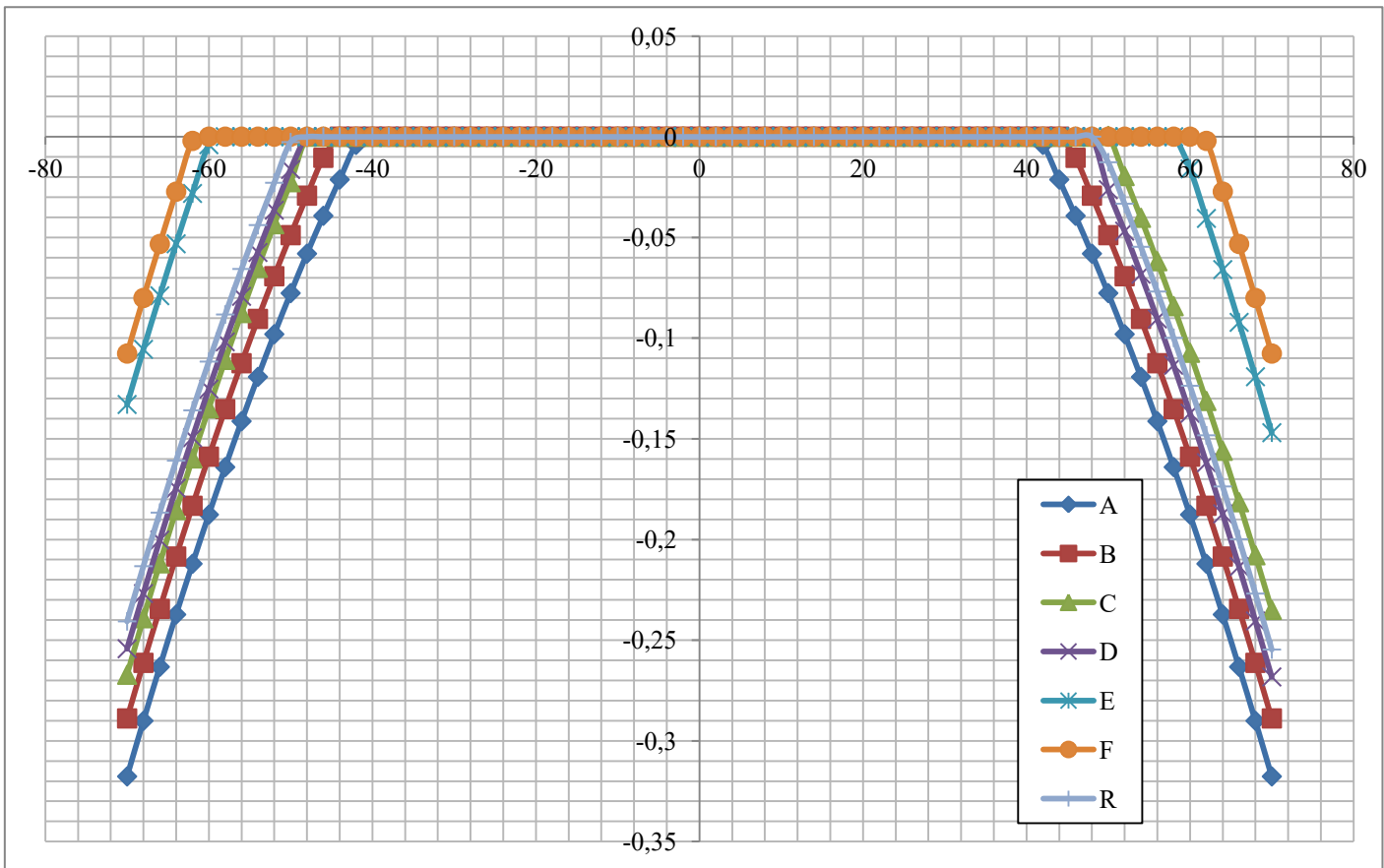


Figure 3.16 - Dependence of Kiel-head insensitivity range with varying the size (i.e. diameter) of the probe

Anyway, in the above-reported picture there are a lot of probes with different external diameters but, although useful for general vision purposes, the test rig harnessed in this research only possesses four-diameter probes, so a huge simplification can be performed of useless types with diameters too much smaller or too much higher.

In this way, neglecting the time constant, it is possible to notice that the probe insensitivity range rises with increasing the external diameter.

In addition, keeping constant all the characteristic values, the only difference between type C and D only consists of the size of the clearance hole, which is 1/2" for the former and 9/16" for the latter. So, it is possible to demonstrate that only the external diameter is important for the present purpose because the inner geometry does not affect the probe performances.

3.1.3. Multi-hole probes

This kind of probes, if used in a fixed, non-nulling configuration, and if properly installed and calibrated, feature a very accurate determination of total pressure as well as flow angle and speed.

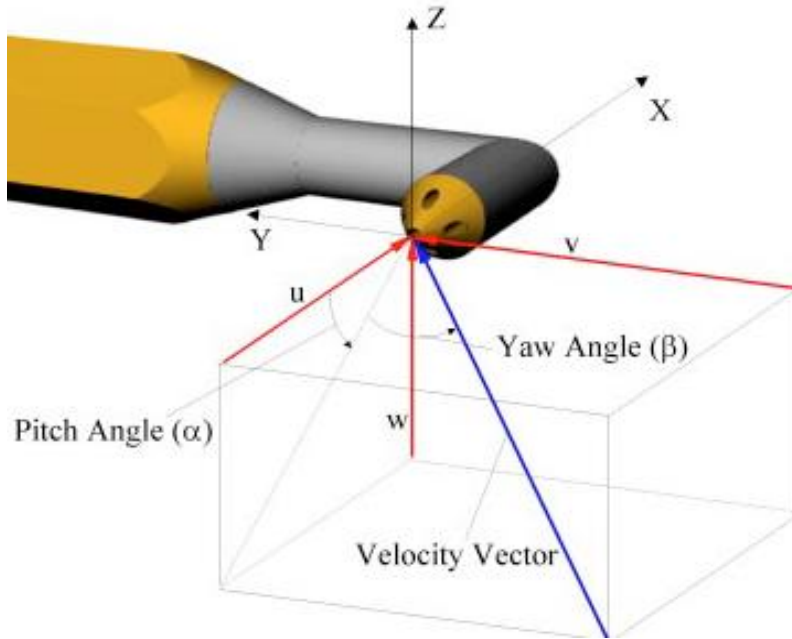


Figure 3.17 - A typical five-hole probe which reference frame suggest the use in a low angle of attack configuration, J. L. Gilarranz et all [2]

According to how greater is the angle of attack of the incoming flow, it is more convenient to use pitch (α) and yaw (β) angles referenced-frame for low angles of attack (smaller than 25 degrees) or, alternatively, cone (ϑ) and roll (φ) angles referenced-frame for higher angles due to the possibility to easily calculate the calibration coefficients in steady calibration even taking into account a possible flow separation over the conical surface.

So, according to these reference frames, it is useful to define different angle dimension-less coefficients based on pressures read by each port that will be determined during the steady calibration procedure, which is not exposed in the present work as this last features unsteady phenomena analysis.

Anyway, a comprehensive study of errors given using steady calibration probes in unsteady environment will be provided.

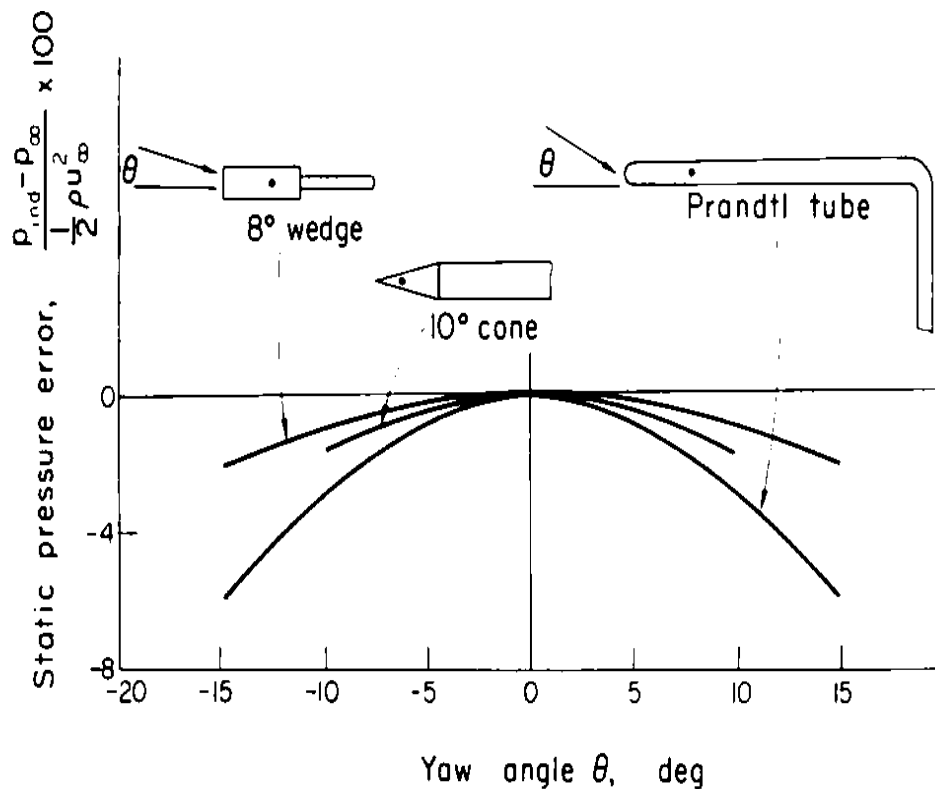


Figure 3.18 - A comparison among different probes' yaw and pitch sensitivity in which it is possible to evaluate the 10° conical shaped one, geometrically similar to multi-hole probes analysed, Chue [3]

As concerns the probes' geometry pitch and yaw sensitivity, Figure 3.18 shows a dependence on the shape of the probe nose. In this way, three different shapes have been analysed by Chue [3], and these are an 8° wedge nosed-probe, a 10° conical probe and a Prandtl tube, with the result that the best misalignment adapting geometry is just the wedge if only the direction of the flow varies on the wedge's symmetry plane. As a matter of facts, changing the plane on which the flow direction varies (in other words, letting it varying around the lateral axis), one face of the wedge is fully wet by the flow and the opposite one is fully darkened, so that turbulent phenomena and strong separation may happen with few degrees of angle of attack. These effects are not so present for conical noses, as its three dimensionality, coupled with Coanda effect, tends to increase the amount of angle of attack (in this case there is not a symmetry plane but a symmetry axis, so doesn't matter if yaw or pitch variations are considered) at which separation happens.

3.2. Flow characteristics study

As regards the influence of flow characteristics on the probe reading, considering that Reynolds number may be assumed negligible according to different authors, the only two effects that can have an appreciable influence in this case are compressibility and turbulence in the flow field.

3.2.1. Compressibility effects

Being the compressibility effect strictly linked to the Mach number, and existing the isentropic law-derived formula between Mach number and the stagnation pressure felt by a probe as a consequence of a flow isentropic freeze, it is possible to write the *equation 3.2*:

$$p^0 = p \left(1 + \frac{\gamma - 1}{2} M^2 \right)^{\frac{\gamma}{\gamma - 1}} \quad (3.2)$$

where:

p^0 is the stagnation pressure;

p is the static pressure;

γ is the specific heats ratio that, as the present study deals with air inside a compressor, is retained equal to 1.4;

M is the local Mach number.

Now, according to Chue [3] and how the *Figure 3.19* shows, as regards all Kiel-head probes there is a local speed range in which the critical angle (i.e. the angle of attack below which the probe is not sensitive to flow direction and gives a pressure read equal to the actual one) remains constant.

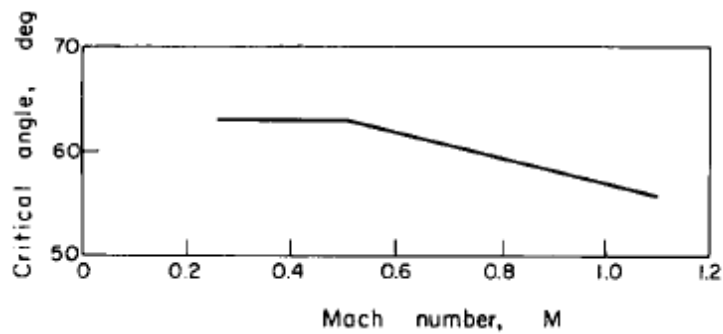


Figure 3.19 - Correlation between critical angle and local Mach number for Kiel-head probes, Chue [3]

Then, at a given Mach number, there is a tendency to decrease the critical angle with rising the local Mach number and the rate of this fall is supposed to depend on the design or the probe.

Talking about Multi-hole probes, instead, the next figure, shows that just like misalignment mistakes, static characteristics of conical or wedged probes changes due to the different designs.

According to *Figure 3.20*, in facts, the contribution of local Mach number starts to be adverted only at high subsonic speeds (about Mach 0.7), exhibiting a sudden rise in terms of static pressure captured due to the formation of local shock wave around the probe's body.

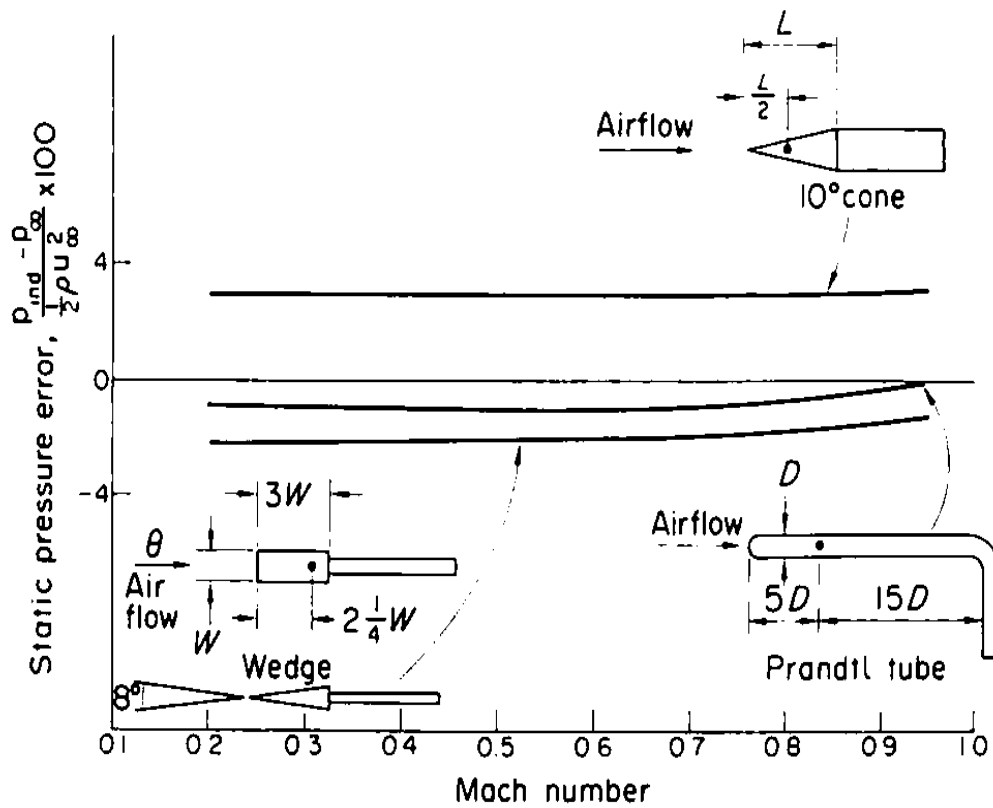


Figure 3.20 - Correlation between static pressure felt by a conical shaped probe and the local Mach number of the flow in which the probe itself is submerged in, Chue [3]

Increasing the speed, till transonic regimes, the unavoidable formation of a bow shock just ahead the probe tip (with consequently strong dissipation and high erratic amounts read) is prevented through the probe head sharpening up to a three degrees cone. This aspect, despite causes a global structural rigidity decrease for small diameters probe, is responsible of the transonic effects delay over Mach one. Furthermore, probes in transonic and supersonic speed, as reported by Chue [3], depict a correlation between the inner probe geometry (i.e. bores diameter, static orifices position along the probe axis, and so on) and the global misalignment performances of the probe.

3.2.2. Turbulence effects

A steady-calibrated probe in an unsteady and turbulent environment may result in a reading as erratic as lower is the pitch and yaw insensitivity range of the probe itself. This is due to the primary effect of turbulence, which features a time distribution of additional velocity components generated by bi-dimensional vortexes. These ones have an influence on both stagnation pressure holes, both on static orifices located all around the probe stem.

Despite less important, there is another effect of turbulent created velocity components that consists of their influence on the probe calibration.

According to different authors, there are a lot of parameters that affects the amount of turbulent phenomena which, among other things, are recognised to be the frequency and the amplitude of phenomena, the vortexes scale respect to the probe reference size (in general the external diameter) and the moving mechanism's physical amounts and phenomena, such as resonance, damping and lag (Chue [3]).

In addition, also the probe nose geometry may have a direct impact on the turbulence errors felt by the probe.

The first theoretical approach to study this kind of effects has been performed by Goldstein which, after ignoring the parameter above mentioned for a simpler study, affirmed that the stagnation pressure felt by a pitot-derived probe submerged in an incompressible flow is given by:

$$p_m = p + \frac{1}{2} \rho \bar{V}^2 \quad (3.3)$$

where p is the static pressure;

ρ is the flow density;

V is the resulting flow mean speed, better described in 3.4, that comprises both steady velocity components in the three dimensional reference frame, both turbulent ones.

$$\bar{V}^2 = q^2 + q'^2 = (u^2 + v^2 + w^2) + (\bar{u}'^2 + \bar{v}'^2 + \bar{w}'^2) \quad (3.4)$$

In general, if the probe is assumed to be aligned with the flow and the resulting flow mean speed vector does not exceed pitch and yaw critical angles, then the q' term (named total turbulent energy) can be replaced by u' (in other words, the terms v' and w' can be neglected).

As Chue [3] reported, *"For the usual turbulence intensity encountered in pipe and wind-tunnel flow, the turbulence error is small, e.g. for a turbulence intensity of 20%, which is too high for practical situations, the impact pressure reads high by only 2% if the static pressure is assumed to be correctly measured. However, for higher degrees of turbulence it is possible for turbulence errors to reach appreciable magnitude in terms of the dynamic pressure, as now the angle of attack at the probe tip may vary over such a wide range that the probe could have instead of just the turbulence error also errors due to both pitch and yaw. In this case, the error is exceedingly difficult to correct"*.

As previously written, turbulence errors can depend also by the probe tip geometry as the turbulent velocity components produce a time averaged pressure distribution. An experimental investigation about this last feature has been carried out by Walsche and Garner [5], which consisted of different kinds of probes' linear and angular oscillations during their steady calibration so that an up to 44% turbulence level could be simulated. According to their study, only if there are horizontal flow fluctuations respect to the flow direction, then the pressure read can be considered as time averaged. As a matter of facts, if this condition is not met, then the pressure value gathered is smaller than the actual time averaged one.

Other results of their study deals with the statement that in highly fluctuating flows, the probes that gather a more accurate dynamic pressure respect to the free-stream value are Kiel-head ones.

What about the possibility to use multi-hole probes, especially five hole probes, they are suitable if it is required to gather the mean flow direction, in addition to stagnation and static pressure.

Finally, they suggest the harness of more sufficient data about Reynolds numbers and oscillations physical characteristics, such as modes, frequencies and amplitudes if the aim is to perform a more comprehensive evaluation of probes' response in highly unsteady environments.

What about the current study, Reynolds number is neglected but all other aspects will be analysed in the next chapter.

Before continuing, is important to define the bi-dimensional turbulence intensity level of the flow, which layout is reported in the picture below:

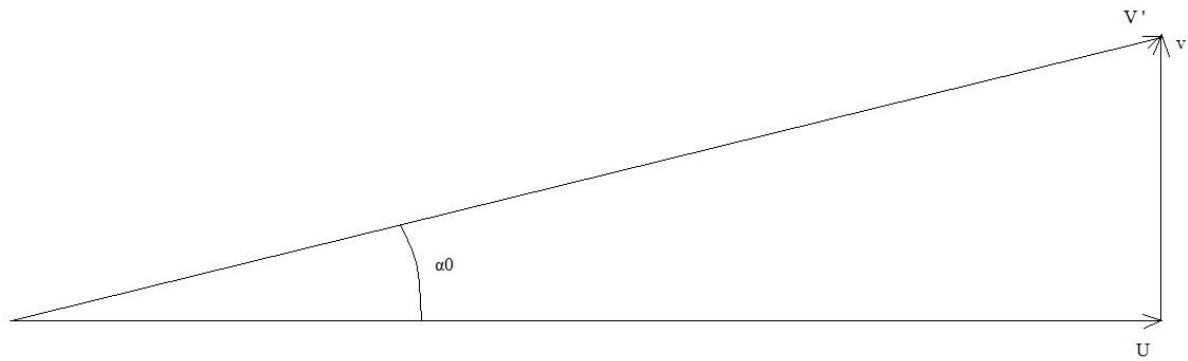


Figure 3.21 - A general speed vector composition useful to analytically threat bi-dimensional turbulence.

According to this layout, the following equations can be written:

$$i [\%] = \frac{v}{U} \quad (3.5)$$

$$\alpha_0 = \text{arctg}(i) \quad (3.6)$$

where i is the percentage turbulence intensity;

U is the free-stream flow speed;

v or w are the turbulent vortexes induced speed components on the plane orthogonal to the probe longitudinal axis;

α_0 is the actual angle of attack, also comprising the vortexes induced speed components.

So, considering the limit case of α_0 equal to the maximum positive or negative critical angle α_{cr} (below which the pressure read differs from the actual free-stream value of 1%), the equation below permits to define the limit turbulence intensity overwhelmed which the probe accuracy falls:

$$i_{lim} = \text{tg}(\alpha_{cr}) \quad (3.7)$$

At this point, to better understand the effects of turbulence on the two types of probes more suitable in this context, a separate discussion is performed for each type.

As concerns multi hole probes, a study about turbulence induced effects must start knowing their insensitivity ranges:

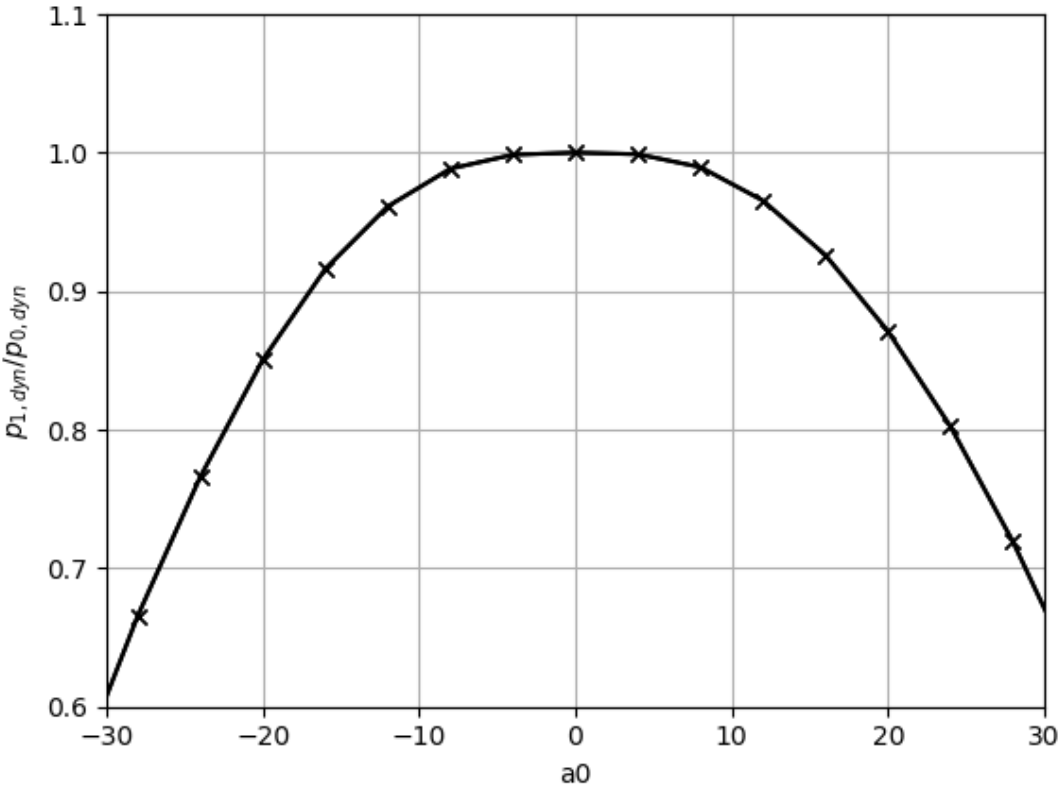


Figure 3.22 - A typical multi-hole probe pitch and yaw sensitivity curve

In this way, in the picture above, it is possible to notice that this kind of probes have a very narrow pitch / yaw range as the critical angle is greatly smaller than those ones possessed by Kiel-head, which leads to the assumption to not consider this probe in highly turbulent flows as the accuracy falls even for lower angles of attack.

In facts, Kiel-head probe is the less sensitive to turbulence induced errors as it has a wider insensitivity range both for pitch and yaw angles (see Figure 3.15). This feature is valid until the flow turbulence intensity remains under 70%, which is the limit turbulence intensity as calculated through equation 3.7 considering a medium Kiel-head critical angle of 35 [°].

To better understand the mutual influence of the flow turbulence intensity and the total pressure felt by a Kiel-head probe it is reported a picture provided by S. Bauinger et al [1]:

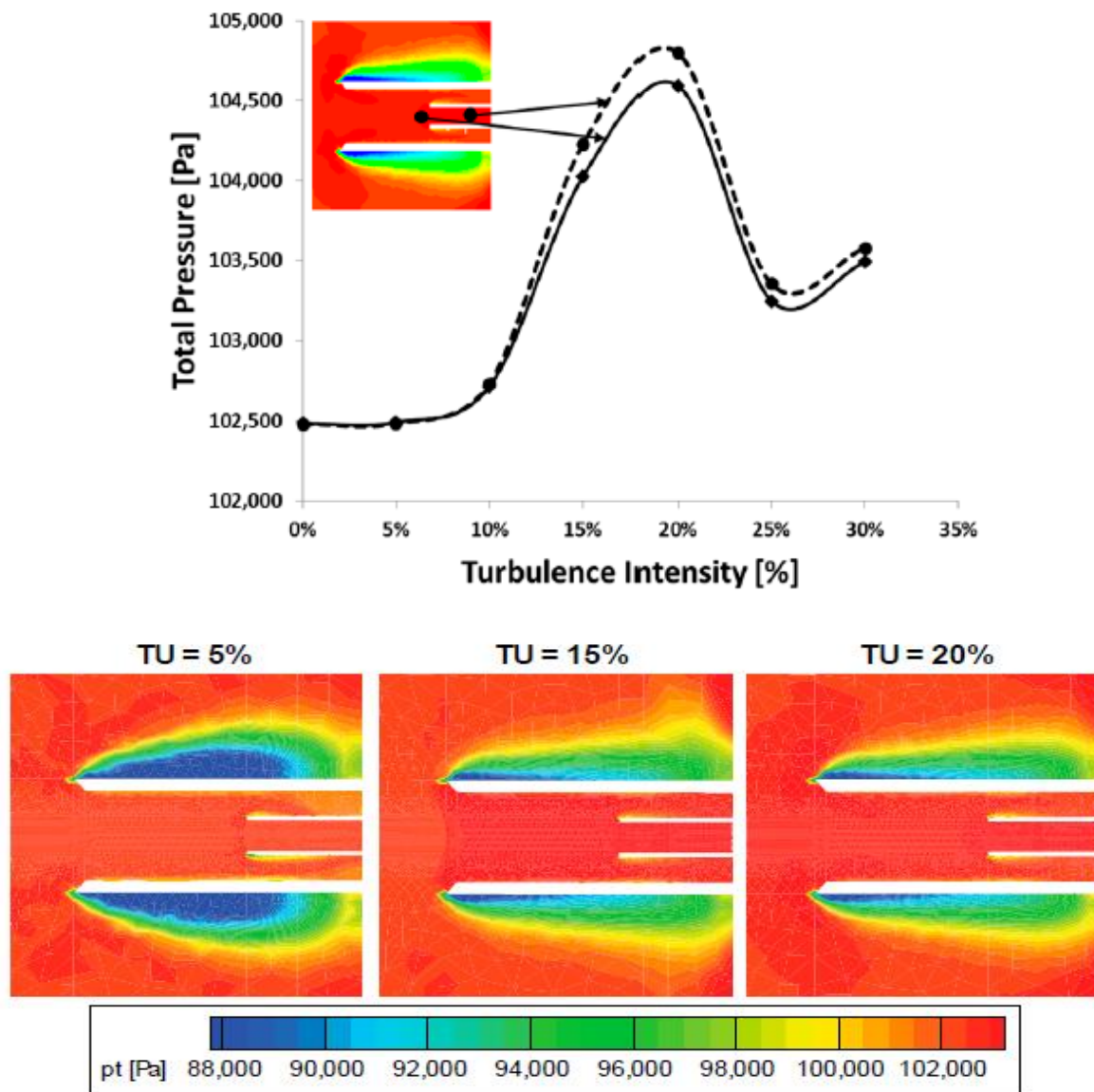


Figure 3.23 - Correlation between total pressure read by Kiel-head probe and the turbulence intensity with a CFD evaluation, S. Bauinger et al [1]

In this picture, anyway, things go differently and total pressure felt differs from the free-stream one at almost 10% of turbulence intensity. This result of course does not agree with the previously specified limit intensity but, nevertheless, here a very different turbulence model have been used.

In facts, in this picture features a three-dimensional model, so there is an additional u' turbulent speed component that tends to increase the total pressure read with increasing the turbulence intensity. In addition, in the previous study a lot of real aspects as well as phenomena have been neglected (numerical diffusivity, for

example), that's why now there is a stagnation pressure peak of 2.09 % higher than the free-stream value at a turbulence intensity where before a null variation had to be resulted.

Anyway, keeping apart these last discussions, the stagnation pressure in this graph features a peak at 17 % of intensity followed by a steep decrease that, according to the authors, is due to a possible separation. As noticeable, there are two similar trends, of which one lower and one higher. The former one is related to the sensor placed before the inner tube intake, the latter one, instead, linked to an equal pressure sensor located after the inner tube intake. About this last feature, the authors only described this trend but did not give any additional information about a possible reason.

3.2.3. Approaches on the analysis of turbulent phenomena

Turbulences are very large domain phenomena in which numerous variable are involved and the full resolution could be highly difficult even in terms of computer resources. Anyway, for very simple geometries like those ones had in probes, in general there is the necessity to use Goldstein's formulation (see *equation 3.8*):

$$p_{t,meas} = \bar{p} + p' + \frac{1}{2}\rho A_i (U^2 + u'^2 + v'^2) \quad (3.8)$$

where $p_{t,meas}$ is the pressure actually measured by the probe;

\bar{p} and p' are time-averaged pressure and fluctuating deterministic value respectively;

U is the free-stream flow speed;

u' and v' are the turbulent vortexes induced speed components;

A_i is a coefficient, determined by unsteady calibration, which takes into account the influence of the probe geometry and the scale of vortexes respect to the reference size;

Nevertheless, this kind of approach has a very strong limitation, which consists of treating the turbulence as isotropic. This feature deals with the fact that statistical properties are invariant under rotations of the reference frame. As perceivable, the imminent consequence is a huge analytical simplification but, on the other hand, there is a 2% error respect to the actual stagnation pressure value just for a 14% turbulence intensity (Chue [3]).

Otherwise, there are two more types of analysis that can be performed:

1. consider, as did by Kronauer and Grant [11], the importance of the asymmetry present in internal probe ducts and couple their inwards flows with asymmetrical fluctuations. This approach leads to the results, already known, that the amplitude of fluctuations is important, but also their frequency must be taken into account. In facts, either if the fluctuating pressure frequencies are much greater than the typical probe frequency or if the amplitude of fluctuations lies under a critical value, no error may be considered. This last error, when the previous conditions are not met, will be at maximum the 15% of the actual value.
2. suppose turbulence as a sum of gradually increasing vortexes. This interesting approach leads, instead, to the importance of considering also the turbulence

geometrical scale, in addition to its intensity, in order to take a correlation with its effects. According to Chue [3], the magnitude of error results to be the double of that one calculated by Goldstein's approach and its sign, instead, is strictly related to the vortexes' size, being positive for small scale turbulence and negative for large scale turbulence.

Other authors, such as Bradshaw and Goodman, in addition, experimentally evaluated the effects of turbulence and reported that the error is directly proportional to the ratio of probe diameter respect to the vortex's typical size.

Finally, those previous authors, considering the small errors induced by turbulence (in the order of 1 or 2%), suggested to overlook any possible correction as surely negligible.

Nevertheless, in the present study it is preferable to have a turbulence error prediction (given by polynomial functions, interpolations and other statistical tools) as, even if small, high precision is required by the project considered.

Chapter 4

4. Analysis of application

In this chapter, a detailed analysis of the fluctuation frequency with different kinds of application will be performed. In fact, as outlined in chapter one, the frequency of fluctuations depends on the application for which a rotating machine is designed. Just to make a quick comparison, wind turbines oscillations are in the order of 1[Hz], as well as common turbojets axial compressors ones are in the range of 1[KHz] to 20 [KHz] while turbochargers fluctuations happen with a frequency of the order of 100 [KHz].

These features are useful to understand because it is important to avoid that, when in service, the amplitude and frequency of rotor blades won't produce deleterious oscillations that can bring to unsteadiness amplification or cause fatigue phenomena on blades' materials.

Then, in order to provide more useful data about this concept comprehension, a table listing the most important physical characteristics for each field of application has been created and here under reported:

Type of rotating machine	blades number	rotational speed [rpm]	f [Hz]	Mach Number	γ
Wind turbine	3	10	3.14	0.10	1.40
Water turbine	22	500	1151.92	0.30	1.33
Turbojet compressor	18	15000	28274.33	0.56	1.40
Turbocharger	13	280000	381179.91	0.70	1.40

Type of rotating machine	α_0 [deg]	α_1 [deg]	α [deg]	tpd
Wind turbine	0.00	0.00	0.00	0.00
Water turbine	0.00	0.00	0.00	0.00
Turbojet compressor	00.00	40.00	40.00	-0.25
Turbocharger	00.00	35.00	35.00	-0.15

Type of rotating machine	tpd	ps [Pa]	pt - ps [Pa]	Δp_{tot} [Pa]	ρ [Kg/m ³]	Δv [m/s]
Wind turbine	0.00	101325.00	711.05	0.28	1.225	34.07
Water turbine	0.00	101325.00	6202.12	2.48	1000.00	3.52
Turbojet compressor	-0.25	101325.00	24041.82	6068.15	1.225	198.12
Turbocharger	-0.15	101325.00	39223.04	6071.48	1.225	253.06

Table 4.1 - empirical evaluation of a set of physical amounts useful to compare different applications rotating machines

where:

- the *blades number* (n_b), *rotational speed* (n) and *Mach number* (M) for each category are average values of those ones possessed by each type of rotating machine;
- the frequency is an abbreviation of the *impeller passing frequency*, defined as done in equation 4.1 as a value depending on physical characteristics of impellers and increases with increasing the number of blades;
- γ is the specific heats ratio;
- α_0 is the incidence angle set up into the rig respect the flow direction. In general, is null as the probe is usually aligned with flow direction but, in chapter five, some examples of probes not aligned will be analysed;
- α_1 is the additional incidence angle coming from fluctuations;
- α is the overall incidence angle, sum of the previously specified angles;
- tdp is the total pressure difference, better defined in equation 4.2;
- ps is the static pressure, in general took at normal conditions;
- $pt - ps$ is the difference between stagnation and static pressure, as defined in equation 4.3 through isentropic correlations;

- Δp_{tot} is the result of equation 4.4, which consists of a product of the differential pressure and the total pressure discharge, so it gives information about the actual error between the measured and the true stagnation pressure;
- ρ is the flow density;
- Δv is the velocity corresponding to the amount of differential pressure, as given by Bernoulli theorem (see equation 4.5);

Now, the equations previously mentioned will be exposed in the same chronological order they have been used:

$$f = \frac{2\pi}{60} n * n_b \quad (4.1)$$

$$tpd = \frac{p_{t_{measured}} - p_t}{p_t - p_s} \quad (4.2)$$

$$p_t - p_s = p_s \left[\left(1 + \frac{\gamma - 1}{2} M^2 \right)^{\frac{\gamma}{\gamma - 1}} - 1 \right] \quad (4.3)$$

$$\Delta p_{tot} = tpd * (p_t - p_s) \quad (4.4)$$

$$\Delta V = \sqrt{\frac{2}{\rho} \left(\frac{\Delta p_{tot}}{tpd} \right)} \quad (4.5)$$

Through these equations, then, it is possible to write the following table and graph useful to describe the trend assumed by the actual error between the measured and the true stagnation pressure with varying the turbulence intensity (i.e. the angle of attack relative to the probe axis) and the type of probe:

i [%]	α [deg]	tpd	tpd %	Δp_{tot} [Pa]	Δp_{tot} [bar]
0.00	0	0.00	-0.04	-9.62	0.00
1.75	1	0.00	-0.03	-8.37	0.00
3.49	2	0.00	-0.03	-7.62	0.00
5.24	3	0.00	-0.03	-7.59	0.00
6.99	4	0.00	-0.04	-8.51	0.00
8.75	5	0.00	-0.04	-10.67	0.00
10.51	6	0.00	-0.06	-14.39	0.00
12.28	7	0.00	-0.08	-20.05	0.00
14.05	8	0.00	-0.12	-28.05	0.00
15.84	9	0.00	-0.16	-38.83	0.00
17.63	10	0.00	-0.22	-52.89	0.00
19.44	11	0.00	-0.29	-70.75	0.00

21.26	12	0.00	-0.39	-92.98	0.00
23.09	13	0.00	-0.50	-120.19	0.00
24.93	14	-0.01	-0.64	-153.03	0.00
26.79	15	-0.01	-0.80	-192.18	0.00
28.67	16	-0.01	-0.99	-238.39	0.00
30.57	17	-0.01	-1.22	-292.41	0.00
32.49	18	-0.01	-1.48	-355.06	0.00
34.43	19	-0.02	-1.78	-427.19	0.00
36.40	20	-0.02	-2.12	-509.69	-0.01
38.39	21	-0.03	-2.51	-603.49	-0.01
40.40	22	-0.03	-2.95	-709.57	-0.01
42.45	23	-0.03	-3.45	-828.93	-0.01
44.52	24	-0.04	-4.00	-962.64	-0.01
46.63	25	-0.05	-4.62	-1111.78	-0.01
48.77	26	-0.05	-5.31	-1277.49	-0.01
50.95	27	-0.06	-6.08	-1460.95	-0.01
53.17	28	-0.07	-6.92	-1663.36	-0.02
55.43	29	-0.08	-7.84	-1885.98	-0.02
57.74	30	-0.09	-8.86	-2130.11	-0.02
60.09	31	-0.10	-9.97	-2397.08	-0.02
62.49	32	-0.11	-11.18	-2688.27	-0.03
64.94	33	-0.12	-12.50	-3005.09	-0.03
67.45	34	-0.14	-13.93	-3349.01	-0.03
70.02	35	-0.15	-15.48	-3721.52	-0.04
72.65	36	-0.17	-17.15	-4124.16	-0.04
75.36	37	-0.19	-18.96	-4558.50	-0.05
78.13	38	-0.21	-20.91	-5026.17	-0.05
80.98	39	-0.23	-23.00	-5528.82	-0.06
83.91	40	-0.25	-25.24	-6068.15	-0.06
86.93	41	-0.28	-27.64	-6645.91	-0.07
90.04	42	-0.30	-30.21	-7263.87	-0.07
93.25	43	-0.33	-32.96	-7923.85	-0.08
96.57	44	-0.36	-35.89	-8627.71	-0.09
100.00	45	-0.39	-39.00	-9377.36	-0.09

Table 4.2 - trend of the actual error between the measured and the true stagnation pressure with varying the turbulence intensity (i.e. the angle of attack relative to the probe axis) and the type of probe. In this case are reported data about a literature provided generic probe but, for the other Kiel-head and multi-hole probes, similar tables have been written.

Through this table and other ones related to five-hole probes and Kiel-head, it is possible to plot the following graph:

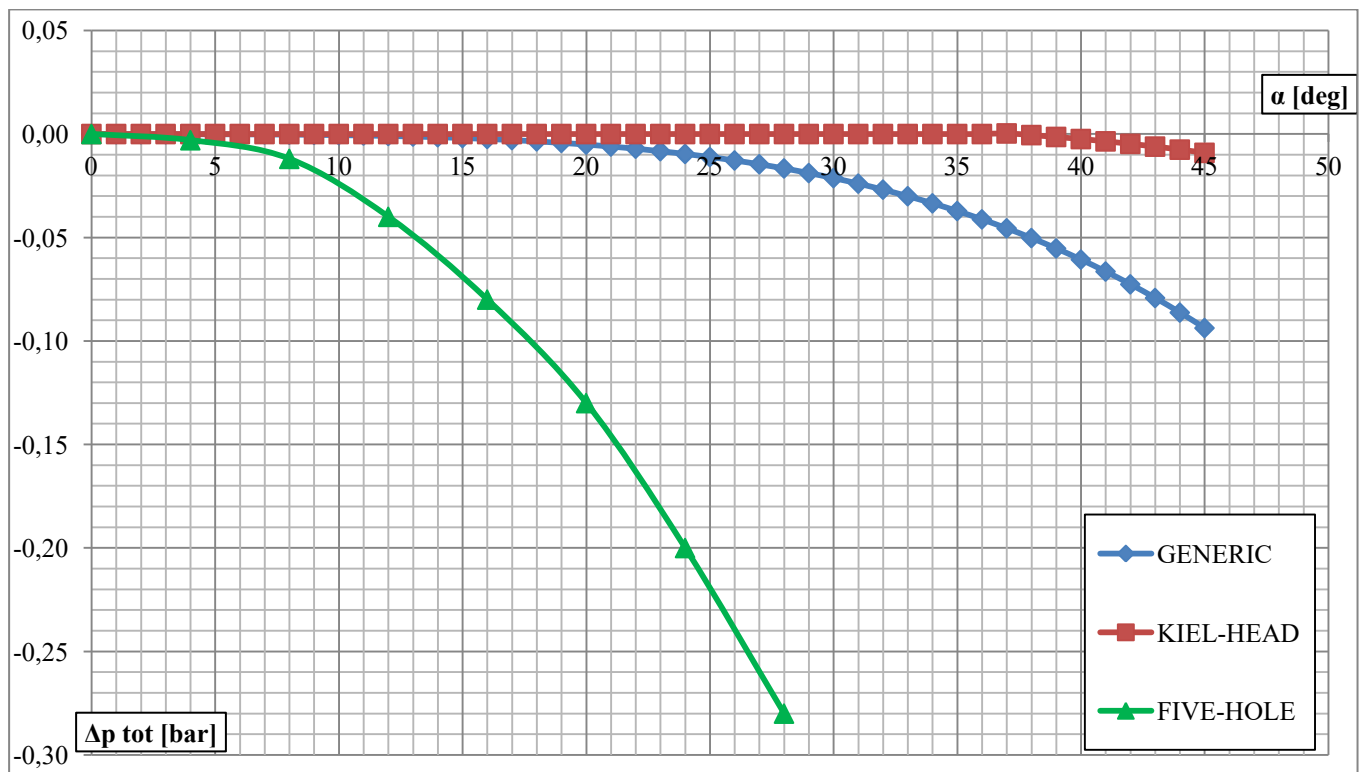


Figure 4.1 - trends of various probe types

As noticeable, the greater error in terms of pressure deviation is given by the five-hole probe instead Kiel-head errors remain negligible until a 70% of turbulence intensity is met.

4.1. Points of strong fluctuations

Unlike stator-installed probes, which may not have influenced by any pressure fluctuation due to the possibility to install rib-lets upstream the probes in order to route the flow along with the probe axis, downstream-the-rotor mounted probes are subjected to important pressure fluctuations owing to wake vortexes generated by the relative motion of rotor blades ahead the probe axis.

These fluctuations have a frequency spectrum that may be dozens time the passing frequency of a blade and, for turbo machinery applications, a feasible frequency range can space from 0 to 50 [KHz].

In general, fluctuations in turbo-machines can be subdivided into:

- periodic;
- nearly periodic;
- stochastic.

Periodic fluctuations, in general, are produced by the blades rotation. This last produces wakes downstream the rotor, inside the flow duct, at a frequency depending on the shaft's angular speed (see *equation 4.1*) and its multiples. Other factors that may cause this kind of fluctuations may be the presence of shock-waves and the interaction among secondary flow rates, which may include bleed and bypass ones, and the core primary flow.

In addition, it is possible to correlate these fluctuations to vortex shedding, which is an oscillating phenomenon that happens when a steady free-stream fluid flows over an obstacle, in this case a rotor blade or a probe cylindrical stem, with the result of creating vortex periodic oscillation in the flow downstream the rotor with a frequency, named *Strouhal* frequency, given by the following equation:

$$f_{st} = \frac{S_t * V}{D} \quad (4.6)$$

where:

- V is the flow speed;
- D is a characteristic size, equal to diameter in case of a cylindrical obstacle and, in case of a rotor blade or an airfoil, its thickness may be considered;

- St is the *Strouhal* number, a dimensionless variable that describes vortex shedding. Even if it varies with varying Reynolds number, a value of 0.2 is habitually used for frequency calculations.

As concerns nearly periodic fluctuations, these are caused by large domain unsteady phenomena, such as rotating stall as well as compressor's surge.

The last type of fluctuations listed, instead, are the most difficult to foresee and threat analytically as they are caused by phenomena such as intermittent blade flutter, boundary layer separation, unsteady transition as well as turbulence.

4.2. Amplitude and frequency assessment

It is clearly known that both amplitude and frequency of pressure fluctuations have a strong influence over the mean pressure values.

Even if periodic fluctuations frequencies are given either by a correlation among the frequency itself, the shaft speed and the number of blades (*equation 4.1*), either by the frequency of vortex shedding (*equation 4.6*), a numerical way must be used in order to determine an analytical description of stochastic fluctuations.

At the state of the art, there are three methods useful to accomplish this goal.

The first one is the Fourier Filtering consist of the subdivision of the measured value of pressure into three components, as specified through the following equation:

$$p(t) = \overline{p(t)} + \langle p(t) \rangle + p'(t). \quad (4.7)$$

As perceivable, the first term is related to the time averaged value, the second one is linked to periodic fluctuations, so it can be seen as a deterministic term, and the ultimate addend is that one that expresses stochastic fluctuations. Now, applying the Fast Fourier Transformations (FFT) over a spread number of samples so that the right resolution is met, it is possible to get the frequency spectrum, an example of which is reported in the following picture taken in the article of S. Bauinger et all [1].

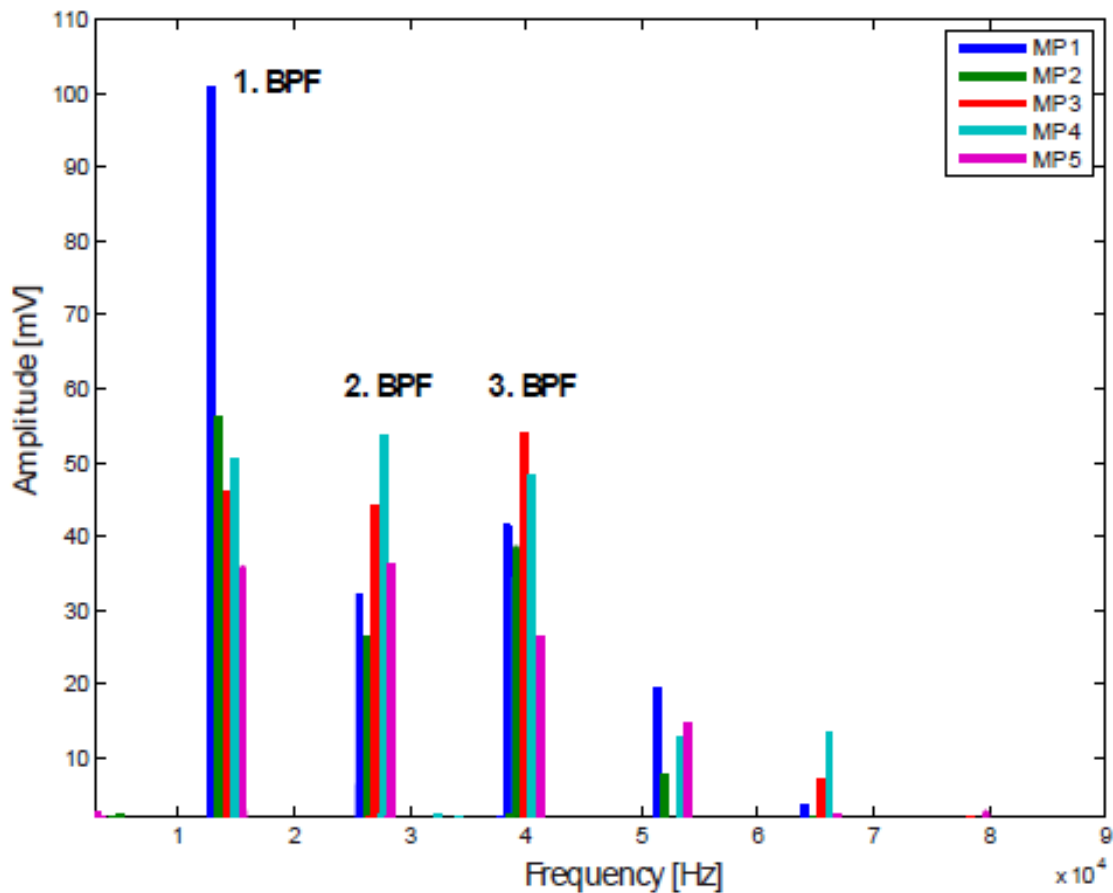


Figure 4.2 – an example of a frequency spectrum obtained by a FFT of a pressure signal containing all periodic, deterministic and stochastic parts of a fluctuating flow, S. Bauinger et al [1]

As noticeable, these kinds of spectrum contain peaks linked to each term previously discussed. As a matter of facts, there is the peak related to the time averaged values, which is placed at 0 [Hz] and it is small if compared to all other peaks, so it can be considered as negligible.

Then, there are peaks located at the blades' rotor passing frequencies (BPF) and their multiples. If these terms are set to null values, the deterministic parts of a pressure signal can be not considered so, at the end of the process, only stochastic-related terms will remain.

At this point, a time domain retransformation will follow. Notice that only the stochastic terms are available, which are just those ones to be evaluated but, as a consequence of the various peaks cancelling procedure, the turbulence intensity will result underestimated.

There are other two methods useful to evaluate the contribution of fluctuations in an unsteady pressure measurement and they consist of coefficients calculation which both at numerator and denominator terms are taken in a reference plane as that ones downstream the rotor.

The first coefficient is the *total pressure coefficient*:

$$C_{pt} = \frac{p_t - \overline{p_{t,ref}}}{\overline{p_{t,ref}} - \overline{p_{ref}}} \quad (4.8)$$

And the second one is called *percentage fluctuation*:

$$PF = \frac{p_{t,RMS}}{\overline{p_{t,ref}}} \cdot 100 \quad (4.9)$$

where:

- p_t is the local total pressure, actually measured by the pneumatic probe;
- $\overline{p_{t,ref}}$ is the mass averaged total pressure;
- $\overline{p_{ref}}$ is the area averaged static pressure;
- $p_{t,RMS}$ is the root mean square total pressure;

These procedures previously exposed deal with experimental methods but, in the past, different authors such as Bennett (1976) and Goldstein (1965) studied theoretical formulations about stochastic fluctuations and tried to write an analytical correlation dealing with the influence of bi-dimensional stochastic fluctuations on the total pressure read by the probe.

Of course, due to the huge analytical difficulties encountered, a lot of simplification have been done, like to consider the fluctuation bi-dimensionality (so the third dimension has been defined as negligible), or to consider only isotropic turbulence, which means that the fluctuating speed components do not vary with rotating the coordinate axes.

These approximations brought the previously discussed authors to write the already encountered analytical correlation dealing with stochastic term factorization:

$$p_{t,meas} = \bar{p} + p' + \frac{1}{2}\rho A_i (U^2 + u'^2 + v'^2) \quad (4.10)$$

where $p_{t,meas}$ is the pressure actually measured by the probe;

p and p' are time-averaged pressure and fluctuating deterministic value respectively;

U is the free-stream flow speed;

u' and v' are the turbulent vortexes induced speed components;

A_i is a coefficient, determined by unsteady calibration, which takes into account the influence of the probe geometry and the scale of vortexes respect to the reference size.

Other authors like J. Xin et all [9] instead, numerically investigated the contribution that different radial inlet geometries may have on the aerodynamic load felt by the impeller, as well as the frequency and amplitude of this response, working with unsteady conditions. Keeping the impeller radius almost constant, the variation in impeller geometries just dealt with the guide vanes disposition.

As a matter of facts, three layouts have been considered:

- OGV, that means radial inlet without guide vanes;
- EGV, referring to radial inlet with evenly deployed guide vanes;

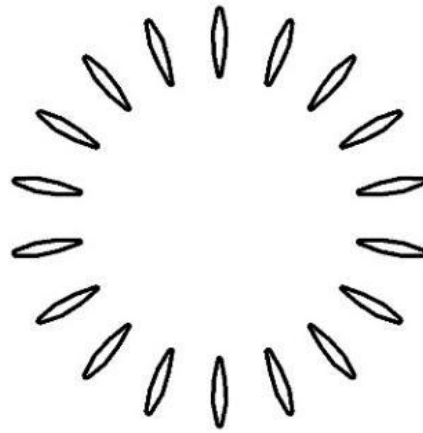


Figure 4.3 – layout of evenly deployed guide vanes, J. Xin et all [9]

- UGV, linked to radial inlet with unevenly deployed guide vanes.

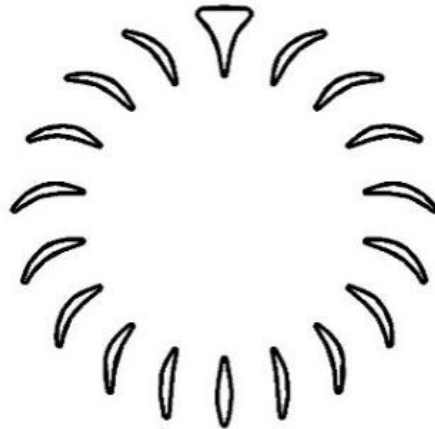


Figure 4.4 – layout of unevenly deployed guide vanes, J. Xin et al [9]

The results they provided show, through computational fluid dynamics (CFD), that the presence of guide vanes will reduce considerably the aerodynamic load and the vorticity on the radial impeller leading edge. Of course, since the probes in this research are placed downstream the rotor (called impeller in radial compressors), one may erroneously conclude that the above mentioned paper is not suitable in this case but, considering that the blade rotation will provide unsteadiness on the blade passing flow field, the mitigation of vortexes contained at the leading edge impacting flow will surely reduce the unsteadiness downstream the blades' trailing edge.

For that reason, it is important to appreciate that guide vanes may lead to a flow vorticity reduction, which is related to a better compressor polytropic performance and a higher exiting pressure but they also feature higher pressure losses. So, being these lasts related to the number of vanes, it is important to install the optimal vanes number so that benefits brought are greater than flaws.

The previously discussed author, furthermore, showed very interesting correlations between the type of vanes deployment and the consequent aerodynamic loads frequency spectra, gained thanks to the Fast Fourier Transformation and reported in the following image:

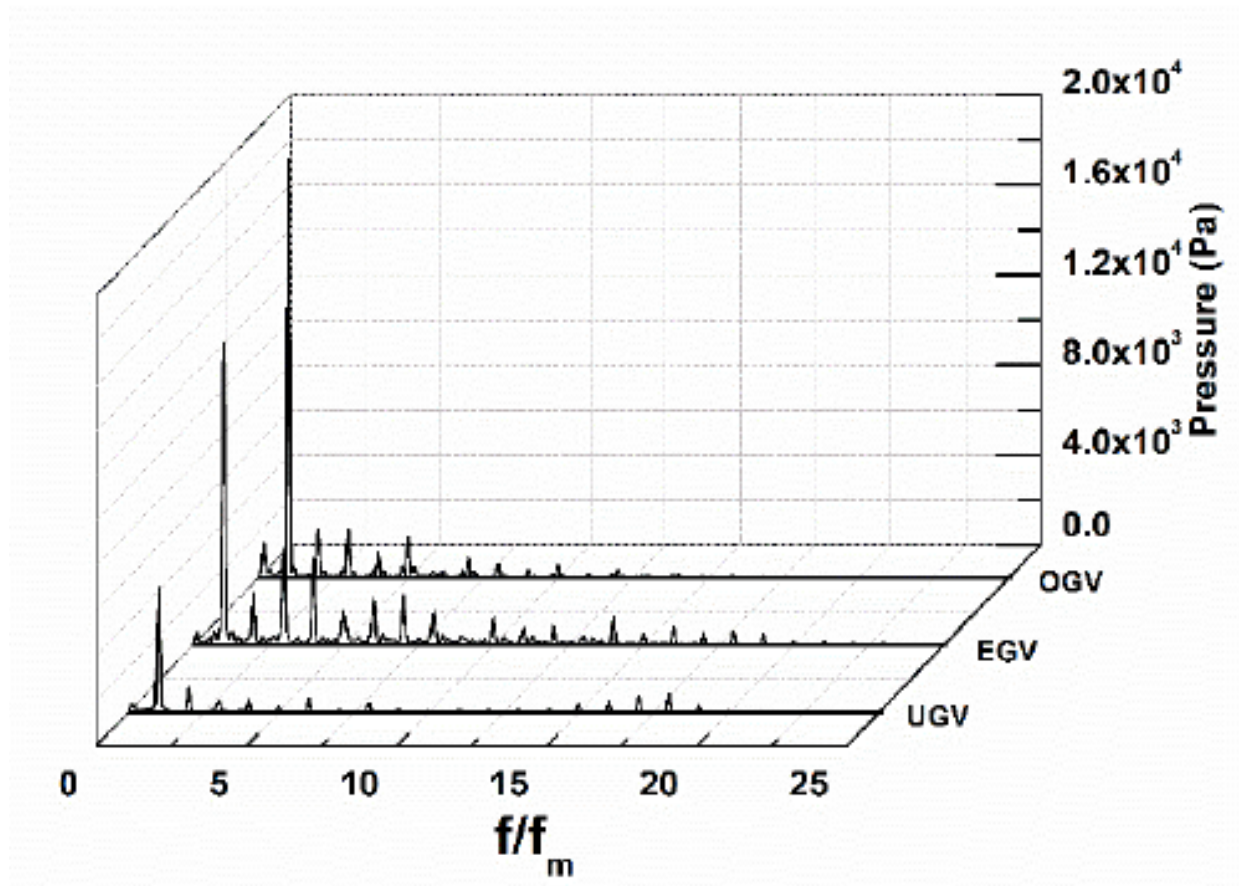


Figure 4.5 – frequency spectra with different guide vanes deployment, J. Xin et al [9]

It is possible to see that the abscissa axis features the frequency domain normalized respect to the machine passing frequency (f_m), which value is dependent on the compressor rotating speed n , as given by equation 4.11.

$$f_m = n/60 \quad (4.11)$$

As noticeable, all the impellers feature peaks of leading edge aerodynamic loads that appear both at this frequency itself, value for which the load amplitude amounts its higher value, both at its multiples.

Multiplying the machine passing frequency for the number of vanes, the results is called impeller passing frequency and, in the paper mentioned, the passing frequencies ratio amounts to eighteen as this is just the number of vanes.

In the end, as previously discussed, the vane-less configuration results in higher load peaks amplitude and the authors state that the reason is due to non-uniformities of flow characteristics distribution both in the tangential and radial directions.

Then, considerably high differences were found between even and uneven configurations. As a matter of facts, even distribution leads to a flow distribution among the different vanes and, even if this distribution is not uniform, contributes to the load peaks amplitude reduction.

Further amplitude mitigation is reached if the flow is uniformly subdivided among the different vanes with other expedients such as uneven guides (see *Figure 4.4*).

Chapter 5

5. Experimental study of reduced model

The aim of the present and the next chapter is to provide, through the analysis of data provided me by my academic supervisors, a comparison of different probes which benefits and flaws were already discussed in the third chapter and for which a variation of the probe setting angle (here called α_0) may have be foreseen.

As a matter of facts, probes here analysed are:

- Five holes probe;
- Kiel-head probe;
- Kiel-head closed probe, which consists of a modification, carried out by a LMFA researcher, in which a metal wall is welded to the downstream facing probe head, and two holes are performed on the lateral, cylindrical face so that the probe chocking is avoided;
- Cylindrical probe, which deals with a cylindrical 4 [mm] diameter stem placed orthogonally the flow direction on which surface is carried out a 1[mm] hole just at 5 [mm] of the submerged stem edge.

All these probes have been tested by LMFA staff on the ECL-B3 reduced model (see chapter two), which is a scaled reconstruction of a real compressor stage on which the suitable probes coming out of this study will be installed and it is used both to get flow-field data for the real probe encumber analysis, both to validate theoretical concepts exposed in the previous chapters.

In facts, the main purpose of this test rig is to get sufficient data about the probe measurement errors and then, after choosing the most appropriate probe among those ones listed and tested, to help the flow mechanic to get the most accurate numerical method so as to foresee the probe behaviour when it will be placed in a real compressor stage. This is done, of course, in order to save resources in terms of compressor developing time and costs and, by varying numerical (i.e. grid meshing) and flow field properties such as Reynolds, Mach Number, etcetera, to adapt the

resulting model to the next designed compressor stages and newer compressor versions.

After that, the main attention may be focused on each probe, for which an already existent FHP analysis *Python* script have been adapted by the undersigned so that each probe could be studied by using the same approach taken by LMFA researchers.

As it will be noticed, two different Mach number analysis have been carried out in order to get a prediction of the influence of flow compressibility and, even for each probe, a setting angle variation mechanism have been adopted also in order to align the probe centre line with the flow direction. An evidence of the harness of this mechanism itself will be provided and a comparison with the blocked stems probes' data will be done.

As concerns the first cases, a cylindrical probe submerged in a Mach 0.5 flow field is now analysed, keeping the following plot:

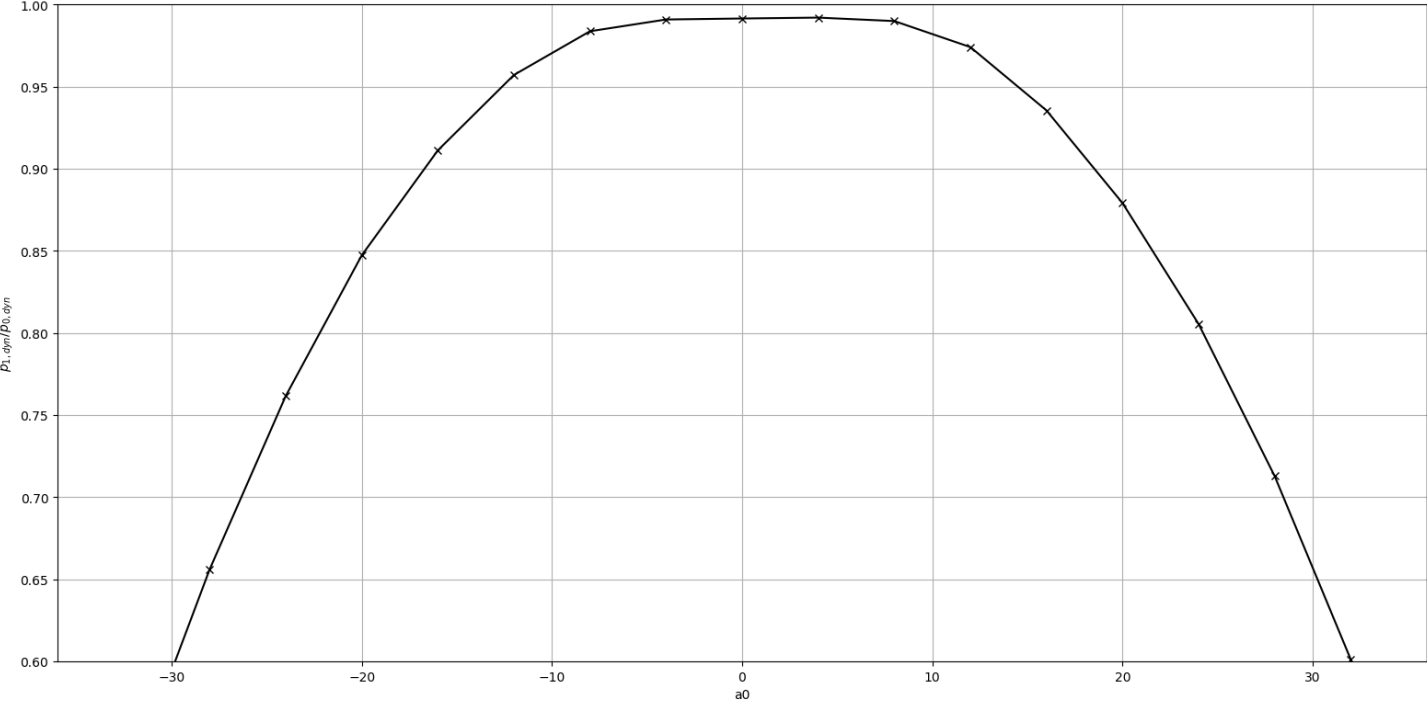


Figure 5.1 – Cylindrical static probe, Mach 0.5

In this plot, among other things, can be seen that the geometrical simplicity of cylindrical probe in comparison with the other ones tested has its drawbacks as the yaw critical angle is the narrower.

Then, this plot and the other ones that will be provided, unless differently specified, feature the yaw angle on the x-axis and total pressure ratio on the y-axis.

For a better plot comprehension, it is important to define the total pressure ratio which, among other things, is the value included both inside the Python files and the matrix "data_matrix" inside the *Matlab* script (see *Appendix 8.2*) :

$$TPR = \frac{p_{felt}^0}{p_{\infty}^0} \quad (5.1)$$

where:

p_{felt}^0 is the total pressure felt by the probe, and

p_{∞}^0 is the real, free stream total pressure.

Of course, if the probe operates within the critical yaw angles, the total pressure ratio will be constant at unitary value as the probe error due to misalignments effects is null. Otherwise, once the yaw angle overtakes the critical value, this ratio will decrease with increasing the real-to-critical yaw angle difference, as noticeable in all the plots provided.

The next picture is about the comparison of the same probe with the dynamic yaw varying mechanism activated:

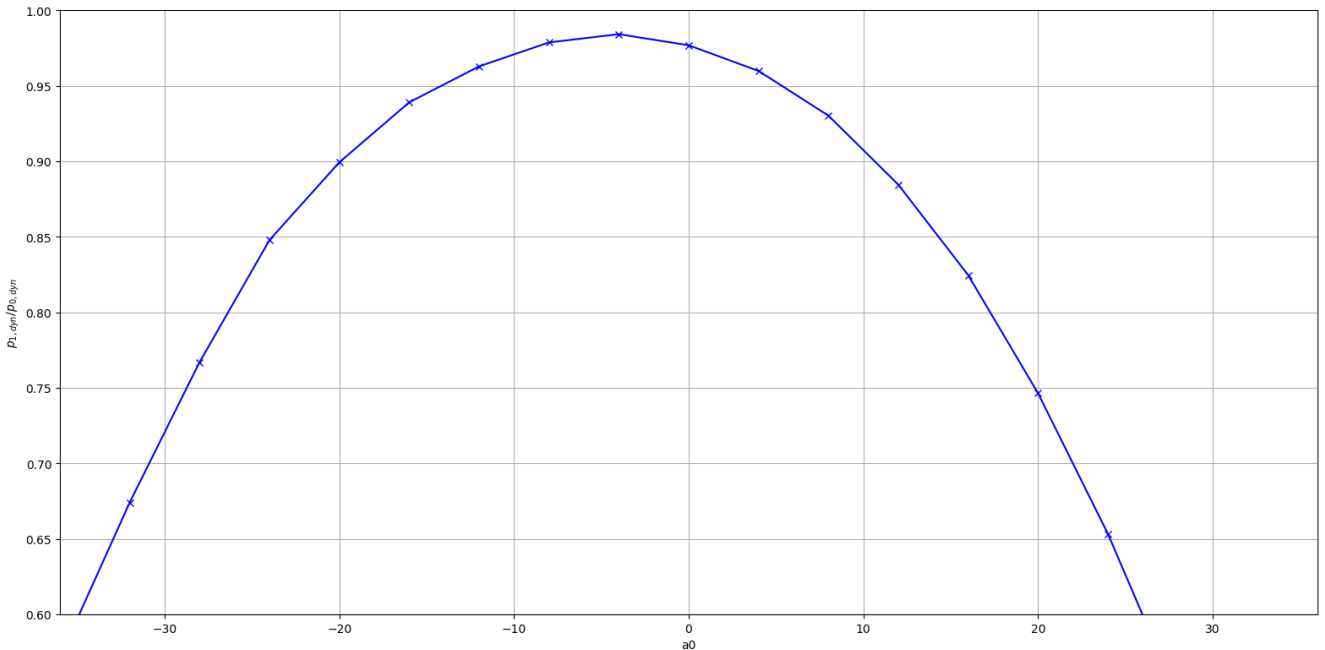


Figure 5.2 – Cylindrical dynamic probe, Mach 0.5

As noticeable, the epithet *dynamic* refers to the yaw varying mechanism activation ("Dremel" activation). In addition, if considering the position of the top of the curve, this graph shows a tendency to a left shifting if compared with inactivated mechanism case.

This feature is related to the test measurement errors and can be cancelled by simply rotating the probe stem axis of an angle read in the same graph reported in Figure 5.2, that is considering an additional yaw angle which is useful to move the represented curve so that the top of the curve will lay on the null yaw angle position. This procedure is carried out only in this case as other types of probes studied have been tested with null or negligible test-related errors.

After this last correction is performed, a comparison of these two cases - static and dynamic cylindrical probe- can be done, reporting the following graph:

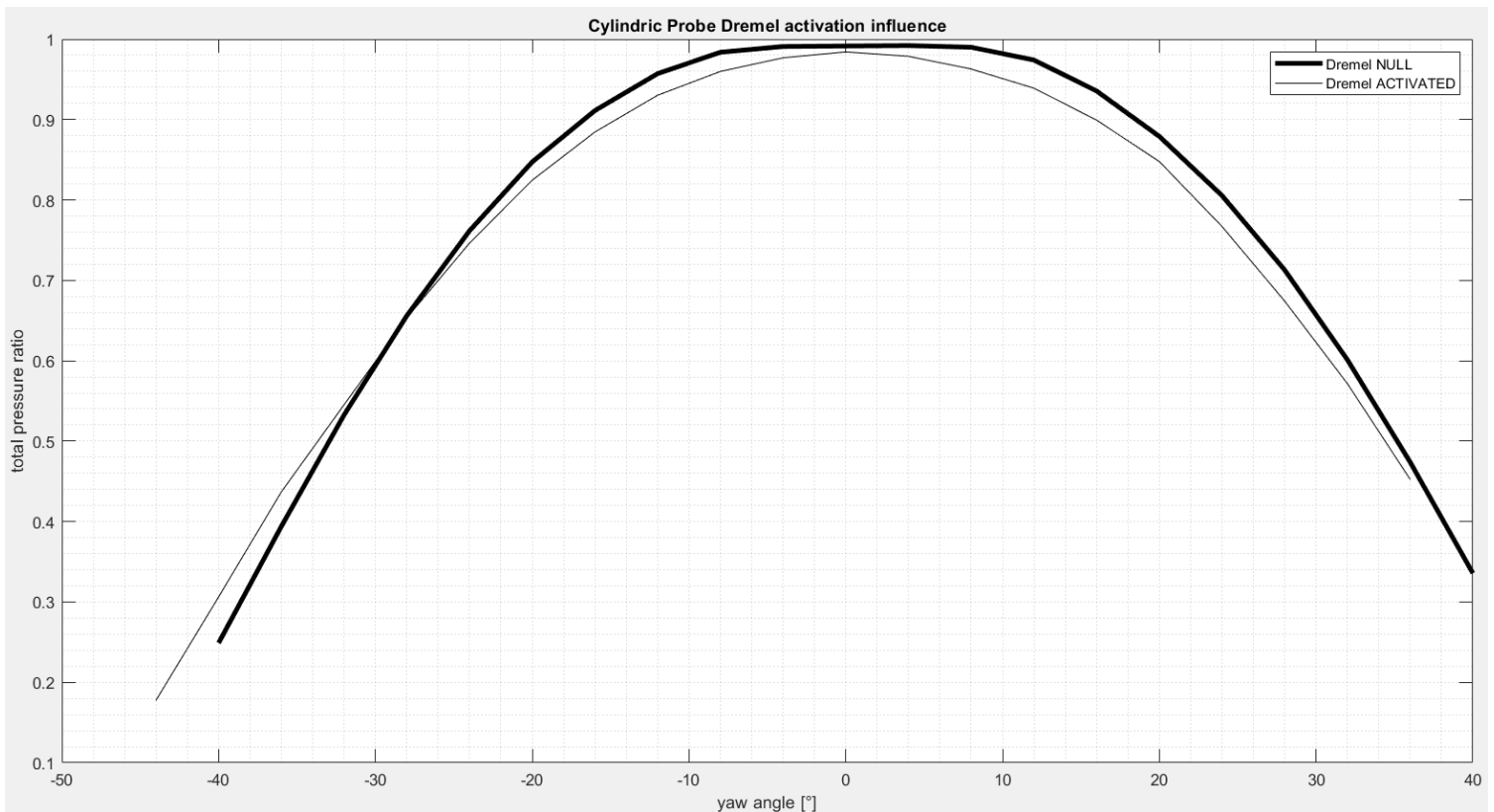


Figure 5.3 – Cylindrical probe comparison, static and dynamic cases, Mach 0.5

Another comparison that can be done deals with compressibility dependence, which consists of considering two different probe measurement data set, the former one linked to Mach 0.5 case, the latter one related to Mach 0.8 case, gathering the following plot:

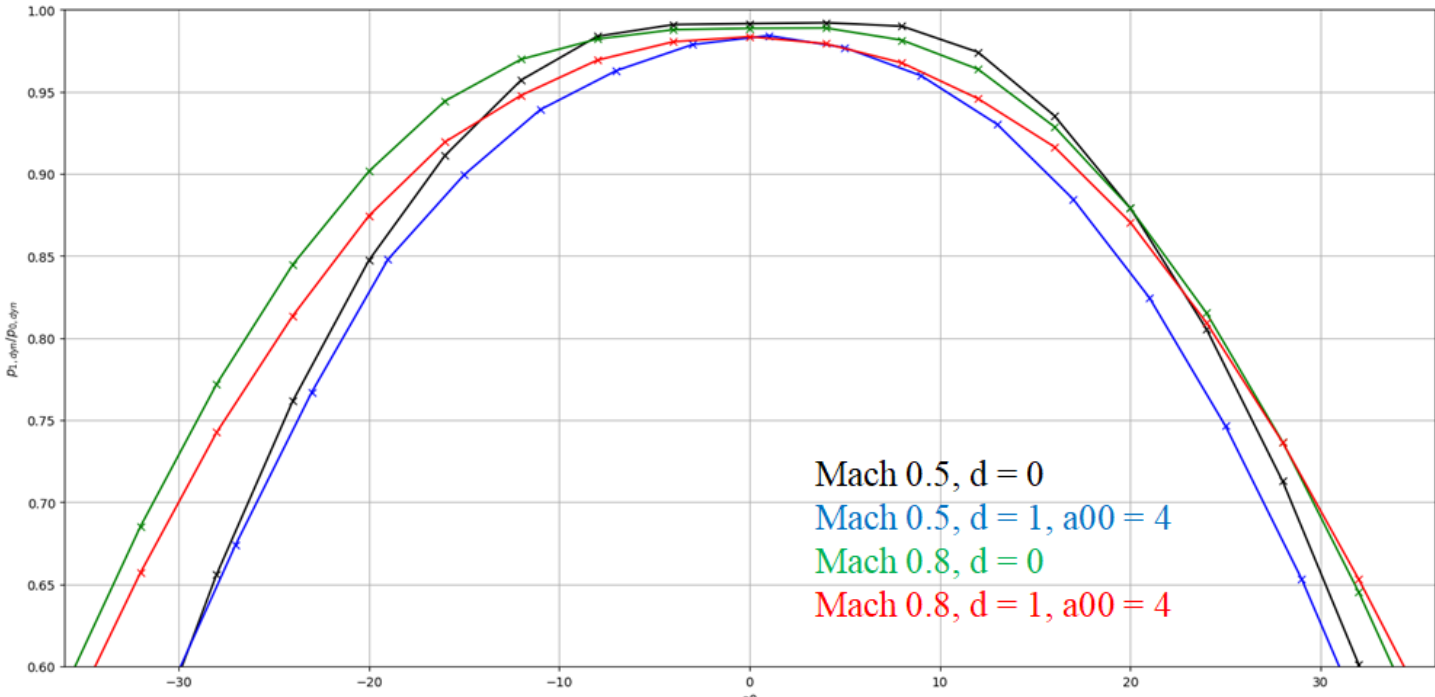


Figure 5.4 – Cylindrical probe, Mach dependence

Through this graph it is possible to notice that, despite the right sides of the curves seem not to be highly sensitive to compressibility and mechanism activation, the left sides show a tendency to spread with increasing Mach number, with a resulting few degrees negative critical angle decrease (increases the modulus).

The same analysis previously performed are reported here under for the other probes' types, such as Kiel-head, Kiel-head blocked and Five Holes Probe respectively, for which almost the same report can be written.

The only difference lays on the Kiel-head and Five Holes Probe Mach dependence, as the curves' tendency to spread with increasing Mach number is symmetrical, unlike the other two probes.

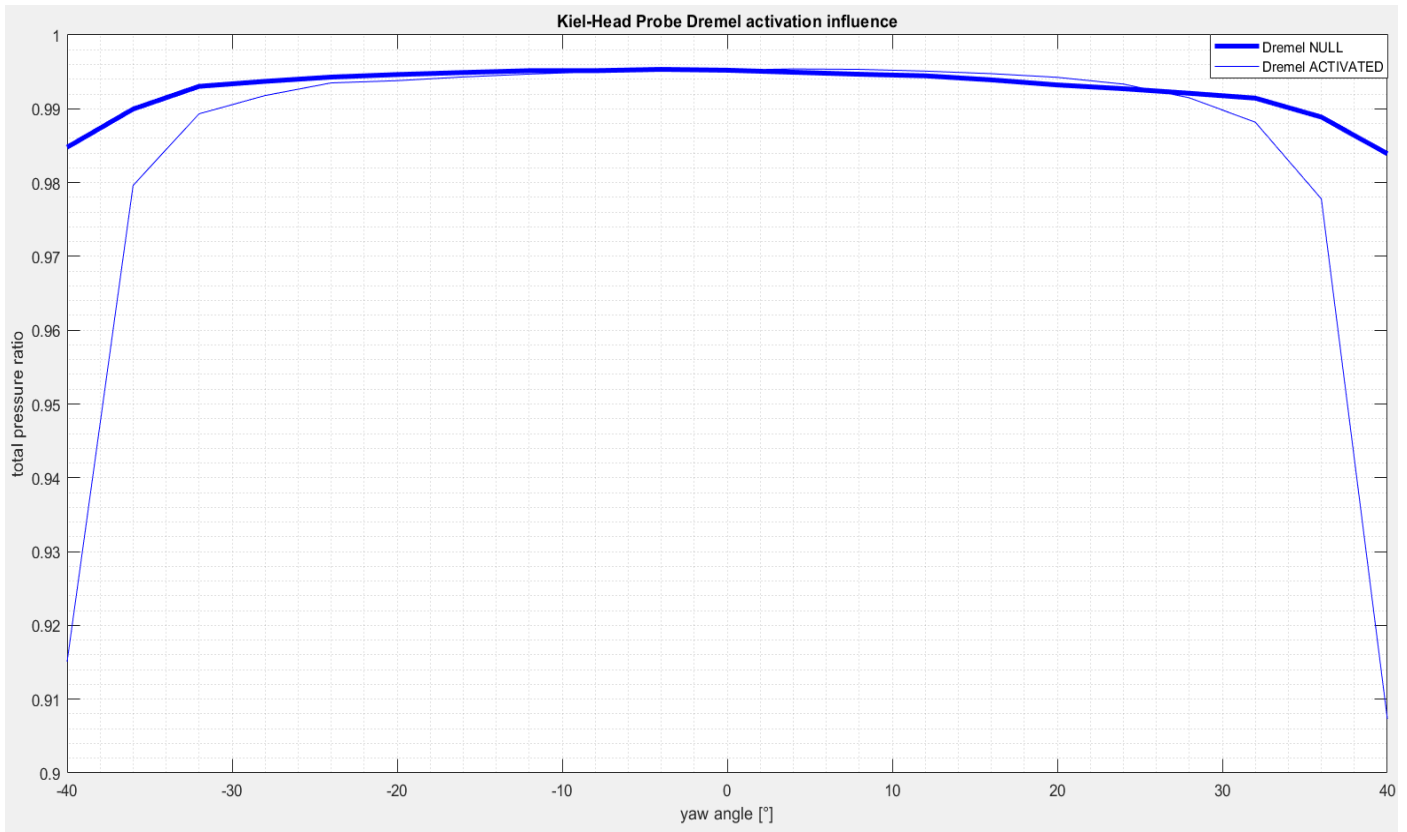


Figure 5.5 – Kiel-head probe comparison, static and dynamic cases, Mach 0.5

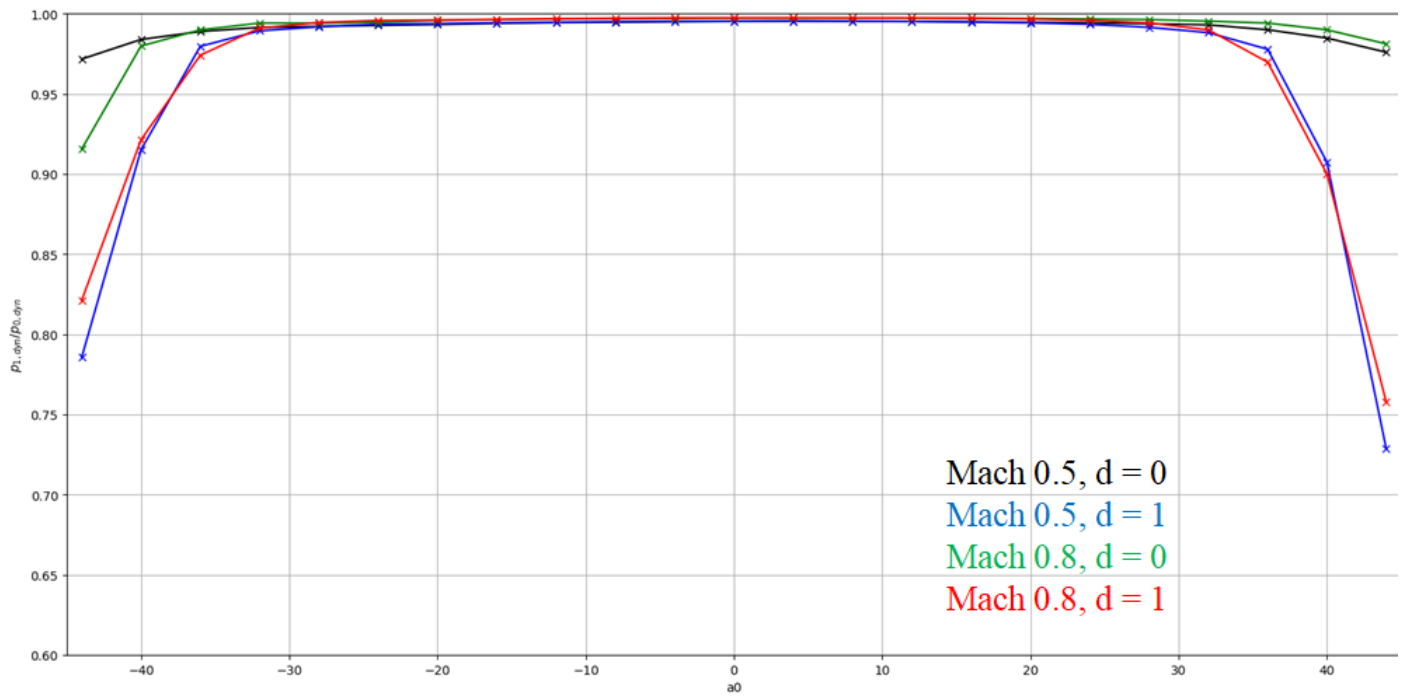


Figure 5.6 – Kiel-head probe, Mach dependence

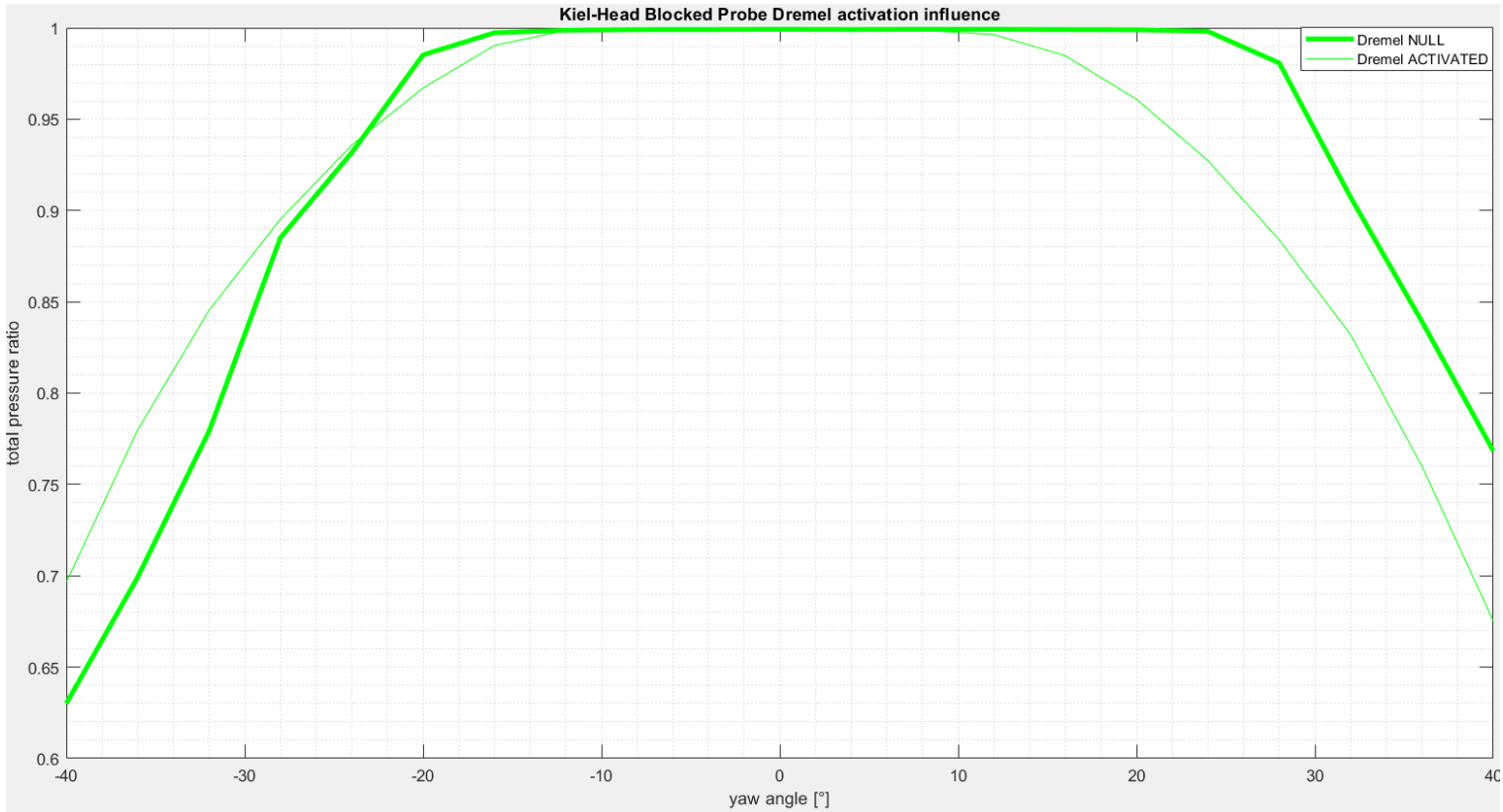


Figure 5.7 – Kiel-head blocked probe comparison, static and dynamic cases, Mach 0.5

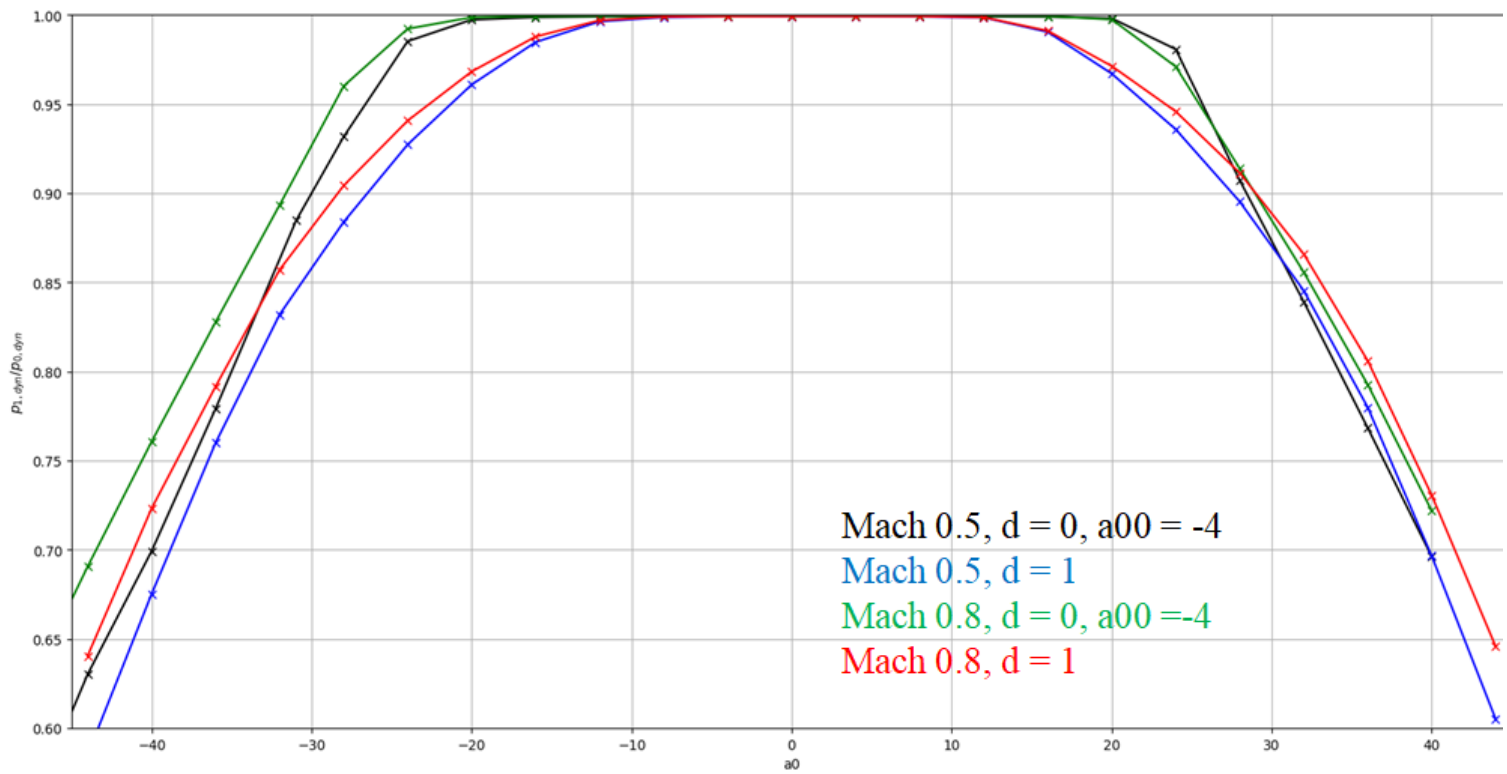


Figure 5.8 – Kiel-head blocked probe, Mach dependence

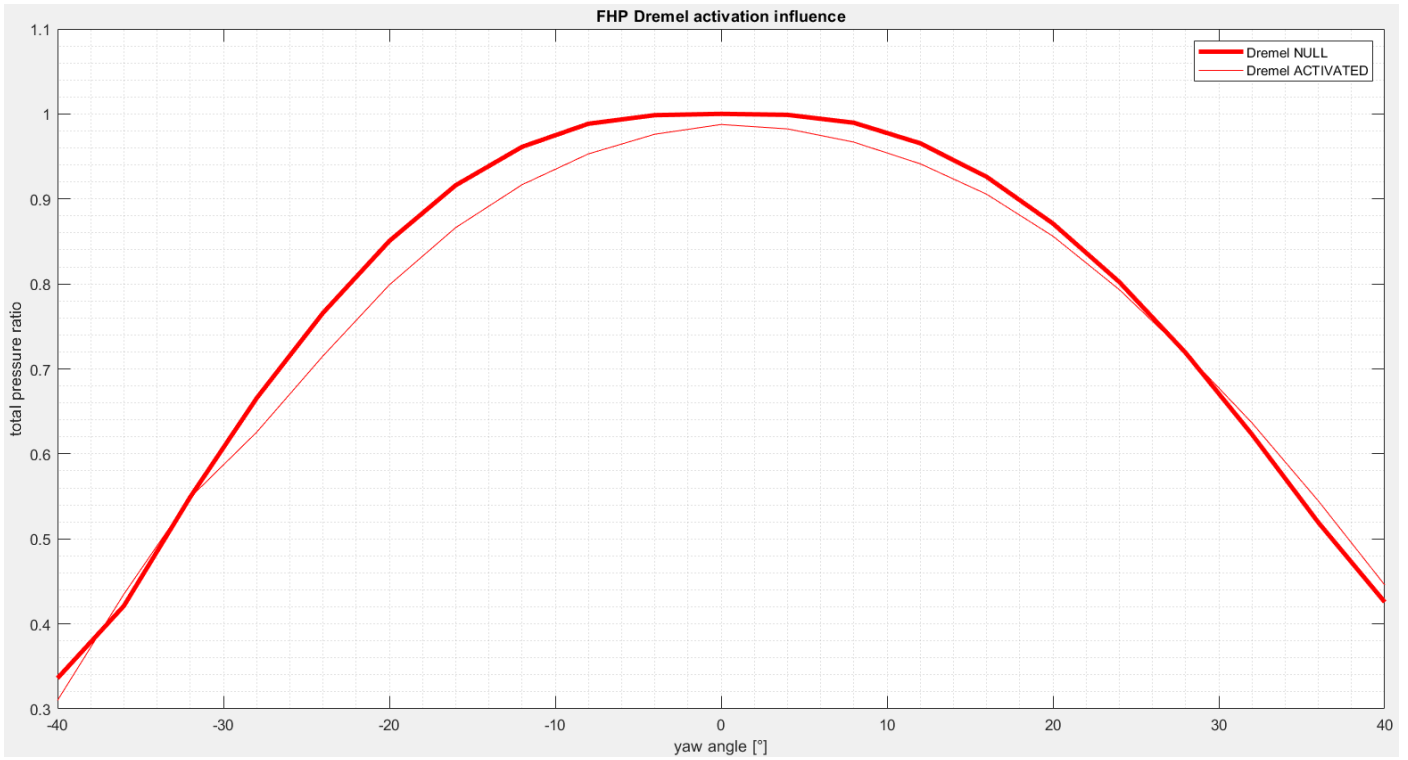


Figure 5.9 – FHP comparison, static and dynamic cases, Mach 0.5

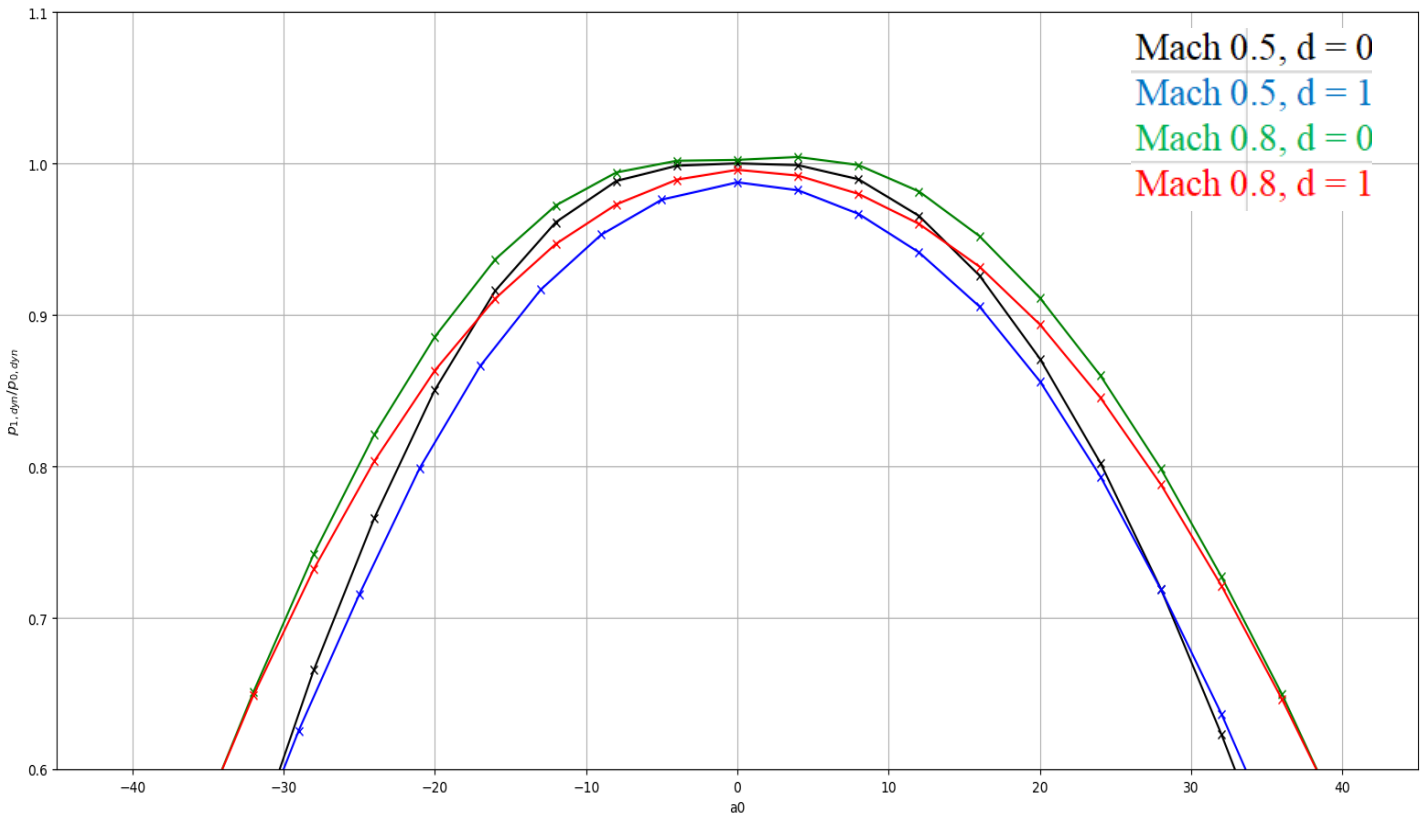


Figure 5.10 – FHP, Mach dependence

Chapter 6

6. Probes cross evaluation

Data analysed in the previous chapter are very important as they provided that, confirming theoretical predictions, Kiel head probes are the most suitable for the highly turbulent unsteady environment.

Final results aside, once gained data for all the probes separately, it is important to interpolate the discrete data set in order to get a polynomial expression of an appropriate degree useful both to extrapolate unavailable data, missing for any reason, both for getting an analytical expression employable to introduce corrective factors that will be used to fix the probe misalignment-induced errors and obtain an accurate pressure read even with highly turbulent flows.

The first step to follow is to interpolate the different probe data, of which the plots reported in the previous chapter constitute an integrated part of the data set under examination.

From now on, a *Matlab* script (fully reported in *Appendix 8.2*) will be used so that different data analysis-related functions will be used, such as *polyfit* and *polyval*, using a sixth degree polynomial function. This choice may seem wrong as to univocally define a data set composed of n elements, a $n-1$ function degree is needed but, if plotted, this data distribution retraces just a sixth degree function.

The result of this process is showed in *Figure 6.1*.

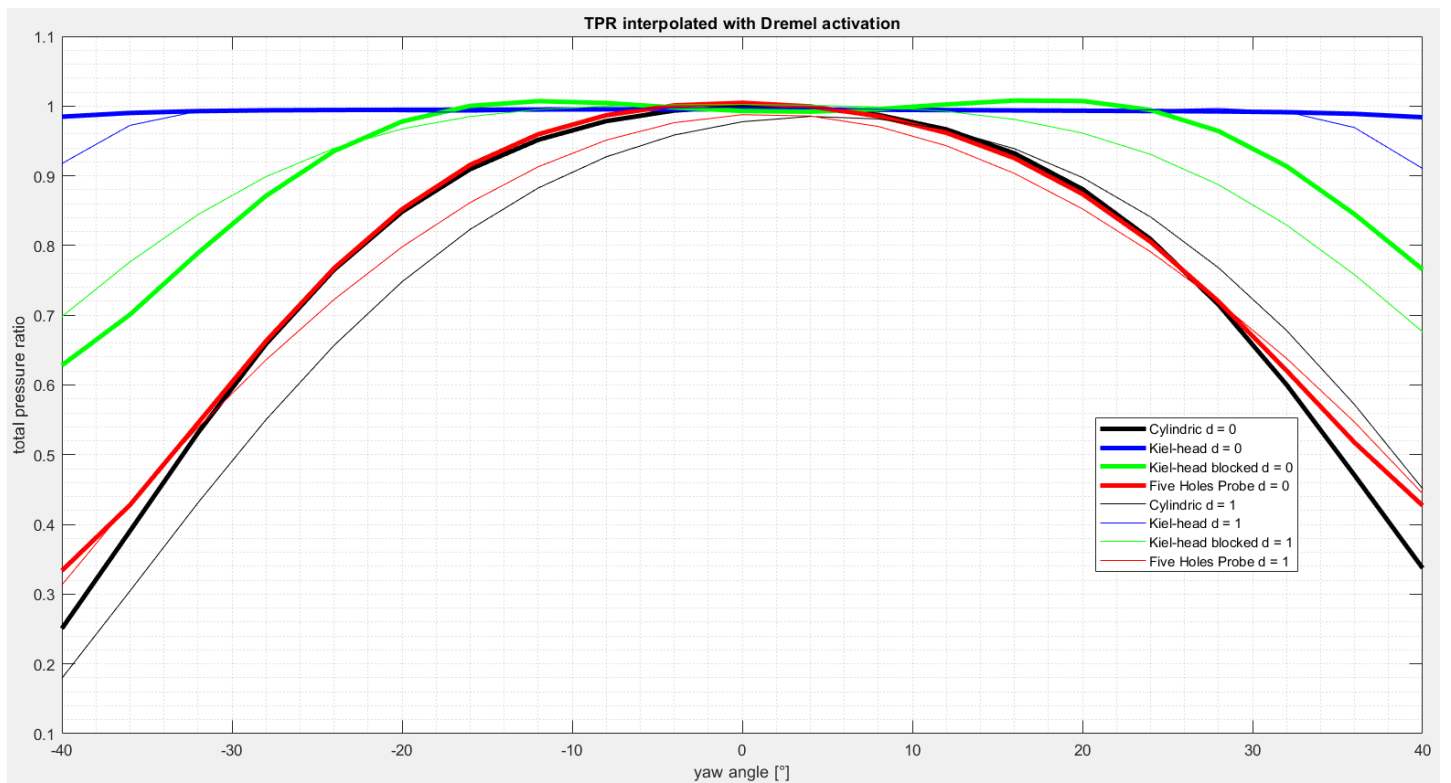


Figure 6.1 – Interpolated curves

Now, it is important to determine the yaw critical angles for each probe, both static and dynamic cases.

To do that, keeping in mind its definition (provided in chapter three), a simple subroutine has been developed and *Figure 6.2* is its results.

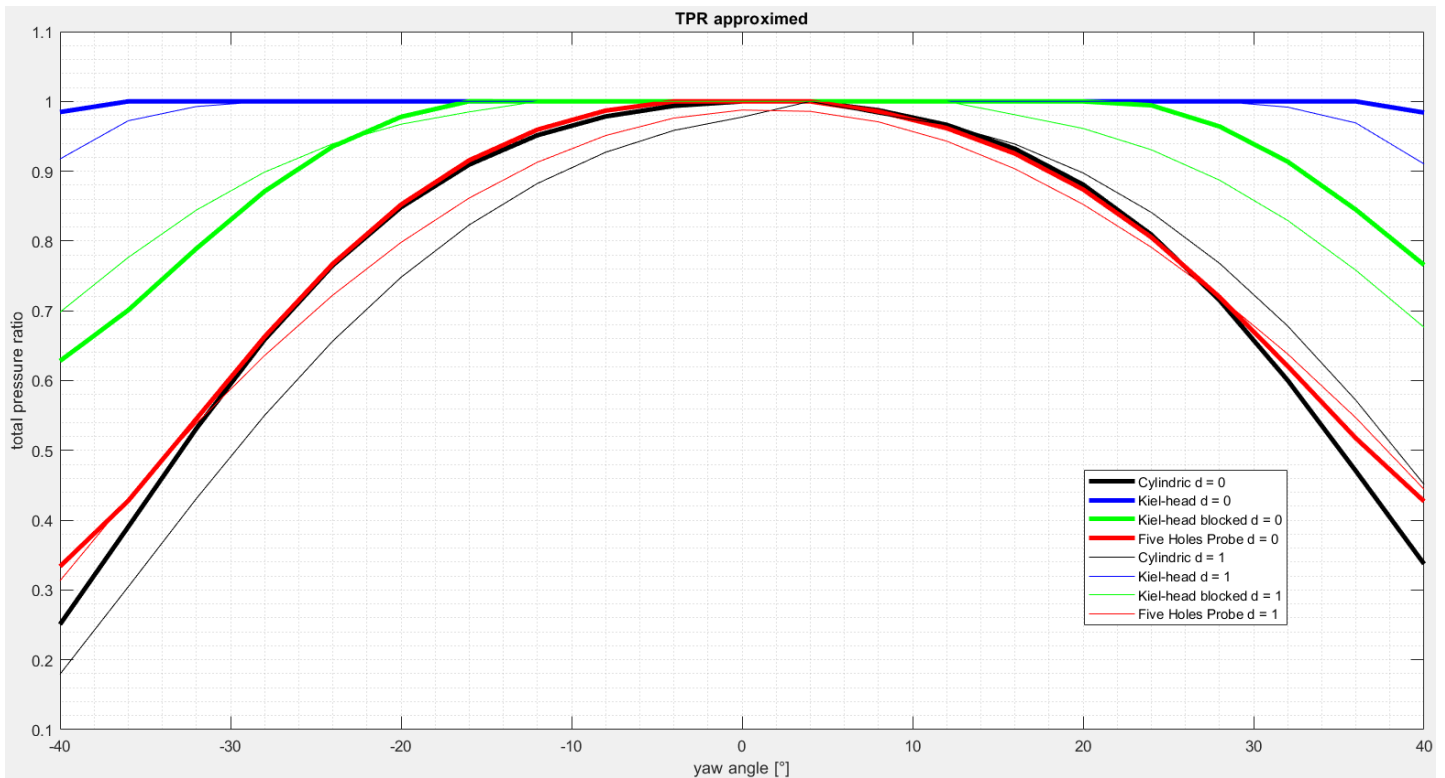


Figure 6.2 – Approximated curves

This last picture features unitary total pressure ratios if yaw angles lay between the two critical angles, otherwise the same points plotted in *Figure 6.1* are reported.

Once here, next step is to calculate the total pressure difference, for each kind of probe analysed, relative to static and dynamic cases.

The results are shown in *Figure 6.3* which, among other things, permits to state that the difference between static and dynamic case is different comparing Kiel-head probes and other kinds as the former ones show a yaw angles segment in which there is no difference between the two cases, in other word the activation of the yaw varying mechanism is useless as this difference amounts to zero. The latter ones, instead, never show a null discrepancy segment, reason for which the mechanism activation influences the reading results.

Increasing the probe misalignment, all these probes feature different error trends even if they're very negligible.

These last statements can be confirmed if these differences are expressed in terms of percentage discrepancy, like in *Figure 6.4*.

In facts, defining the total pressure discrepancy as:

$$\delta_{TP} = \frac{TPR_{static} - TPR_{dynamic}}{TPR_{static}} * 100 \quad (6.1)$$

it is possible to plot this function for each kind of probe and evaluate how much the dynamic probes (which, in order to better understand, consist of a rotating stem mechanism) differ from the static, not rotating probes.

As noticeable, the trends are almost similar for all probes: lower for null or small yaw angles and highly increasing as much as the probe misalignment is getting higher.

Nevertheless, as regards the right probe selection for highly unsteady environments, the Kiel-head probes are the most suitable even in this point of view. As a matter of facts, even with yaw angles higher than the critical ones, the pressure difference between the static stem probe and the one with dynamically yaw varying stem is negligible and quite symmetrical. This means, in terms of percentage error, not only that corrective factors are relatively simple to calculate arithmetically, but only highly turbulent flows will let errors increase in a way to invalidate the amounts read. Of course, keeping in mind that in turbo-machinery turbulence intensities won't overwhelm a 10% value, the errors will be negligible every time.

These last features absolutely can't be reproduced if using other types of probes analyzed. As a matter of facts blocked Kiel-head probes, even if their error curves are similar to the original Kiel-head, show asymmetrical error trends, which can be treated with more difficult polynomial functions, but their insensitivity ranges are much more smaller than the ones had by original, not blocked probes.

As regards the other kinds of probes, they feature asymmetrical, randomly rising and decreasing error trends, which leads to the statement that in these cases the accuracy predictions can't be absolutely done with a satisfying precision as well as the simplicity that characterizes the former two types.

This last sentence is proved with a lot of broken segments in the related plots, probably majorly owing to measurement and sampling errors rather than geometry and secondary flow field effects related ones.

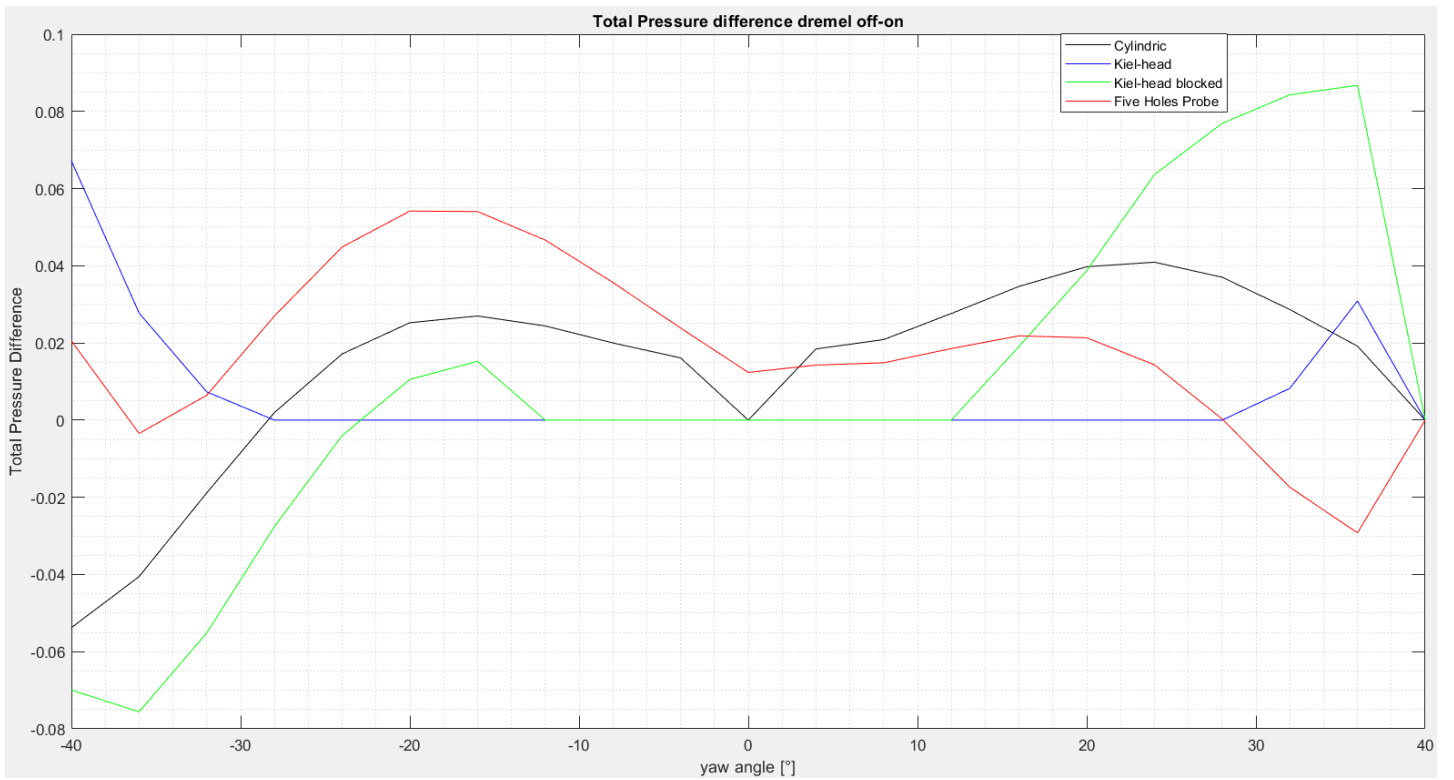


Figure 6.3 – Total pressure difference between static and dynamic situations for each kind of probe

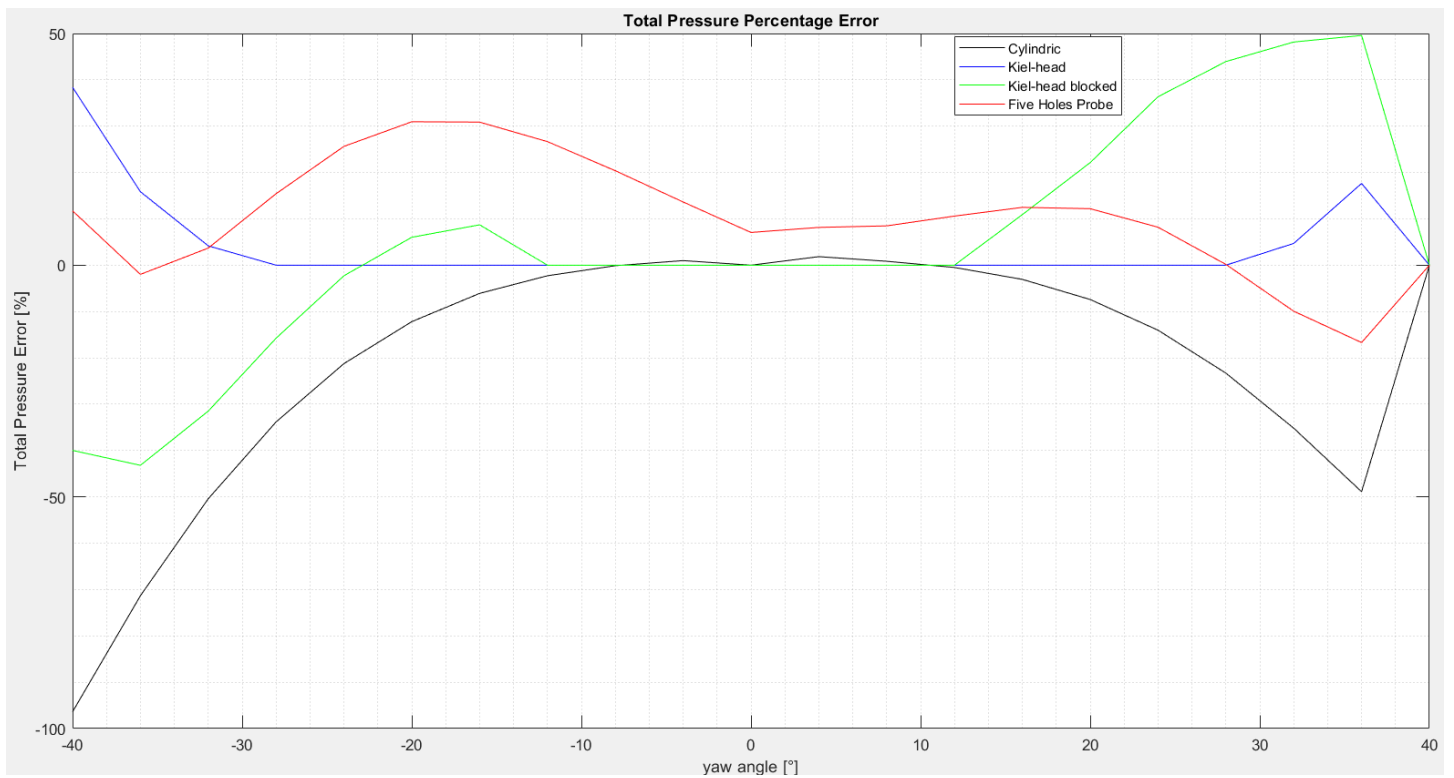


Figure 6.4 - Total Pressure Percentage discrepancy

Anyway, being these data some pressure-related ones, it is more convenient to harness pressure coefficient distribution with varying the yaw angle.

In general, for the incompressible case, the stagnation pressure remains constant and so it is possible to write the following passages:

$$p^0 = cost = p_\infty + \frac{1}{2}\rho_\infty U_\infty^2 = p + \frac{1}{2}\rho U^2 \quad (6.2)$$

where:

p_∞ , U_∞ and ρ_∞ are the free stream static pressure, speed and density respectively;

p , U and ρ are the probe related static pressure, speed and density respectively.

Considering that the pressure coefficient is defined as the difference between actual to free-stream static pressures non-dimensionalized through the free stream dynamic pressure:

$$cp = \frac{p - p_\infty}{\frac{1}{2}\rho_\infty U_\infty^2} \quad (6.3)$$

the following formula can be written also keeping in mind that the density does not vary within the flow-field:

$$cp = \frac{p - p_\infty}{\frac{1}{2}\rho_\infty U_\infty^2} = 1 - \left(\frac{U}{U_\infty}\right)^2 \quad (6.4)$$

Nevertheless, the present studies deal with compressible cases ($M > 0.3$), reason for which the same coefficient has to be calculated considering that dynamic pressure is not the difference between stagnation and static pressures anymore as the stagnation pressure now varies within the flow-field, which leads to a compressible case pressure coefficient greater than the incompressible case one.

So, starting from *equation 6.3*, it is possible to divide both the numerator and denominator of the second member for p_∞ , obtaining :

$$cp = \frac{p - p_\infty}{\frac{1}{2}\rho_\infty U_\infty^2} = \frac{\frac{p}{p_\infty} - 1}{\frac{1}{2}\frac{\rho_\infty}{p_\infty} U_\infty^2} \quad (6.5)$$

Now, keeping in mind the ideal gases state equation :

$$\frac{p}{\rho} = RT$$

and the speed of sound as well as the Mach number definition, it is possible to write the following passages in which there is also the need to multiply all for γ :

$$cp = \frac{2\left(\frac{p}{p_{\infty}} - 1\right)}{\frac{\rho_{\infty}}{p_{\infty}} U_{\infty}^2} = \frac{2\left(\frac{p}{p_{\infty}} - 1\right)}{\frac{1}{RT} \gamma U_{\infty}^2} = \frac{2\left(\frac{p}{p_{\infty}} - 1\right)}{\frac{1}{c^2} \gamma U_{\infty}^2} = \frac{2}{\gamma M^2} \left(\frac{p}{p_{\infty}} - 1\right) \quad (6.6)$$

where:

γ is the air specific heats ratio, equal to 1.4;

M is the free stream Mach number, equal either to 0.5 or 0.8;

p_{∞} is the free stream static pressure;

p is the probe related static pressure, found by *equation 6.7*;

$$p = \frac{TPR * p_{\infty}^{\circ}}{\left(1 + \frac{\gamma - 1}{2} M^2\right)^{\left(\frac{\gamma}{\gamma - 1}\right)}} \quad (6.7)$$

By doing the same operations previously described, it is possible to obtain the following graphs that lead to the same conclusions already expressed:

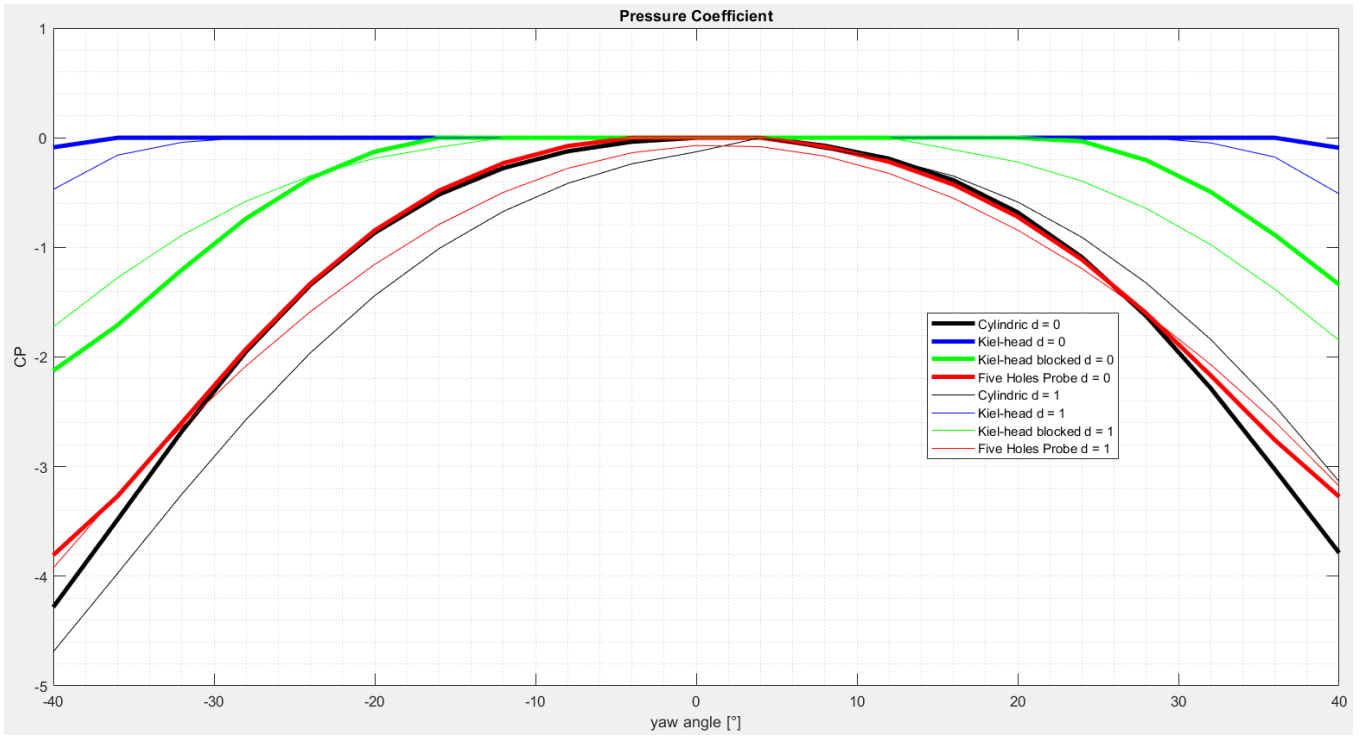


Figure 6.5 - Pressure coefficient distribution for all probes, both in static and dynamic cases

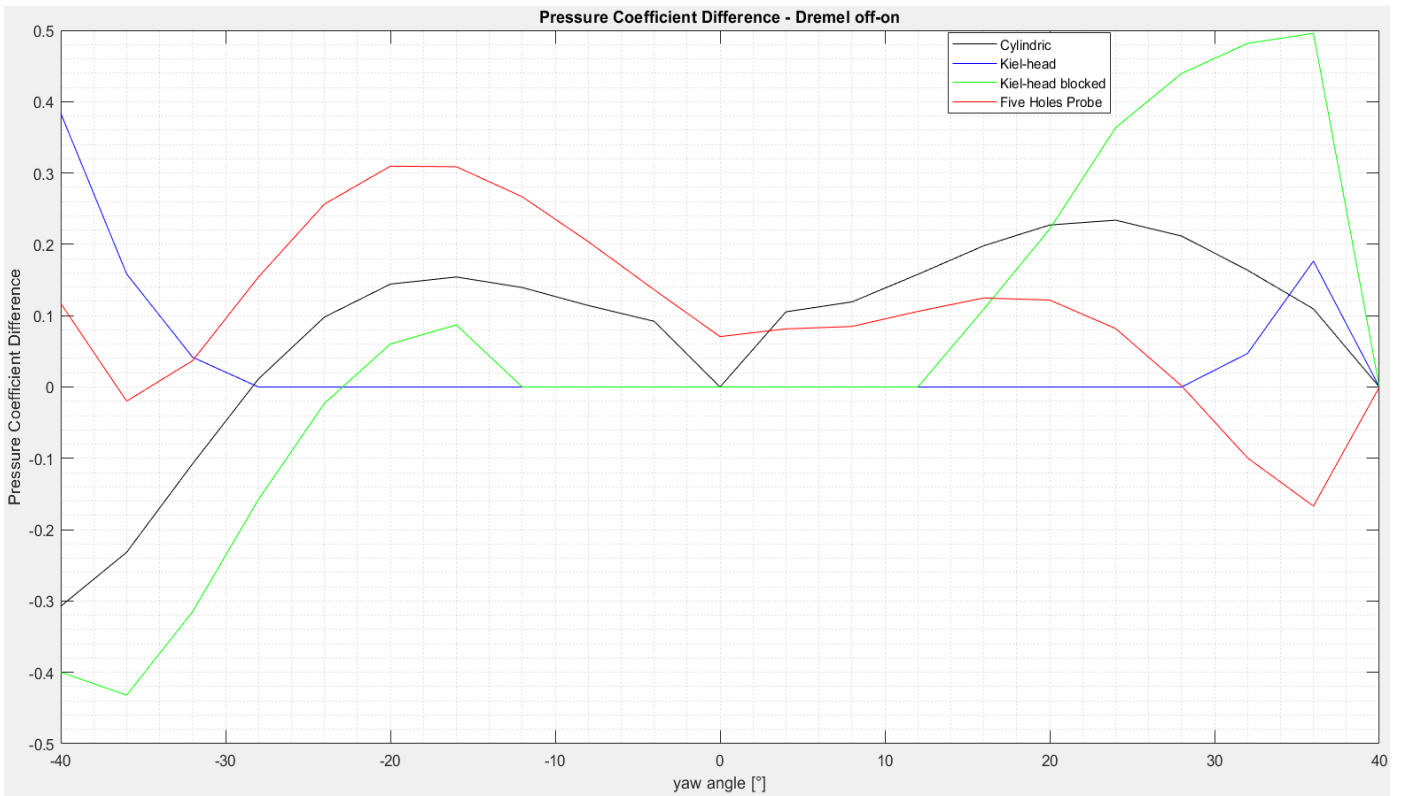


Figure 6.6 - static-to-dynamic pressure coefficient differences, for each kind of probe

In general, as regards pressure coefficients plots, it is possible to confirm the same trends and comments previously done, and this is synonym of the present formulation accuracy.

Next step is to determine corrective factors useful to obtain the actual stagnation pressure value. For this purpose, if critical angles are greater than the total, both geometrical and turbulence induced yaw angle, then corrective factor amounts to unity as there is no probe misalignment error. Otherwise, the corrective factor is given by data extrapolation and the final step is to divide the real, wrong pressure value by the correction factor calculated right now.

For a better comprehension of the procedures adopted in the whole data analysis flow chart, please see the *Appendix 8.2* containing all the instructions written in the *Matlab* script compiled by the undersigned.

7. Conclusions

The present chapter represents the end of the study carried out, by the undersigned, at the LMFA (*Laboratoire de Mécanique des Fluides et d'Acoustique*) sited into École Centrale de Lyon.

Within the proposed work, the author tried to analyse the specific influence of periodic unsteadiness in order to investigate the validity of calibrations under steady conditions. In addition, they have conducted a systematic variation of flow and probe parameters so that sensitivities have been derived and measurement accuracy has been quantified.

In other words, the present study dealt with the comprehension of how much the size and the geometry of pneumatic probes used in today's centrifugal compressors can affect the precision of the pressure amounts read downwards compressors' rotors, environments well known as fully unsteady.

Despite these values could seem useless due to the strong importance of inter-stage pressure values, which correspond to data get downwards both rotor and stator, into performance determination the knowledge of downstream-of-the rotor pressure values can provide very useful information about compressor stall and surge predictions, as well as they can assess and certify the good design of rotor blades.

In this way, the aim of this study consisted of performing a parametric analysis about the study of the influence of both probe geometry (number of holes, probe's intake, length, diameter, radial position and so on) and flow characteristics (Mach number, velocity vector direction respect to the probe front axis, Reynolds number, kind of unsteadiness - if periodic or randomly fluctuating);

Then, another feature on which the attention has been focused has been to get a prediction, about the points along with the flow path, where there could be strong fluctuations.

So, during the first one this five months' period, a huge bibliography research has been conducted in order to gather sufficient data to begin the study but, owing to the very broad and variegated field such as this one debated, very few scientific articles and papers resulted suitable for the case under consideration.

In addition, what about the study conducted by the undersigned, despite the results are not highly representative of the real physics of the studied phenomena as a lot of approximations have been done, such as the turbulence model (Goldstein's, isotropic

turbulence) as well as variables (Reynolds) and secondary effects (wall proximity effects) neglected even if other authors stated their importance, the same results constitute a valid tool to state that Kiel head probes are the most suitable for highly unsteady environments as:

- they have a greater critical angle, which means that the yaw insensitivity ranges are the most wide in comparison with other probes in this study analyzed;
- their insensitivity range rises with increasing the external diameter (geometrical dependence);
- there is a local speed range in which the critical angle remains constant. Then, at a given Mach number, there is a tendency to decrease the critical angle with rising the local Mach number and the rate of this fall is supposed to depend on the design or the probe (compressibility dependence);
- having a wider insensitivity range both for pitch and yaw angles, this kind of probes is the less sensitive to turbulence induced errors. This feature is valid until the flow turbulence intensity remains under 70%, which is the limit turbulence intensity as calculated through *equation 3.7* considering a medium Kiel-head critical angle of 35 [°] (turbulence effects on the read values);
- even with yaw angles higher than the critical ones, the pressure difference between the static stem probe and the one with dynamically yaw varying stem is negligible and quite symmetrical. This means, in terms of percentage error, not only that corrective factors are relatively simple to calculate arithmetically, but only highly turbulent flows will let errors increase in a way to invalidate the amounts read. Of course, keeping in mind that in turbo-machinery turbulence intensities won't overwhelm a 10% value, the errors will be negligible every time.

Now, as specified in chapter five, experiments have been carried out on ECL-B3 reduced model, which is a scaled reconstruction of a real compressor stage, and the main results permits to analyze flow-field data for the real probe encumber analysis and are able to validate theoretical concepts reported in the first chapters in terms of probe measurement errors.

Anyway, even if the most suitable probe has been chosen, the present studies will result useless if future numerical studies carried out upon these bases won't use the most accurate numerical method so as to foresee the probe behaviour when it will be placed in a real compressor stage. In other words, the resulting numerical outcomes will be useful to complete the project started by the undersigned through the present work.

8. Appendix

8.1. Kiel-head probe specifications

Kiel Probes

General Information

Aerodynamic Properties

Kiel probes are used to measure total pressure in a fluid stream where the direction of flow is unknown or varies with operating conditions. Their correction factor is 0 when used within the ranges outlined below.

Mach Number Range

True total pressure is indicated up to a Mach Number of 1.0. There is a slight drop in yaw insensitive range above Mach Number 0.3. This decrease averages about 4% for all types at a Mach Number of 1.0.

Reynolds Number Range

The probes are insensitive to Reynolds Number except at extremely low velocities for Pitot-Static probes. For air this limiting velocity is about 4 ft/sec for the smallest size Kiel probes listed.

Time Constant

Time constant depends on the complete installation, probe, pressure lines, and manometer. With 1/8" connecting hose up to 20 ft. long and a liquid manometer of 1/4" ID, the Type B probe will reach equilibrium reading in approximately 15 seconds. Using this time "t" as a standard the other time constants for average stem lengths will be:

Type	Constant
A	2.4 t
C, D, H	.04 t
E, F	.02 t

Turbulence Errors

Turbulence errors are negligible, especially since the probe is yaw insensitive. Very High turbulence may cut down the yaw and pitch insensitive ranges however.

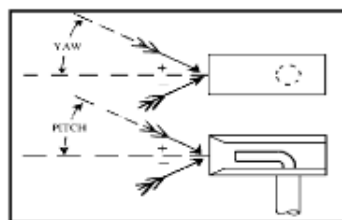


Figure 1. Flow Angles

Yaw and Pitch Angle Range

The outstanding advantage of Kiel probes compared with other total pressure probes is complete insensitivity to direction of flow within certain limits. Their yaw and pitch characteristics are generally the same although stem interference on some designs will change one from the other. Fig. 1 shows these flow angles and Fig. 2 is a typical calibration curve of a Type A probe. It can be seen that the correction factor equals 0 up to the limits of the yaw range and then drops very sharply. The range is arbitrarily defined as the point where the error equals 1% of velocity pressure.

Symbols used in these figures are:

- Pt: Total Pressure
- Ps: Static Pressure
- Ptp: Indicated Total Pressure

The yaw and pitch range for all types listed below at a Mach Number of .25 are:

Type	Yaw Range	Pitch Range
A	±52°	±47° - 40°
B	±48°	±45°
C	±54°	±49°
D	±54°	±49°
E	±63°	±58°
F	±67°	±61°
R	±54°	±49°

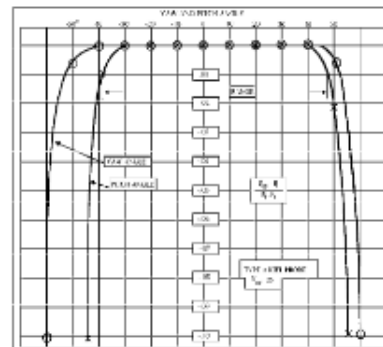
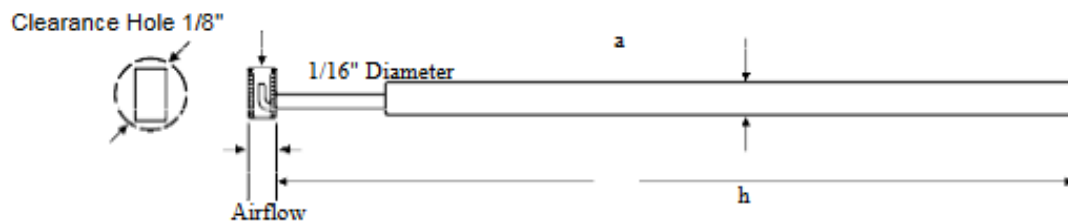


Figure 2. Typical Calibration Curve of a Type A Probe

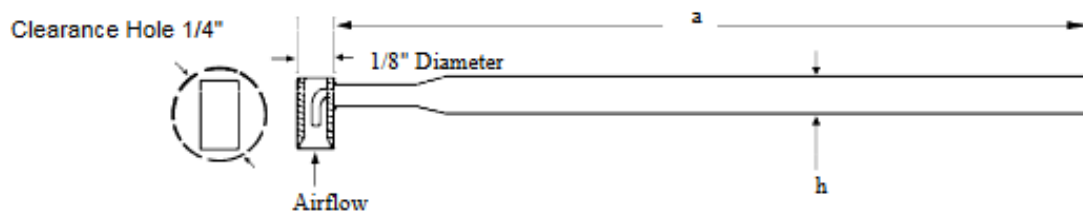
SELECT FROM THESE KIEL MODELS / SPECIFICATIONS

Ordering Part Number	Sensing Head Description	Probe Diameter r h	Probe Length a	Yaw Range **	Pitch Range **	Time † Constant (Sec.)
KAA-"a"	1/16" Dia. Miniature Type KA 	1/16"	Standard Probe Lengths are 6" 8" 12" 24"	± 52°	+ 47° - 40°	36
KAC-"a"		1/8"				
KBA-"a"	1/8" Dia. Standard Type KB 	1/16"		± 48°	± 45°	
KBC-"a"		1/8"				
KBC-"a"-W						

Type KA:



Type KB:



** "Range" is defined as the point at which error equals 1% of velocity pressure.
 † See qualifications under "Time Constant", front page.



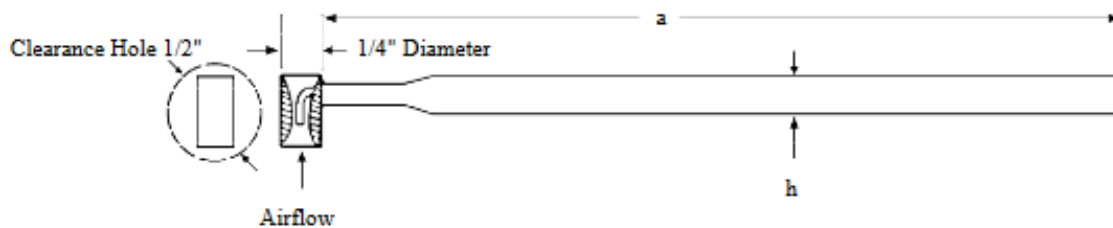
TECHMARK

— Industriesteuerungen GmbH — <http://www.techmark.de> — e-mail: info@techmark.de —
 Kirschstrasse 20 • D-80999 München • Telefon (+49-89) 89.26.57-0 • Telefax (+49-89) 89.26.57-33

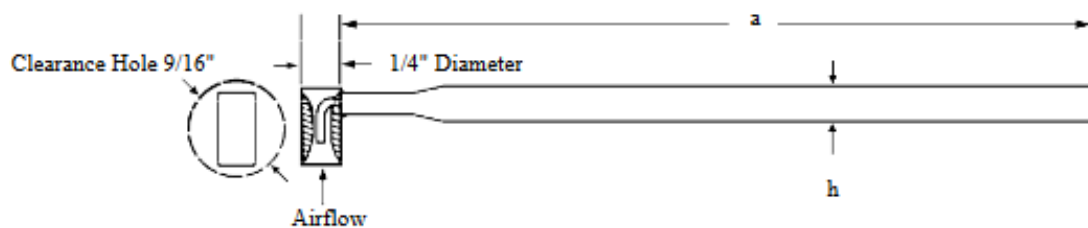
SELECT FROM THESE KIEL MODELS / SPECIFICATIONS

Ordering Part Number	Sensing Head Description	Probe Diameter r h	Probe Length a	Yaw Range **	Pitch Range **	Time † Constant (Sec.)
KCC-"a"	1/4" Dia. Venturi Type KC 	1/8"	Standard Probe Lengths are 6" 8" 12" 24"	± 54°	± 49°	0.6
KCE-"a"		3/16"				
KCF-"a"		1/4"				
KCF-"a"-W						
KDC-"a"	1/4" Dia. Venturi Type KD 	1/8"		± 54°	± 49°	0.6
KDE-"a"		3/16"				
KDF-"a"-W		1/4"				

Type KC:



Type KD:



** "Range" is defined as the point at which error equals 1% of velocity pressure.

† See qualifications under "Time Constant", front page.



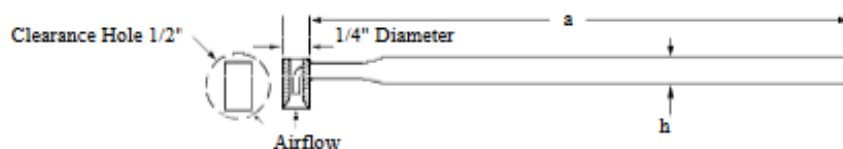
TECHMARK

— Industriesteuerungen GmbH — <http://www.techmark.de> — e-mail: info@techmark.de —
Kirschstrasse 20 • D-80999 München • Telefon (+49-89) 89.26.57-0 • Telefax (+49-89) 89.26.57-33

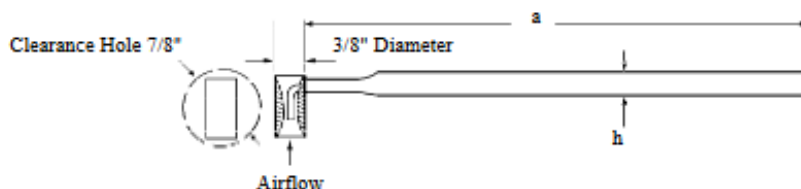
SELECT FROM THESE KIEL MODELS / SPECIFICATIONS

Ordering Part Number	Sensing Head Description	Probe Diameter	Probe Length	Yaw Range **	Pitch Range **	Time † Constant (Sec.)
KRC-"a"	1/4" Dia. High-Range Type KR 	1/8"	Standard Probe Lengths are 6" 8" 12" 24"	± 54°	± 49°	0.6
KRF-"a"		1/4"				
KEC-"a"	3/8" Dia. Venturi Type KE 	1/8"		± 63°	± 58°	0.3
KEE-"a"-W		3/16"				
KEF-"a"		1/4"				
KFF-"a"	3/4" Dia. Venturi Type KF 	1/4"		± 67°	± 61°	0.3

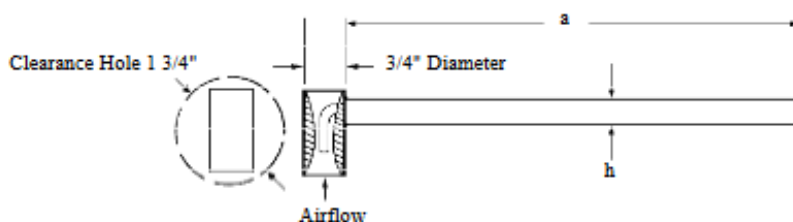
Type KR:



Type KE:



Type KF:



** "Range" is defined as the point at which error equals 1% of velocity pressure.

† See qualifications under "Time Constant", front page.



TECHMARK

— Industriesteuerungen GmbH — <http://www.techmark.de> — e-mail: info@techmark.de —
Kirschstrasse 20 • D-80999 München • Telefon (+49-89) 89.26.57-0 • Telefax (+49-89) 89.26.57-33

Boundary Effects

Boundary effects are small as in all total pressure probes. However, in steep total pressure gradients as near solid boundaries or in "trough" behind guide vanes a shift in the effective center of the probe occurs, so the total pressure measured corresponds to the streamline 0.5d away from the geometrical center of the head in the direction of the higher total pressure as shown in Fig. 3.

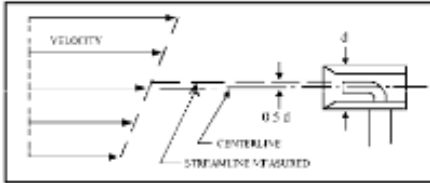


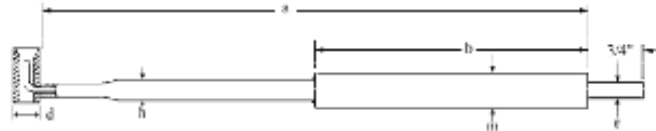
Figure 3. Shift in Effective Probe Center

Installation

These probes are usually installed through holes large enough to pass the head as listed on the Kiel Specification pages. See each individual type for the minimum size.

Special construction including other material, designs to customer's specifications, special take-offs, and mounting adapters quoted as requested.

Ordering Information



Typical Example: KBC-12-F-10-C-W

- K: Class = K (Kiel) All stainless steel construction
- B: d = See chart and table – Type A, B, C, D, E, F, R
- C: h = 1/8" - see chart for range in each type

A	C	D	E	F	H	J
1/16"	1/8"	5/32"	3/16"	1/4"	5/16"	3/8"

- 12: a = 12" - Overall length - inches
- F: m = 1/4" - Reinforcing tube diameter (Omit if no reinforcing required)

C	D	E	F	H	J	L	M	N
1/8"	5/32"	3/16"	1/4"	5/16"	3/8"	1/2"	5/8"	3/4"

- 10: b = Reinforcing tube length – inches (Omit if no reinforcing required)
- C: e = 1/8" - Take-off diameter (Omit if take-off is same size as stem; i.e.

"h")

A	C	D	F
1/16"	1/8"	5/32"	1/4"

- W: Welded for use up to 2,000°F

High temperature braze for use up to 1,500°F, use N in place of W.

Omit if Welded or Microbraze is not required. Standard Braze is Silver soldered for use up to 900°F.



TECHMARK

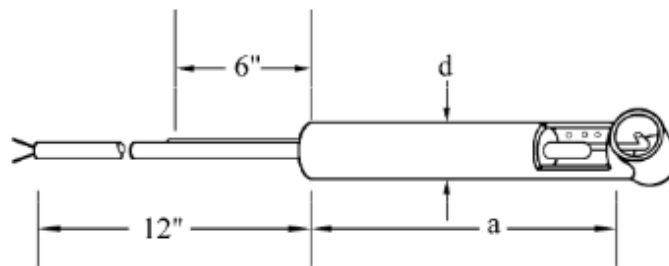
— Industriesteuerungen GmbH — <http://www.techmark.de> — e-mail: info@techmark.de —
Kirschstrasse 20 • D-80999 München • Telefon (+49-89) 89.26.57-0 • Telefax (+49-89) 89.26.57-33

Kiel Temperature Probes

Combination Pressure/ Temperature Probes

KT: Special purpose Kiel-Temperature Probe measures total pressure and temperature in one unit. The Kiel Head is insensitive to pitch and yaw angles of flow up to +/- 45°. Thermocouple has grounded junction with bleed holes. Exposed and ungrounded junctions are available. Thermocouple accessories and pressure connectors are also available upon request. Please consult United Sensor.

Ordering Information



Typical Example: KT-8-K-12-C

KT: Type KT
8: a = 8" – Probe Length
K: Thermocouple Wire Calibration
K: Chromel – Alumel
J: Iron – Constantan
T: Copper – Constantan
E: Chromel – Constantan

12: 12" - Leadwire Length
C: d = 1/8" – Probe Diameter

C	E	F
1/8"	3/16"	1/4"



TECHMARK

— Industriesteuerungen GmbH — <http://www.techmark.de> — e-mail: info@techmark.de —
Kirschstrasse 20 • D-80999 München • Telefon (+49-89) 89.26.57-0 • Telefax (+49-89) 89.26.57-33

8.2. MATLAB script for the probes cross evaluation

8.2.1. Variables definition and data loading

```
%% Pneumatic Probe Data Interpolation - Mach 0.5 - with Total Pressure, Pressure
Coefficients Determination and Dremel activation influence
clear all;
clc;
M = 0.5;%free stream Mach Number
gamma = 1.4;%specific heats ratio
ps = 18600;%static pressure [Pa]
Ts = 273.15+22.4;%static temperature [K]
R = 287.05;%dry air specific constant [J/(Kg*K)]
alfa_0 = 4;%probe setting angle, read by a plot through the Python script
i = 0;%turbulence intensity
err_max = 0.02;
alfa_max = 40;
max_degree = 6;%maximum polynomial interpolation degree
alfa_vect = [-alfa_max:4:alfa_max];
data_matrix = zeros(9,(length(alfa_vect)));
interp_coeff = zeros(9,(max_degree+1));
data_interp = zeros(9,(length(alfa_vect)));
data_approx = zeros(9,(length(alfa_vect)));
tpd_matrix = zeros(9,(length(alfa_vect)));
c_f = zeros(9,2);%correction factor matrix, composed of two columns : the left-side
one is related to the negative critical yaw angle, the right side one is related to the
positive critical yaw angle
ptot_diff = zeros(5,(length(alfa_vect)));%dremel off - on total pressure difference
matrix
ptot_perc = zeros(5,(length(alfa_vect)));%dremel off - on total pressure percentage
error
cp_matrix = zeros(9,(length(alfa_vect)));
cp_diff = zeros(5,(length(alfa_vect)));%dremel off - on pressure coefficient difference
matrix
for i = 1:(length(alfa_vect))
    data_matrix(1,i) = alfa_vect(i);
    data_interp(1,i) = alfa_vect(i);
    ptot_diff(1,i) = alfa_vect(i);
end

%insertion of measurement data related to different pneumatic probes
%      -40      -36  -32  -28   -24  -20  -16  -12  -8   -4   0
4      8   12   16   20   24   28   32   36   40
```

%DREMEL NULL

```
data_matrix(2,:) = [0.248993 0.394008 0.53257 0.655956 0.761572 0.847304  
0.911194 0.957114 0.983746 0.990897 0.991509 0.992045 0.989941 0.974093  
0.93554 0.879098 0.805453 0.71281 0.601158 0.473907 0.33578]; %data related to  
Cylindric probe d=0
```

```
data_matrix(3,:) = [0.984782 0.989962 0.99304 0.993717 0.994295 0.994639  
0.994913 0.995162 0.995165 0.99534 0.995224 0.994952 0.994681 0.994468  
0.993917 0.993229 0.99272 0.992099 0.991442 0.988878 0.983906]; %data related to  
Kiel-head probe d=0
```

```
data_matrix(4,:) = [0.630105 0.699259 0.779167 0.885069 0.931665 0.98524  
0.997315 0.9987 0.999037 0.9991 0.99922 0.999107 0.999221 0.999218 0.999058  
0.998949 0.998074 0.98078 0.907245 0.839164 0.768378]; %data related to Kiel-head  
blocked probe d=0
```

```
data_matrix(5,:) = [0.33608 0.421145 0.54923 0.665486 0.765831 0.850467 0.916064  
0.961275 0.988474 0.998573 1.00009 0.998938 0.989637 0.965484 0.926072  
0.871086 0.802261 0.718962 0.622902 0.51929 0.425703]; %data related to FHP d=0
```

%DREMEL ACTIVATED

```
data_matrix(6,:) = [0.177558 0.306268 0.436966 0.545248 0.653221 0.746369  
0.824589 0.884547 0.930224 0.959829 0.976838 0.984182 0.978713 0.962864  
0.939047 0.899357 0.847824 0.767004 0.674082 0.571497 0.452429]; %data related  
to Cylindric probe d=1 (angolo di rotazione consigliato 4°)
```

```
data_matrix(7,:) = [0.91507 0.979626 0.989319 0.991796 0.993507 0.993809  
0.994317 0.994704 0.994998 0.995203 0.99525 0.995399 0.995342 0.995107 0.99476  
0.994263 0.993344 0.991486 0.988181 0.977799 0.907331]; %data related to Kiel-  
head probe d=1 (angolo di rotazione consigliato 0°)
```

```
data_matrix(8,:) = [0.696534 0.779894 0.845391 0.895295 0.935822 0.967091  
0.990427 0.99857 0.999052 0.999109 0.999176 0.999118 0.998677 0.99632 0.984772  
0.960903 0.927305 0.883857 0.83196 0.760013 0.675204]; %data related to Kiel-head  
blocked probe d=1 (angolo di rotazione consigliato 0°)
```

```
data_matrix(9,:) = [0.310008 0.434987 0.548726 0.625429 0.715219 0.798857  
0.866255 0.916723 0.952997 0.976122 0.987587 0.982396 0.966811 0.941376  
0.905602 0.856176 0.793332 0.71867 0.636444 0.544639 0.44576]; %data related to  
FHP d=1 (angolo di rotazione consigliato 0°)
```

8.2.2. Interpolation coefficients generation

%interpolation coefficients generation - Kiel-head blocked

```
x = data_matrix(1,:);  
p = polyfit(data_matrix(1,:),data_matrix(4,:),max_degree);  
y = polyval(p,x);  
data_interp(4,:) = y;  
for i = 1:(max_degree+1)  
    interp_coeff(4,i) = p(i);
```

end

8.2.3. Critical yaw angles determination

```
%critical yaw angles determination - d = 0
alfa_crit = zeros(9,2); %two columns : the left-side one is related to the negative
critical yaw angle, the right side one is related to the positive critical yaw angle
aux = zeros(1,length(alfa_vect)); %auxiliary array reset
%cylindric probe
for i = 1:length(alfa_vect)
    if (data_interp(2,i)>(1-err_max))
        aux(i) = alfa_vect(i);
    end
end
alfa_crit(2,1) = min(aux);
alfa_crit(2,2) = max(aux);
```

8.2.4. Approximated curves calculation

```
%APPROXIMATED CURVES CALCULATION
```

```
x = data_matrix(1,:);
for i = 2:9
    for j = 1:length(alfa_vect)
        if (x(j)<alfa_crit(i,2) && x(j)>alfa_crit(i,1))
            data_approx(i,j) = 1;
        else
            data_approx(i,j) = data_interp(i,j);
        end
    end
end
end
```

8.2.5. Pressure coefficients calculation

```
%PRESSURE COEFFICIENTS CALCULATION
```

```
pt_real = ps*((1+((gamma-1)/2)*M^2)^(gamma/(gamma-1)));
rho = ps/(R*Ts);
V_inf = M*sqrt(gamma*R*Ts);
x = data_matrix(1,:);
for i = 2:9
    for j = 1:length(alfa_vect)
        cp_matrix(i,j) = (((data_approx(i,j).*pt_real)/((1+((gamma-1)/2)*M^2)^(gamma/(gamma-1))))/ps)-1)*(2/(gamma*M^2));
    end
end
end
```

8.2.6. *Dremel* off - on total pressure difference, total pressure percentage error and CP difference matrixes calculation

```
for i = 2:5
    for j = 1:(length(alfa_vect)-1)
        if (i==2)
            ptot_diff(i,j) = data_approx(i,j) - data_approx(i+4,j+1);
            ptot_perc(i,j) = 100*(data_approx(i,j) - data_approx(i+4,j+1)/data_approx(i,j));
            cp_diff(i,j) = cp_matrix(i,j) - cp_matrix(i+4,j+1);
        else
            ptot_diff(i,j) = data_approx(i,j) - data_approx(i+4,j);
            ptot_perc(i,j) = 100*(cp_matrix(i,j) - cp_matrix(i+4,j));
            cp_diff(i,j) = cp_matrix(i,j) - cp_matrix(i+4,j);
        end
    end
end
```

8.2.7. Fluctuations-related angle and corrective factors determination

%fluctuations-related angle determination

%input of the probe setting angle - alfa_0

```
continue_iteration = true;
while continue_iteration
    prompt = 'Insert the probe setting angle alfa_0 [°] (must be -45 <= alfa_0 <= 45) : ';
    alfa_0 = input(prompt);
    if ((alfa_0 >= -45) && (alfa_0 <= 45))
        continue_iteration = false;
    end
end
```

%input of the expected fluctuation intensity - i

```
continue_iteration = true;
while continue_iteration
    prompt = 'Insert the expected turbulence intensity [%] (must be 0 <= i <= 10 in turbomachinery applications) : ';
    i = input(prompt);
    if ((i >= 0) && (i <= 10))
        continue_iteration = false;
    end
end
```

```
alfa_1 = radtodeg(atan(i/100));
```

```

%stagnation pressure determination
alfa_min = alfa_0 - alfa_1;
alfa_max = alfa_0 + alfa_1;
for i = 2:5
    if (alfa_min > alfa_crit(i,1) && alfa_min < alfa_crit(i,2))
        c_f(i,1)= 1;
    else
        c_f(i,1)= polyval(interp_coeff(i,:),alfa_min);
    end
    if (alfa_max < alfa_crit(i,2) && alfa_max > alfa_crit(i,1))
        c_f(i,2)= 1;
    else
        c_f(i,2)= polyval(interp_coeff(i,:),alfa_max);
    end
end

pt_ind = zeros(5,2);
for i = 2:5
    pt_ind(i,1) = pt_real.*(c_f(i,1));
    pt_ind(i,2) = pt_real.*(c_f(i,2));
end

```


9. Bibliography

- [1] **S. Bauinger, A. Marn, E. Göttlich, F. Heitmeir**, "Influence of Pressure Fluctuations on the Mean Value of Different Pneumatic Probes", *Int. J. Turbomach. Propuls. Power*, 2017;
- [2] **J. L. Gilarranz, A. J. Ranz, J. A. Kopko, J. M. Sorokes**, "On the Use of Five-Hole Probes in the Testing of Industrial Centrifugal Compressors ", *ASME*, 2005;
- [3] **S. H. Chue**, "Pressure probes for fluid measurement", *Prog. Aerospace Sci.*, Vol.16, No. 2, pp.147-223, 1975;
- [4] **L. Toni, V. Ballarini, S. Cioncolini, P. Gaetani, G. Persico**, "Unsteady Flow Field Measurements In An Industrial Centrifugal Compressor", *Texas A&M University. Turbomachinery Laboratories*. Available electronically from <http://hdl.handle.net/1969.1/163050>, 2010;
- [5] **D. E. Walsche, H.C. Garner**, "Usefulness of various pressure probes in fluctuating low speed flows", *Brit. ARC* 21714, 1960;
- [6] **P. Kupferschmied, P. Koppel, W. Gizzi, C. Roduner and . Gyarmathy**, "Time-resolved flow measurements with fast-response aerodynamic probes in turbomachines", *ETH Zurich (Swiss Federal Institute of Technology), Institute of Energy Technology, Turbomachinery Laboratory, CH-8092 Zurich, Switzerland*, 2000;
- [7] **A. L. Treaster, A. M. Yocum**, "The calibration and Application of Five-Hole Probes", *The Pennsylvania State University, Institute for Science and Engineering, applied research laboratory*, 1978;
- [8] **K. N. Everett, A. A. Gerney and D. A. Durston**, "Seven-Hole Cone Probes for High Angle Flow Measurement: Theory and Calibration", *AIAA Journal* vol. 21, no. 7, 1983;
- [9] **J. Xin, X. Wang, L. Zhou, Z. Ye and H. Liu**, "Numerical investigation of the flow field and aerodynamic load on impellers in centrifugal compressor with different radial inlets", *ASME*, 2016;
- [10] **S. Goldstein**, "A Note on the Measurement of Total Head and Static Pressure in a Turbulent Stream", 1936;
- [11] **R.E. Kronauer and H.P. Grant**, "Pressure probe response in fluctuating flows", *Proc. 2nd U.S. National Congr. Appl. Mech.*, pp. 163-9, 1954;

- [12] **X. Ottavy**, "Banc ECL-B3 de l'EquipEx PHARE", ECL, 27 février 2014;
- [13] **C. Lonati**, "Caratterizzazione del campo di moto a valle di schiere di turbina a disegno 3d in una galleria del vento anulare di nuova concezione", Politecnico di Milano, A.A. 2008/2009;
- [14] **G.E. Maselli**, "Indagine sugli effetti del numero di Reynolds nella calibrazione ed applicazione di sonde pneumatiche direzionali", Politecnico di Milano, A.A. 2009/2010;
- [15] **G.E. Glawe, L.N. Krause, and T.J. Dudzinski**, "A small combination sensing probe for measurement of temperature, pressure, and flow direction", Lewis Research Center, NASA, October 1968;
- [16] **F. Han, Y. Mao, J. Tan, C. Zhao and Y. Zhanu**, "Flow measurement and simulation of a radial inlet for centrifugal compressor", SAGE, 2015;
- [17] **P.Duquesne, C.Deschênes, M.Iliescu, G.D.Ciocani**, "Calibration in a potential water jet of a five-hole pressure probe with embedded sensors for unsteady flows measurement", Proceedings of SPIE - The International Society for Optical Engineering, January 2010;
- [18] **J. Schlienger, A. Pfau, A.I. Kalfas, R.S. Abhari**, "Measuring unsteady 3d flow with a single pressure transducer", Laboratory for Turbomachinery, ETH Zurich, Switzerland;
- [19] **R. J. Miller, R. W. Ainsworth**, "Accuracy of fast-response probes in unsteady turbine flows", Cambridge, UK, September 2002;
- [20] **D. J. Anderson**, "Velocity measurements in a transonic compressor using a calibrated pressure probe", US Navy, Naval Postgraduate School, March 1975;
- [21] **A. Stein**, "Computational analysis of stall and separation control in centrifugal compressors", Georgia Institute of Technology, May 2000;
- [22] **M.Y. Ding, C. Groth, S. Kacker, D. Roberts**, "CFD Analysis of Off-design Centrifugal Compressor Operation and Performance";
- [23] **T. F. Øvervåg**, "Centrifugal Compressor Load Sharing with the use of MPC", Norwegian University of Science and Technology, March 2013;
- [24] **X. Medina, G. Pisani, F. Lopez**, "Centrifugal Compressor Optimization", Florida International University, November 2014;

- [25] **J. van Helvoirt**, "Centrifugal compressor surge : modeling and identification for control", Technische Universiteit Eindhoven DOI: 10.6100/IR629084, 2007;
- [26] **M. Chernov**, "Design of a test stand for a centrifugal compressor", Lappeenranta University of Technology, 2013;
- [27] **J. Liedman, R. Månsson**, "Dynamic simulation of a centrifugal compressor system", Chalmers university of technology, Gothenburg, Sweden, 2013;
- [28] **Y. A. Wu**, "Numerical Investigation of the Performance and Flow Behaviour of Centrifugal Compressors", University of Manchester, 2014;
- [29] **M.H.L. Ogink**, "Analyses and dynamic modelling of the compressor section in a PCC-process for coal-fired power plants with offshore storage", Delft University of Technology, June 2015;
- [30] **K.J Elliott**, "Numerical investigation of highly curved turbulent flows in centrifugal compressors and in a simplified geometry", Electronic Thesis and Dissertation Repository. 556, <https://ir.lib.uwo.ca/etd/556>, June 2012;
- [31] **S. S. Solaesa**, "Analytical prediction of turbocharger compressor performance : a comparison of loss models with numerical data", Universidad Politécnica de Madrid, KTH Royal Institute of Technology, September 2016;